1989

Kinetic study of the reaction of ferrocenes and ferrocenium ions with ground and excited states of tris (2,2'-bipyridine) chromium ions and the preparation and homolysis of organocobalt complexes

Shaoyung Lee
Iowa State University

Order Number 9014921

Kinetic study of the reaction of ferrocenes and ferrocenium ions with ground and excited states of tris(2,2′-bypyridine)chromium ions and the preparation and homolysis of organocobalt complexes

Lee, Shaoyung, Ph.D.

Iowa State University, 1989

U·M·I
300 N. Zeeb Rd.
Ann Arbor, MI 48106

Kinetic study of the reaction of ferrocenes and ferrocenium ions with ground and excited states of tris(2,2'-bipyridine)chromium ions and the preparation and homolysis of organocobalt complexes

by

Shaoyung Lee

A Dissertation Submitted to the
Graduate Faculty in Partial Fulfillment of the
Requirements for the Degree of
DOCTOR OF PHILOSOPHY

Department: Chemistry
Major: Inorganic Chemistry

Approved:

Signature was redacted for privacy.

In Charge of Major Work

Signature was redacted for privacy.

For the Major Department

Signature was redacted for privacy.

For the Graduate College

Iowa State University
Ames, Iowa
1989

TABLE OF CONTENTS

GENERAL INTRODUCTION 1

CHAPTER I. REACTIONS OF FERROCENES AND FERROCENIUM IONS WITH GROUND AND EXCITED STATES OF TRIS(2,2'-BIPYRIDINE)CHROMIUM IONS 2

INTRODUCTION 3

EXPERIMENTAL 6

Reagents 6

Methods 7

RESULTS 10

Quenching of $^*Cr(bpy)_3^{3+}$ by d^6 metallocenes 10

Quenching of $^*Cr(bpy)_3^{3+}$ by ferrocenium ions 11

Kinetic reaction of ferrocenium ions with $Cr(bpy)_3^{2+}$ 14

Yield of $Cr(bpy)_3^{2+}$ in the quenching of $^*Cr(bpy)_3^{3+}$ with d^6 metallocenes 17

DISCUSSION 21

Quenching of $^*Cr(bpy)_3^{3+}$ by d^6 metallocenes 21

Quenching of $^*Cr(bpy)_3^{3+}$ by ferrocenium ions 24

Kinetics of the reaction of $Cr(bpy)_3^{2+}$ with ferrocenium ions $(Fe(C_5H_4R)(C_5H_4R')^+)$ 30

Summary 32

BIBLIOGRAPHY 33

APPENDIX 36

CHAPTER II. PREPARATION AND HOMOLYSIS OF A SERIES MACROCYCLIC ORGANOCOBALT COMPLEXES 63

INTRODUCTION 64

EXPERIMENTAL 68

Reagents 68

Synthesis of organocobalt complexes 71

Methods 72

X-ray Crystallography of rac-$CH_2ClCo(Me_6[14]4,11$ $dieneN_4(ClO_4)_2$ 73

RESULTS 76

^1H NMR and UV-Visible spectra 76

X-ray crystal structure of $[(H_2O)(Me_6[14]4,11$-$dieneN_4CoCH_2Cl](ClO_4)_2$ 76

Isomerization of $RCo(Me_6[14]4,11\text{-}dieneN_4)^{2+}$ 90

Homolysis of $EtCo(Me_6[14]4,11\text{-}dieneN_4)^{2+}$ 90

Activation parameters (ΔH, ΔS) 95

Rate constant of the reaction of Me· with $MeCo(Me_6[14]4,11\text{-}dieneN_4)^{2+}$ 97

Reaction of $RCoL^{2+}$ with Cr^{2+} 100

DISCUSSION 105

Preparation of the organocobalt compexes 105

Crystal structure of $CH_2ClCo(Me_6[14]4,11\text{-}dieneN_4)^{2+}$ 109

Isomerization of $RCo(Me_6[14]4,11\text{-}dieneN_4)^{2+}$ 113

Homolysis 114

Reaction of radical(R°) with $RCoL^{2+}$ complexes 119

Reaction of $RCoL^{2+}$ with Cr^{2+} 121

Summary 122

BIBLIOGRAPHY 123

APPENDIX 128

GENERAL SUMMARY 143

ACKNOWLEDGMENTS 144

LIST OF TABLES

Table I-1. Rate constants for the quenching of $^*Cr(bpy)_3^{3+}$ by d^6 metallocene 13

Table I-2. Rate constants for the quenching of $^*Cr(bpy)_3^{3+}$ by ferrocenium ions 16

Table I-3. Rate constants for the reduction of ferrocenium ions by $Cr(bpy)_3^{2+}$ 19

Table I-4. Yield of $Cr(bpy)_3^{2+}$ for the quenching of $^*Cr(bpy)_3^{3+}$ with d^6 metallocenes 20

Table I-5. Summary of electrochemical and experimental kinetic data for the reaction of $^*Cr(bpy)_3^{3+}$ with d^6 metallocenes 22

Table I-6. Summary of electronic and kinetic data for the reaction of $^*Cr(bpy)_3^{3+}$ with ferricenium ions ($Fe(C_5H_4R)(C_5H_4R')$) 28

Table I-7. Summary of electrochemical and kinetic data for the reaction of $Cr(bpy)_3^{2+}$ with ferricenium ions ($Fe(C_5H_4R)(C_5H_4R')$) 31

Table A-1. Kinetic data of the reaction of $Fe(Cp)_2$ with $^*Cr(bpy)_3^{3+}$
Conditions: $[Cr(bpy)_3^{3+}] = 1.0 \times 10^{-5}$ M
$\lambda = 727$ nm, $\mu = 0.05$ M
T = 25 °C, in 70% CH_3CN/H_2O 36

Table A-2. Kinetic data for the reaction of $Fe(Cp)(C_5H_4\text{-}nBu)$ with $^*Cr(bpy)_3^{3+}$
Conditions: $[Cr(bpy)_3^{3+}] = 1.13 \times 10^{-5}$ M
$\lambda = 727$ nm, $\mu = 0.05$ M
T = 25 °C, in 70% CH_3CN/H_2O 37

Table A-3. Kinetic data for the reaction of $Fe(C_5H_4CH_3)_2$ with $^*Cr(bpy)_3^{3+}$
Conditions: $[Cr(bpy)_3^{3+}] = 1.1 \times 10^{-5}$ M
$\lambda = 727$ nm, $\mu = 0.05$ M
T = 25 °C, in 70% CH_3CN/H_2O 38

Table A-4. Kinetic data for the reaction of $Fe(Cp)(C_5H_4CHO)$ with $^*Cr(bpy)_3^{3+}$
Conditions: $[Cr(bpy)_3^{3+}] = 1.1 \times 10^{-5}$ M
$\lambda = 727$ nm, $\mu = 0.05$ M
T = 25 °C, in 70% CH_3CN/H_2O 39

Table A-5. Kinetic data of the reaction of

$Fe(Cp)(C_5H_4CH_2OH)$ with $^*Cr(bpy)_3^{3+}$
Conditions: $[Cr(bpy)_3^{3+}] = 5 \times 10^{-5}$ M
$\lambda = 727$ nm, $\mu = 0.05$ M
T = 25 °C, in 70% CH_3CN/H_2O 40

Table A-6. Kinetic data for the reaction of
$Fe(Cp)(C_5H_4COOH)$ with $^*Cr(bpy)_3^{3+}$
Condition: $[Cr(bpy)_3^{3+}] = 1 \times 10^{-5}$ M
$\lambda = 727$ nm, $\mu = 0.05$ M
T = 25 °C, in 70% CH_3CN/H_2O 41

Table A-7. Kinetic data for the reaction of
$Fe(C_5H_4COOH)_2$ with $^*Cr(bpy)_3^{3+}$
Conditions: $[Cr(bpy)_3^{3+}] = 5.7 \times 10^{-6}$ M
$\lambda = 727$ nm, $\mu = 0.05$ M
T = 25 °C, in 70% CH_3CN/H_2O 42

Table A-8. Kinetic data for the reaction of
$Fe(Cp)(C_5H_4CH_2NMe_2)$ with $^*Cr(bpy)_3^{3+}$
Conditions: $[Cr(bpy)_3^{3+}] = 1.1 \times 10^{-5}$ M
$\lambda = 727$ nm, $\mu = 0.05$ M
T = 25 °C, in 70% CH_3CN/H_2O 43

Table A-9. Kinetic data for the reaction of $Ru(Cp)_2$
with $^*Cr(bpy)_3^{3+}$

Conditions: $[Cr(bpy)_3^{3+}] = 1.1 \times 10^{-5}$ M
$\lambda = 727$ nm, $\mu = 0.05$ M
T = 25 °C, in 70% CH_3CN/H_2O 44

Table A-10. Kinetic data for the reaction of $Os(Cp)_2$ with $^*Cr(bpy)_3^{3+}$
Conditions: $\lambda = 727$ nm, $\mu = 0.05$ M
T = 25 °C, in 70% CH_3CN/H_2O 45

Table A-11. Kinetic data for the reaction of $Fe(Cp)_2PF_6$ with $^*Cr(bpy)_3^{3+}$
Conditions: $[Cr(bpy)_3^{3+}] = 3.77 \times 10^{-4}$ M
$\lambda = 727$ nm, $\mu = 0.05$ M ($HClO_4$)
T = 25 °C, in 70% CH_3CN/H_2O 46

Table A-12. Kinetic data for the reaction of $Fe(Cp)(C_5H_4\text{-}nBu)PF_6$ with $^*Cr(bpy)_3^{3+}$
Conditions: $[Cr(bpy)_3^{3+}] = 5 \times 10^{-5}$ M
$\lambda = 727$ nm, $\mu = 0.05$ M
T = 25 °C, in 70% CH_3CN/H_2O 47

Table A-13. Kinetic data for the reaction of $Fe(Cp)(C_5H_4CH_2NMe_2)PF_6$ with $^*Cr(bpy)_3^{3+}$
Conditions: $[Cr(bpy)_3^{3+}] = 5.0 \times 10^{-5}$ M
$\lambda = 727$ nm, $\mu = 0.05$ M

T = 25 °C, in 70% CH_3CN/H_2O 48

Table A-14. Kinetic data for the reaction of $Fe(Cp)(C_5H_4CH_2OH)PF_6$ with $*Cr(bpy)_3^{3+}$
Conditions: $[Cr(bpy)_3^{3+}] = 5 \times 10^{-5}$ M
λ = 727 nm, μ = 0.05 M
T = 25 °C, in 70% CH_3CN/H_2O 49

Table A-15. Kinetic data for the reaction of $Fe(C_5H_4CH_3)_2PF_6$ with $*Cr(bpy)_3^{3+}$
Conditions: $[Cr(bpy)_3^{3+}] = 5 \times 10^{-5}$ M
λ = 727 nm, μ = 0.05 M
T = 25 °C, in 70% CH_3CN/H_2O 50

Table A-16. Kinetic data for the reaction of $Fe(C_5H_4\text{-}nBu)_2PF_6$ with $*Cr(bpy)_3^{3+}$
Conditions: $[Cr(bpy)_3^{3+}] = 3.7 \times 10^{-4}$ M
λ = 727 nm, μ = 0.05 M
T = 25 °C, in 70% CH_3CN/H_2O 51

Table A-17. Kinetic data for the reaction of $Fe(Cp^*)_2PF_6$ with $*Cr(bpy)_3^{3+}$
Conditions: $[Cr(bpy)_3^{3+}] = 5 \times 10^{-5}$ M
λ = 727 nm, μ = 0.05 M
T = 25 °C, in 70% CH_3CN/H_2O 52

Table A-18. Kinetic data for the reaction of $Fe(C_5H_4COOH)_2^+$ with $Cr(bpy)_3^{2+}$
Conditions: λ = 560 nm, μ = 0.05 M
T = 25 °C, in 70% CH_3CN/H_2O 53

Table A-19. Kinetic data for the reaction of $Fe(Cp)(C_5H_4CHO)^+$ with $Cr(bpy)_3^{2+}$
Conditions: λ = 560 nm, μ = 0.05 M
T = 25 °C, in 70% CH_3CN/H_2O 54

Table A-20. Kinetic data for the reaction of $Fe(Cp)(C_5H_4COOH)^+$ with $Cr(bpy)_3^{2+}$
Conditions: λ = 560 nm, μ = 0.05 M
T = 25 °C, in 70% CH_3CN/H_2O 55

Table A-21. Kinetic data for the reaction of $Fe(Cp)(C_5H_4CH_2OH)^+$ with $^*Cr(bpy)_3^{2+}$
Conditions: λ = 560 nm, μ = 0.05 M
T = 25 °C, in 70% CH_3CN/H_2O 56

Table A-22. Kinetic data for the reaction of $Fe(Cp)(C_5H_4\text{-}nBu)^+$ with $Cr(bpy)_3^{2+}$
Conditions: λ = 560 nm, μ = 0.05 M
T = 25 °C, in 70% CH_3CN/H_2O 57

Table A-23. Kinetic data for the reaction of $Fe(C_5H_4CH_3)_2^+$ with $Cr(bpy)_3^{2+}$
Conditions: λ = 560 nm, μ = 0.05 M
T = 25 °C, in 70% CH_3CN/H_2O 58

Table A-24. Kinetic data for the reaction of $Fe(Cp)(C_5H_4CH_2NMe_2)^+$ with $Cr(bpy)_3^{2+}$
Conditions: λ = 727 nm, μ = 0.05 M
T = 25 °C, in 70% CH_3CN/H_2O 59

Table A-25. Kinetic data for the reaction of $Fe(Cp)_2^+$ with $Cr(bpy)_3^{2+}$
Conditions: $[Cr(bpy)_3^{3+}] = 3.77 \times 10^{-4}$ M
λ = 560 nm, μ = 0.01 M
T = 25 °C, in 70% CH_3CN/H_2O 60

Table A-26. Kinetic data for the reaction of $Fe(Cp^*)_2PF_6$ with $^*Cr(4,4'\text{-}Me_2bpy)_3^{3+}$
Conditions: $[Cr(4,4'\text{-}Me_2bpy)_3^{3+}]$
$= 2.0 \times 10^{-5}$ M
λ = 727 nm, μ = 0.05 M (HCl)
T = 25 °C, in 70% CH_3CN/H_2O 61

Table A-27. Kinetic data for the reaction of $Fe(Cp^*)_2PF_6$ with $^*Cr(5\text{-}Clphen)_3^{3+}$

Conditions: $[Cr(5\text{-}Clphen)_3^{3+}]$
= 2.0×10^{-5} M
λ = 727 nm, μ = 0.05 M (HCl)
T = 25 °C, in 70% CH_3CN/H_2O 62

Table II-1. UV-Visible spectra data for the $RCoL^{2+}$ 77

Table II-2. ^1H NMR spectra data for the $RCoL^{2+}$ 78

Table II-3. Crystallographic data for $CoC_{17}H_{36}Cl_3N_4O_9$ 81

Table II-4. Calculated bond distances for $CH_2ClCo(Me_6[14]4,11\text{-}dieneN_4)(H_2O)(ClO_4)_2$ 82

Table II-5. Bond angles in $CH_2ClCo(Me_6[14]4,11\text{-}dieneN_4)(H_2O)(ClO_4)_2$ 83

Table II-6. Atomic coordinates for $CH_2ClCo(Me_6[14]4,11\text{-}dieneN_4)(H_2O)(ClO_4)_2$ 85

Table II-7. Torsion angles in $CH_2ClCo(Me_6[14]4,11\text{-}dieneN_4)(H_2O)^{2+}$ 87

Table II-8. Kinetic result and product analysis from the decomposition of $EtCo(Me_6[14]4,11\text{-}$

dieneN$_4$)$^{2+}$ with the presence of scavengers[a] 96

Table II-9. Activation parameters of unimolecular homolysis and D_{Co-C} of alkylcobalt complexes, $RCoL^{n+}$ 98

Table II-10. Summary of kinetic result for the reaction of $RCoL^{2+}$ with Cr^{2+} 104

Table II-11. Comparison of axial bond lengths in macrocyclic cobalt(III) complexes 110

Table II-12. Least-Squares plane[a] 111

Table II-13. Kinetic data and activation parameters of unimolecular homolysis for alkylcobalt complexes, $RCoL^{n+}$ 118

Table A-1. Kinetic data for the reaction of Cr^{2+} with $EtCo(Me_6[14]4,11\text{-dieneN}_4)^{2+}$
Conditions: λ = 480 nm, μ = 0.14 M
T = 25.0 ± 0.1 °C 128

Table A-2. Kinetic data for the reaction of $Co(NH_3)_5Br^{2+}$ with $EtCo(Me_6[14]4,11\text{-dieneN}_4)^{2+}$

Conditions: λ = 480 nm, μ = 0.5 M
T = 25.0 ± 0.1 °C 128

Table A-3. Homolysis Rate constants of $EtCo(Me_6[14]4,11\text{-}dieneN_4)^{2+}$ in different temperatures 129

Table A-4. Homolysis rate constants for $n\text{-}PrCo(Me_6[14]4,11\text{-}dieneN_4)^{2+}$ in different temperatures 130

Table A-5. Homolysis rate constants for $EtCo(Me_6[14]aneN_4)^{2+}$ in different temperatures 131

Table A-6. Homolysis Rate constants for $n\text{-}PrCo(Me_6[14]aneN_4)^{2+}$ in different temperatures 132

Table A-7. Kinetic result of the reaction of Me· with $MeCo(Me_6[14]4,11\text{-}dieneN_4)^{2+}$ 133

Table A-8. Kinetic data for the reaction of Cr^{2+} with $MeCo(Me_6[14]4,11\text{-}dieneN_4)^{2+}$
Conditions: λ = 470 nm, μ = 1.0M

T = 25.0 ± 0.1 °C 134

Table A-9. Kinetic data for the reaction of Cr^{2+} with $EtCo(Me_6[14]4,11\text{-}dieneN_4)^{2+}$
Conditions: λ = 480 nm, μ = 1.0 M
T = 25 .0 ± 0.1 °C 135

Table A-10. Kinetic data for the reaction of Cr^{2+} with $n\text{-}PrCo(Me_6[14]4,11\text{-}dieneN_4)^{2+}$
Conditions: λ = 480 nm, μ = 1.0 M
T = 25.0 ± 0.1 °C 136

Table A-11. Kinetic data for the reaction of Cr^{2+} with $MeCo(Me_6[14]aneN_4)^{2+}$
Conditions: λ = 480 nm, μ = 1.0 M
T = 25.0 ± 0.1 °C 137

Table A-12. Kinetic data for the reaction of Cr^{2+} with $EtCo(Me_6[14]aneN_4)^{2+}$
Conditions: λ = 390 nm, μ = 1.0 M
T = 25.0 ± 0.1 °C 138

LIST OF FIGURES

Figure I-1. Quenching of the emission from $^*Cr(bpy)_3^{3+}$ by various metallocenes following a linear relation of k_{obs} vs $[M(Cp)_2]$. Kinetic data were obtained in 70:30 CH_3CN/H_2O at 25 °C. In order of decreasing rate constant, data are shown for $Fe(C_5H_5)_2$, $Fe(C_5H_5)(C_5H_4CH_2OH)$, $Ru(C_5H_5)_2$, and $Fe(C_5H_5)(C_5H_4CH_2NMe_2)$ 12

Figure I-2. Quenching of the emission from $^*Cr(bpy)_3^{3+}$ by various metallocenes following a linear relation of k_{obs} vs $[M(Cp)_2^+]$. Kinetic data were obtained in 70:30 CH_3CN/H_2O at 25 °C. In order of decreasing rate constant, data are shown for $Fe(C_5H_5)^+$, $Fe(C_5H_5)(C_5H_4NMe_2)^+$, $Fe(C_5H_4CH_3)_2^+$, and $Fe(C_5H_4\text{-}nBu)_2^+$ 15

Figure I-3. Plot of $-\ln(k_q/k_q')_{corr}$ versus the donor acceptor distance. The ferrocenium ions are numbered in order of their appearance in Table I-6 29

Figure II-1. Structures of Me_6[14]4,11-dieneN$_4$ and C-meso-Me_6[14]aneN$_4$ 66

Figure II-2. The ORTEP of $CH_2ClCo(Me_6[14]4,11\text{-}dieneN_4)(H_2O)^{2+}$ 79

Figure II-3. The stereoview of $CH_2ClCo(Me_6[14]4,11\text{-}dieneN_4)(H_2O)^{2+}$ 80

Figure II-4a. ^1H NMR spectrum of $MeCo(Me_6[14]4,11\text{-}dieneN_4)^{2+}$ in D_2O, t = 20 min 91

Figure II-4b. ^1H NMR spectrum of $MeCo(Me_6[14]4,11\ dieneN_4)^{2+}$ in D_2O, t = 45 min 92

Figure II-4c. ^1H NMR spectrum oh $MeCo(Me_6[14]4,11\ dieneN_4)^{2+}$ in D_2O, t = 86 min 93

Figure II-4d. ^1H NMR spectrum of $MeCo(Me_6[14]4,11\ dieneN_4)^{2+}$ in D_2O, t = 775 min 94

Figure II-5. The dependence of k_{corr} on $[CH_3Co(Me_6\text{-}[14]4,11\text{-}dieneN_4)^{2+}]$ for the reaction of $\cdot CH_3$ with $MeCo(Me_6[14]4,11\text{-}dieneN_4)^{2+}$ 101

Figure II-6. The dependence of k_{obs} on $[Cr^{2+}]$ for the reaction of $MeCoL^{2+}$ with Cr^{2+}. The upper line is for $MeCo(Me_6[14]aneN_4)^{2+}$. The lower line is for $MeCo(Me_6[14]4,11\text{-}dieneN_4)^{2+}$ 103

Figure A-1. The plot of Eyring equation for the homolysis of $EtCo(Me_6[14]4,11\text{-}dieneN_4)^{2+}$ 139

Figure A-2. The plot of Eyring equation for the homolysis of $n\text{-}PrCo(Me_6[14]4,11\text{-}dieneN_4)^{2+}$ 140

Figure A-3. The plot of Eyring equation for the homolysis of $EtCo(Me_6[14]aneN_4)^{2+}$ 141

Figure A-4. The plot of Eyring equation for the homolysis of $n\text{-}PrCo(Me_6[14]aneN_4)^{2+}$ 142

GENERAL INTRODUCTION

Chapter I describes the kinetics of the quenching of $^*Cr(bpy)_3^{3+}$ by d^6 metallocenes and by ferrocenium ions. The $Cr(bpy)_2^{2+}$ and the ferroceniums, formed by electron transfer quenching of $^*Cr(bpy)_3^{3+}$ with ferrocenes, undergo rapid back electron transfer reaction.

Chapter II describes the preparation and characterization of a series of organocobalt complexes, $RCo(Me_6[14]4,11\text{-}dieneN_4)^{2+}$ and $RCo(Me_6[14]aneN_4)^{2+}$(R = primary and substituted primary alkyl group). The unimolecular homolyses have been studied for some of these complexes. The kinetics and mechanism for the reaction of $RCoL^{2+}$(L = $Me_6[14]4,11\text{-}dieneN_4$ and $Me_6[14]aneN_4$) with Cr^{2+} are also discussed.

CHAPTER I. REACTIONS OF FERROCENES AND FERROCENIUM IONS WITH GROUND AND EXCITED STATES OF TRIS(2,2'-BIPYRIDINE)CHROMIUM IONS

INTRODUCTION

Quenching of an electronically excited state by energy[1]- or electron-transfer[2,3] processes is a subject of great theoretical and practical interest. In the last few years, the photochemistry of tris(2,2'-bipyridine)chromium(III) ion and the reactivity of the excited state, $^*Cr(bpy)_3^{3+}$, have received much attention. The long life time of $^*Cr(bpy)_3^{3+}$ (~70 μs in 1 M HCl)[4] provides an excellent opportunity for studying the quenching process. The $^*Cr(bpy)_3^{3+}$ is a very active transition metal complex in photochemistry owing to its high reduction potential[5,6] as well as the well-known activity for energy-transfer[7-9] quenching. Furthermore, if

$$^*Cr(bpy)_3^{3+} + e^- \longrightarrow Cr(bpy)_3^{2+} \qquad E^\circ = 1.44\ V \qquad (1)$$

$$^*Cr(bpy)_3^{3+} \longrightarrow Cr(bpy)_3^{3+} \qquad E_{0-0} = 1.70\ eV \qquad (2)$$

the excited state undergoes an electron transfer reaction, $Cr(bpy)_3^{2+}$ will be formed; it is a good reducing agent with a high self-exchange rate constant[10]. Therefore, a return electron transfer reaction should be observed after quenching process. This makes the system more interesting.

$$^*Cr(bpy)_3^{3+} + Q \longrightarrow Cr(bpy)_3^{2+} + Q^+ \qquad (3)$$

$$Cr(bpy)_3^{2+} + Q^+ \longrightarrow Cr(bpy)_3^{3+} + Q \qquad (4)$$

Since its discovery in 1951[11,12], ferrocene has played an important role in organometallic chemistry. Numerous investigations have been developed, both theoretically and experimentally, on understanding of the electronic structures[13-15] of organometallic compounds. The quenching ability of ferrocene has also created a considerable amount of interest in photochemistry. It is well-known that ferrocene is an excellent energy transfer quencher for many triplets of organic compounds[16-18]. Meanwhile, a series of related ferrocenes with different potentials provides a great scope to study Marcus theory for electron transfer reaction[19-20].

The purpose of the research described here was to investigate i) the quenching efficiency of certain d^6 metallocenes and the mechanism of those reactions, ii) the quenching efficiency of certain ferrocenium ions and to establish the relation between these rate constants and the size of these ions, iii) the reactivities of certain ferrocenium ions with $Cr(bpy)_3^{2+}$ and to establish the relation between these rate constants and reduction potentials. The set of these reactions are shown in Scheme I. The use of

Scheme I.

$$Cr(bpy)_3^{3+} + h\nu \longrightarrow {}^*Cr(bpy)_3^{3+} \quad (5)$$

$${}^*Cr(bpy)_3^{3+} + M(Cp)_2 \longrightarrow Cr(bpy)_3^{2+} + M(Cp)_2^{+} \quad (6)$$

$${}^*Cr(bpy)_3^{3+} + M(Cp)_2 \longrightarrow Cr(bpy)_3^{3+} + {}^*M(Cp)_2 \quad (7)$$

$${}^*Cr(bpy)_3^{3+} + Fe(Cp)_2^{+} \longrightarrow Cr(bpy)_3^{3+} + {}^*Fe(Cp)_2^{+} \quad (8)$$

$$Cr(bpy)_3^{2+} + Fe(Cp)_2^{+} \longrightarrow Cr(bpy)_3^{3+} + Fe(Cp)_2 \quad (9)$$

laser flash photolysis permits the monitoring of these reactions on a microsecond time scale and also provides a simple method to prepare the $Cr(bpy)_3^{2+}$ reagent.

EXPERIMENTAL

Reagents

Metallocene derivatives All the compounds used in this study were previously known and commercially available. 1,1'-Dimethylferrocene ($Fe(C_5H_4CH_3)_2$), was recrystallized from water-ethanol (1:1, v/v). Hydroxymethylferrocene ($Fe(Cp)(C_5H_4CH_2OH)$) was recrystallized from Skelly B. Ferrocene carboxaldehyde ($Fe(Cp)(C_5H_4CHO)$) was purified by vacuum sublimation. All the others were used without further purification.

Ferrocenium salts The ferrocenes were converted to the respective ferrocenium hexafluorophosphate salts by the method of Yang et al.[21] 0.5 g Ferrocene was dissolved in 10 ml concentrated sulfuric acid in which oxidation occurred during a 15-60 minutes period, then the solution was poured into 150 ml of water. The dilute solution was filtered to remove sulfur, etc., and an aqueous solution of KPF_6 was added. The resulting precipitate was filtered, washed several times with ether and dried under vacuum.

Hydroxymethylferrocenium hexafluorophosphate was synthesized by reacting the ferrocene with excess iron(III).[19] This was done by dissolving the ferrocene in petroleum ether and an acidic aqueous solution of ferric nitrate containing a

twofold stoichiometric excess of iron(III) was added. The solution was stirred strongly until the yellow color of the ferrocene was no longer evident in the organic layer. The aqueous layer, containing the ferrocenium ion, was then treated with a saturated solution of potassium hexafluorophosphate. The precipitated ferrocenium salt was then washed with ether and dried under vacuum.

Chromium complexes ($CrL_3(ClO_4)_3$) The polypyridinechromium(III) complexes were prepared[10,22] by adding under argon a 1M perchloric acid solution of chromium(II) to a slurry of a twofold stoichiometric excess of the ligand in water. The resultant green mixture was stirred for 1 hour. Saturated bromine water was then added (the precipitate turned yellow) and the mixture was filtered. The solid was dissolved in water, the pH was adjusted to ~ 6, and the solution was extracted with chloroform until the chloroform was free of ligand. Sodium perchlorate saturated solution was added to give the perchlorate salt which was separated and washed with water and ether.

Methods

Analysis The identity and purity of the metallocenes were established by NMR and UV-visible spectrophotometry. The NMR spectrum of each compound was in agreement with the assumed identity. All of the solutions of the metallocenes

were characterized with UV-visible spectroscopy and showed values consistent with literature data. The concentrations of solutions of these complexes were most easily determined by the intensity of their absorption spectrum. Concentrations were determined spectrophotometrically using the following absorption maxima[20,23]: $Fe(Cp)_2$, λ440 nm, ε = 96 $M^{-1}cm^{-1}$; $Fe(C_5H_4CH_3)_2$, λ435 nm, ε = 104 $M^{-1}cm^{-1}$; $Fe(Cp)(C_5H_4$-nBu), λ450 nm, ε = 100 $M^{-1}cm^{-1}$; $Fe(Cp)(C_5H_4CH_2OH)$, λ435 nm, ε = 100 $M^{-1}cm^{-1}$; $Fe(Cp)(C_5H_4CH_2NMe_2)$, λ435 nm, ε = 102 $M^{-1}cm^{-1}$; $Fe(Cp)(C_5H_4COOH)$, λ440 nm, ε = 267 $M^{-1}cm^{-1}$; $Fe(Cp)(C_5H_4CHO)$, λ 460nm, ε = 765 $M^{-1}cm^{-1}$; $Fe(C_5H_4COOH)_2$, λ450 nm, ε = 282 M^{-1} cm^{-1}; $Ru(Cp)_2$, λ277 nm, ε = 195 $M^{-1}cm^{-1}$; $Os(Cp)_2$, λ245 nm, ε = 2630 $M^{-1}cm^{-1}$.

The identity and purity of the ferrocenium salts were also established by UV-visible spectrophotometry in comparison with literature values. Concentrations were determined spectrophotometrically using following absorption maxima[19,24]: $Fe(Cp)_2^+$, λ617 nm, ε = 410 $M^{-1}cm^{-1}$; $Fe(C_5H_4CH_3)_2^+$, λ650 nm, ε = 332 $M^{-1}cm^{-1}$; $Fe(Cp)(C_5H_4$-nBu$)^+$, λ625 nm, ε = 352 $M^{-1}cm^{-1}$; $Fe(C_5H_4$-nBu$)_2^+$, λ650 nm, ε = 380 $M^{-1}cm^{-1}$; $Fe(Cp)(C_5H_4CH_2OH)^+$, λ627 nm, ε = 400 $M^{-1}cm^{-1}$; $Fe(Cp)(C_5H_4CH_2NMe_2)$, λ627 nm, ε = 198 $M^{-1}cm^{-1}$; $Fe(C_5Me_5)_2^+$, λ778 nm, ε = 394 $M^{-1}cm^{-1}$.

Kinetics Kinetic runs were carried out using laser flash photolysis. The laser system used has been described by Connolly[25] and is based on another system in the literature[26].

In a typical kinetic run, the deaerated sample solution was prepared in a square one centimeter quartz cell. The solution was then flashed by a 0.6 μs laser pulse from a Phase-R model DL-1100 pulsed dye laser. At right angles to the laser beam was a monitoring beam, provided by a 50 W quartz-halogen lamp, which passed through the cell. The light transmitted through the cell then passed through an Instruments SA grating monochromator, and was detected by a Hamamatsu R928 photomultiplier tube. The signal from the photomultiplier tube was collected and stored on a Nicolet model 2090-3A digitizing oscilloscope. The Nicolet oscilloscope was interfaced with an Apple II Plus microcomputer which converted the voltage vs time data from the oscilloscope to absorbance vs time data (voltages being proportional to transmittance).

RESULTS

Quenching of $^*Cr(bpy)_3^{3+}$ by d^6 metallocenes

The kinetics of the reaction of d^6 metallocenes with $^*Cr(bpy)_3^{3+}$ were studied by using the flash-photolysis method. The general photochemical sequence for the production and the reaction of the excited state of tris(2,2'-bipyridine)chromium (III) ion is represented in Equation (5), (6) and (7).

$$Cr(bpy)_3^{3+} + h\nu \longrightarrow {}^*Cr(bpy)_3^{3+} \qquad (5)$$

$$^*Cr(bpy)_3^{3+} + M(Cp)_2 \begin{cases} \longrightarrow Cr(bpy)_3^{2+} + M(Cp)_2^{+} & (6) \\ \longrightarrow Cr(bpy)_3^{3+} + {}^*M(Cp)_2 & (7) \end{cases}$$

The excited state of the $Cr(bpy)_3^{3+}$ ion is produced by irradiating the absorption band at 420-460 nm. This can be quenched by the appropriate metallocene in the solution. Quenching rate constants in 70% CH_3CN/H_2O were obtained by monitoring at λ727 nm.

All the reactions of metallocenes with $Cr(bpy)_3^{3+}$ were studied kinetically under pseudo-first-order conditions with metallocene in excess. The rate constants for the reactions

were obtained from an analysis of the emission at 727 nm vs. time data. The pseudo-first-order rate constants are listed in Table A-1 to A-10 for all d^6 metallocenes. Plots of k_{obs} vs. [metallocene], Fig. I-1, are linear in all the cases, showing the first order dependence of the rate on metallocene concentration. Thus the reaction between the $^*Cr(bpy)_3^{3+}$ and metallocene follow the second-order rate law shown in equation 10. Table I-1 gives the second-order rate constants for the reaction of $^*Cr(bpy)_3^{3+}$ with all the d^6 metallocene complexes.

$$-d[^*Cr(bpy)_3^{3+}]/dt = (k_o + k_q\,[M(Cp)_2])\,[^*Cr(bpy)_3^{3+}] \qquad (10)$$

$$k_{obs} = k_o + k_q\,[M(Cp)_2] \qquad (11)$$

Quenching of $^*Cr(bpy)_3^{3+}$ by ferrocenium ions

The kinetics of the reaction of ferrocenium ions with $^*Cr(bpy)_3^{3+}$ were studied by laser flash-photolysis. Quenching rate constants were obtained by monitoring at λ727 nm under pseudo-first-order kinetic conditions in 70% CH_3CN/H_2O. The pseudo-first-order rate constants are listed in Table A-11 to A-17. Plots of k_{obs} vs. [ferrocenium ion], Fig. I-2, are linear in all the cases, showing the first order dependence of the rate on ferrocenium ion concentration. Thus the rate law of the reaction between $^*Cr(bpy)_3^{3+}$ and ferrocenium ions is shown in equation 12. Table I-2 gives the second order rate

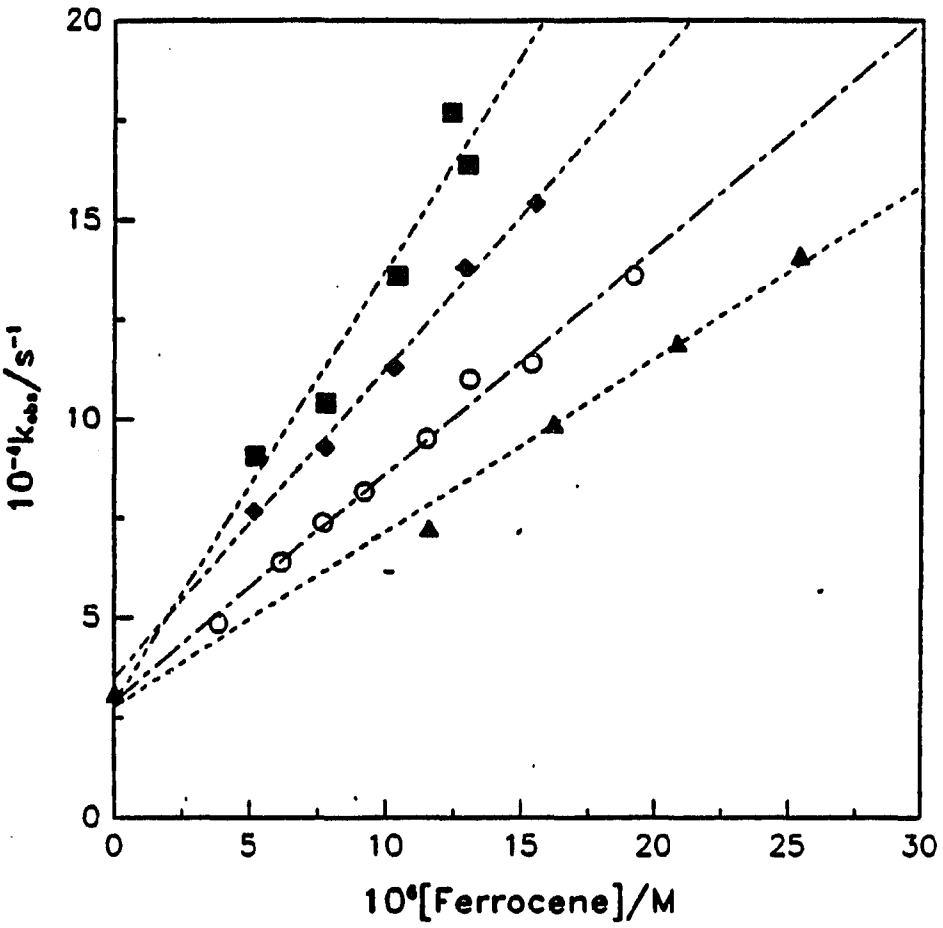

Figure I-1. Quenching of the emission from $^*Cr(bpy)_3^{3+}$ by various metallocenes following a linear relation of k_{obs} vs $[M(Cp)_2]$. Kinetic data were obtained in 70:30 CH_3CN/H_2O at 25 °C. In order of decreasing rate constant, data are shown for $Fe(C_5H_5)_2$, $Fe(C_5H_5)(C_5H_4CH_2OH)$, $Ru(C_5H_5)_2$, and $Fe(C_5H_5)(C_5H_4CH_2NMe_2)$

Table I-1. Rate constants for the quenching of $^*Cr(bpy)_3^{3+}$ by d^6 metallocene

metallocene	10^6[metallocene]/M	$10^{-9}k/M^{-1}s^{-1}$ [a]
$Fe(Cp)_2$	5.19 - 24.8	10.3 ± 0.3
$Fe(Cp)(C_5H_4$-nBu)	4.20 - 12.6	10.0 ± 0.2
$Fe(C_5H_4CH_3)_2$	2.84 - 11.4	9.6 ± 0.2
$Fe(Cp)(C_5H_4CHO)$	4.90 - 21.2	8.3 ± 0.2
$Fe(Cp)(C_5H_4CH_2OH)$	5.17 - 15.5	8.1 ± 0.1
$Fe(Cp)(C_5H_4COOH)$	6.20 - 25.0	7.1 ± 0.3
$Fe(C_5H_4COOH)_2$	3.02 - 15.1	6.2 ± 0.1
$Fe(Cp)(C_5H_4CH_2NMe_2)$	11.6 - 43.9	4.5 ± 0.1
$Ru(Cp)_2$	3.85 - 19.2	5.9 ± 0.1[b]
$Os(Cp)_2$	3.02 - 15.1	9.3 ± 0.2

[a] At 25 °C, in 70% CH_3CN and μ = 0.05 M ($LiClO_4$), except as noted.

[b] μ = 0.05 M (HCl).

constants for the reaction of $^*Cr(bpy)_3^{3+}$ with all the ferrocenium ions.

$$-d[^*Cr(bpy)_3^{3+}]/dt = (k_o + k_q[Fe(Cp)_2^+])\ [^*Cr(bpy)_3^{3+}] \quad (12)$$

$$k_{obs} = k_o + k_q\ [Fe(Cp)_2^+] \quad (13)$$

These quenching processes were also examined by monitoring at λ560 nm which is the maximum of $Cr(bpy)_3^{2+}$. Continuously decreasing curves at λ560 nm were observed which indicate there was no significant amount of $Cr(bpy)_3^{2+}$ being formed in these steps. These results strongly suggest that these reactions are energy quenching processes.

Kinetic reaction of ferrocenium ions with $Cr(bpy)_3^{2+}$

Since the quenching reactions of ferrocene derivatives with $^*Cr(bpy)_3^{3+}$ are very fast ($k_q = 10^9$~10^{10} $M^{-1}s^{-1}$) and a significant amount of $Cr(bpy)_3^{2+}$ was formed in most cases, the kinetics of the reaction of $Cr(bpy)_3^{2+}$ with ferrocenium ion ($Fe(C_5H_4R)(C_5H_4R')^+$) were therefore studied by monitoring at λ560 nm. The general photochemical sequence for the production and reaction of tris(bipyridyl)chromium(2+) is represented in the following equations.

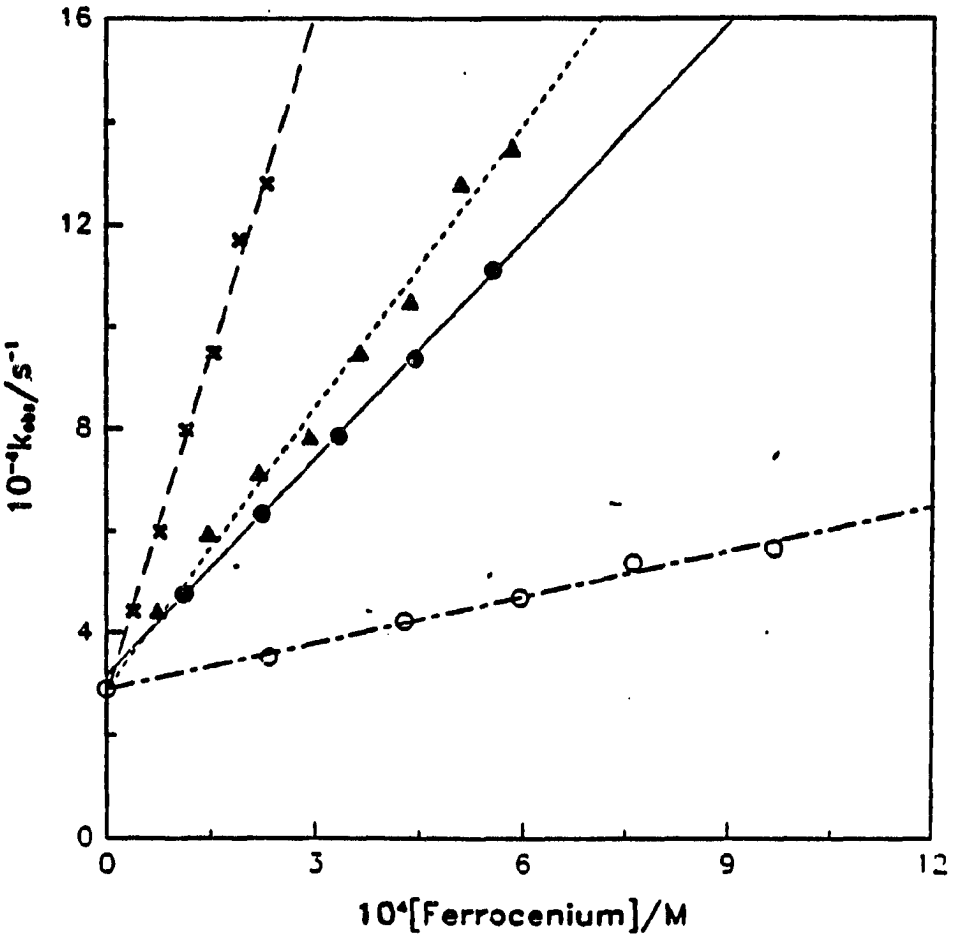

Figure I-2. Quenching of the emission from $^*Cr(bpy)_3^{3+}$ by various metallocenes following a linear relation of k_{obs} vs $[M(Cp)_2^+]$. Kinetic data were obtained in 70:30 CH_3CN/H_2O at 25 °C. In order of decreasing rate constant, data are shown for $Fe(C_5H_5)^+$, $Fe(C_5H_5)(C_5H_4NMe_2)^+$, $Fe(C_5H_4CH_3)_2^+$, and $Fe(C_5H_4\text{-}nBu)_2^+$

Table I-2. Rate constants for the quenching of $^*Cr(bpy)_3^{3+}$ by ferrocenium ions

ferrocenium ion	$10^4[Fe(C_5H_4R)(C_5H_4R')^+]/M$	$10^{-8}k/M^{-1}s^{-1}$ [a]
$Fe(Cp)_2^+$	0.38 - 2.31	4.5 ± 0.1
$Fe(Cp)(C_5H_4\text{-}nBu)^+$	1.13 - 7.80	3.2 ± 0.1
$Fe(Cp)(C_5H_4CH_2NMe_2)^+$	0.73 - 8.76	1.89 ± 0.03
$Fe(Cp)(C_5H_4CH_2OH)^+$	1.30 - 5.76	1.6 ± 0.1
$Fe(C_5H_4CH_3)_2^+$	1.11 - 5.57	1.40 ± 0.03
$Fe(C_5H_4\text{-}nBu)_2^+$	2.34 - 9.68	0.30 ± 0.01
$Fe(Cp^*)_2^+$	9.50 - 40.1	0.23 ± 0.01

[a] At 25 °C, in 70% CH_3CN and μ = 0.05 M ($HClO_4$).

$$Cr(bpy)_3^{3+} + h\nu \longrightarrow {}^*Cr(bpy)_3^{3+} \quad (5)$$

$${}^*Cr(bpy)_3^{3+} + Fe(Cp)_2 \longrightarrow Cr(bpy)_3^{2+} + Fe(Cp)_2^{+} \quad (8)$$

$$Cr(bpy)_3^{2+} + Fe(Cp)_2^{+} \longrightarrow Cr(bpy)_3^{3+} + Fe(Cp)_2 \quad (9)$$

All the reactions of $Fe(C_5H_4R)(C_5H_4R')^+$ with $Cr(bpy)_3^{2+}$ studied kinetically under second-order conditions. Table A-18 to A-25 give the second-order rate constants for each ferrocenium ion ($Fe(Cp)_2^+$). Table I-3 gives the rate constants for the reaction of $Cr(bpy)_3^{2+}$ with all the ferrocenium ions.

Yield of $Cr(bpy)_3^{2+}$ in the quenching of ${}^*Cr(bpy)_3^{3+}$ with d^6 metallocenes

The yields of $Cr(bpy)_3^{2+}$ in the quenching step of ${}^*Cr(bpy)_3^{3+}$ with d^6 metallocenes were determined for all the cases by measuring the ratio between the concentration of $Cr(bpy)_3^{2+}$ formed in the quenching step and the concentration of ${}^*Cr(bpy)_3^{3+}$ formed in the laser pulse. The reference amount of ${}^*Cr(bpy)_3^{3+}$ formed in the laser photolysis was determined by flashing a solution in the absence of metallocene and monitoring at λ445 nm. The concentration of ${}^*Cr(bpy)_3^{3+}$ could be estimated by using Beer's Law and the absorbance change at λ445 nm ($\Delta\varepsilon = -2640\ M^{-1}cm^{-1}$). The concentration of $Cr(bpy)_3^{2+}$ formed in the quenching step was

determined in a similar way. A sample solution in the presence of metallocene with the same amount of $Cr(bpy)_3^{3+}$ was flashed and monitored at λ560 nm. Therefore the concentration of $Cr(bpy)_3^{2+}$ could be estimated by using Beer's Law and the absorption change at λ560 nm. Table I-4 gives the yield of $Cr(bpy)_3^{2+}$ found in the quenching step of $^*Cr(bpy)_3^{3+}$ with all d^6 metallocenes.

Table I-3. Rate constants for the reduction of ferrocenium ions by $Cr(bpy)_3^{2+}$

Ferrocenium ion	$10^{-9}k/M^{-1}s^{-1}$ [a]
$Fe(C_5H_4COOH)_2^+$	8.9 ± 0.3
$Fe(Cp)(C_5H_4CHO)^+$	8.8 ± 0.3
$Fe(Cp)(C_5H_4COOH)^+$	6.2 ± 0.3
$Fe(Cp)(C_5H_4CH_2OH)^+$	6.0 ± 0.4
$Fe(Cp)(C_5H_4$-nBu$)^+$	5.3 ± 0.1
$Fe(C_5H_4CH_3)_2^+$	4.5 ± 0.1
$Fe(Cp)(C_5H_4CH_2NMe_2)^+$	3.6 ± 0.1
$Fe(Cp)_2^+$	3.5 ± 0.2

[a] At 25 °C, in 70% CH_3CN and μ = 0.05 M ($HClO_4$).

Table I-4. Yield of $Cr(bpy)_3^{2+}$ for the quenching of $^*Cr(bpy)_3^{3+}$ with d^6 metallocenes

metallocene	yield
$Fe(C_5H_4CH_3)_2$	61%
$Fe(Cp)(C_5H_4\text{-}nBu)$	59%
$Fe(Cp)(C_5H_4CH_2OH)$	50%
$Fe(Cp)_2$	44%
$Fe(Cp)(C_5H_4CH_2NMe_2)$	42%
$Fe(Cp)(C_5H_4CHO)$	19%
$Fe(Cp)(C_5H_4COOH)$	20%
$Fe(C_5H_4COOH)_2$	13%
$Ru(Cp)_2$	5%
$Os(Cp)_2$	7%

DISCUSSION

Quenching of $^*Cr(bpy)_3^{3+}$ by d^6 metallocenes

The quenching reactions of the metallocenes with $^*Cr(bpy)_3^{3+}$ are very fast (k_q = 0.45-1.03 x 10^{10} $M^{-1}s^{-1}$, Table I-5). Because these values are so close to the limit of diffusion control, they have been corrected by equation (14) and listed as k_{corr} in Table I-5. However, all the rate

$$1/k_{corr} = 1/k_q - 1/k_1 \qquad (14)$$

where k_1 = 1.55 x 10^{10} $M^{-1}s^{-1}$

constants listed in Table I-5 clearly suggest that d^6 metallocenes of Fe, Ru, Os are strong quenchers of $^*Cr(bpy)_3^{3+}$ The rate constants for electron transfer are given by the product of k_{corr} x f_{et}. The values (Table I-5) range from 1.4 x 10^9 to 1.7 x 10^{10} $M^{-1}s^{-1}$. Because the electron transfer rate constants are so large, no effort was made to attempt an analysis in terms of the Marcus equation.

Ohno and Kato[27] reported that the quenching rate constants for $^*Cr(bpy)_3^{3+}$ by ferrocene and ferrocene carboxylic acid are 6.2 and 7.3 x 10^9 $M^{-1}s^{-1}$ (15 °C), respectively. Those values are in good agreement with the results obtained in this work, although the yield of $Cr(bpy)_3^{2+}$ is quite low in their study (0.18 for ferrocene and

Table I-5. Summary of electrochemical and experimental kinetic data for the reaction of $^*Cr(bpy)_3^{3+}$ with d^6 metallocenes

metallocene	E°(V, NHE)	$k_q/M^{-1}s^{-1}$ [a]	$k_{corr}/M^{-1}s^{-1}$ [b]	$k_{el}/M^{-1}s^{-1}$ [c]	$k_{en}/M^{-}s^{-1}s^{-1}$	yield
$Fe(Cp)_2$	0.51	1.0×10^{10}	3.0×10^{10}	1.3×10^{9}	1.7×10^{9}	0.44
$Fe(Cp)(C_5H_4\text{-}nBu)$	0.50	1.0×10^{10}	2.8×10^{10}	1.7×10^{10}	1.1×10^{9}	0.59
$Fe(C_5H_4CH_3)_2$	0.43	9.6×10^{9}	2.5×10^{10}	1.5×10^{10}	1.0×10^{10}	0.61
$Fe(Cp)(C_5H_4CHO)$	0.55	8.3×10^{9}	1.8×10^{10}	3.4×10^{9}	1.46×10^{10}	0.19
$Fe(Cp)(C_5H_4CH_2OH)$	0.52	8.1×10^{9}	1.7×10^{10}	1.4×10^{10}	3×10^{9}	0.50
$Fe(Cp)(C_5H_4COOH)$	0.77	7.1×10^{9}	1.3×10^{10}	5.8×10^{9}	7.2×10^{9}	0.20
$Fe(C_5H_4COOH)_2$	0.98	6.2×10^{9}	1.1×10^{10}	2.5×10^{9}	8.5×10^{9}	0.13
$Fe(Cp)(C_5H_4CH_2NMe_2)$	0.55	4.5×10^{9}	6.4×10^{9}	2.7×10^{9}	3.7×10^{9}	0.42
$Ru(Cp)_2$	0.91	5.9×10^{9} [d]	9.8×10^{9}	7.8×10^{8}	9.0×10^{9}	0.05
$Os(Cp)_2$	0.85	9.3×10^{9} [d]	2.5×10^{10}	2.8×10^{9}	2.2×10^{10}	0.07

[a] At T= 25 °C and μ = 0.05 M ($HClO_4$), except as noted. In 70% CH_3CN/30% H_2O.

[b] Calculated according to equation 14.

[c] $k_{el} = k_q$ x yield.

[d] μ = 0.05 M (HCl).

0.069 for carboxylicacidferrocene). The discrepancy may arise from their use of an incorrect spectrum for the excited state.

In view of the large driving force of the electron transfer step as well as the high self-exchange rate constants for metallocene and $Cr(bpy)_3^{3+}$ redox couples, it is not unexpected to find that d^6 metallocenes can quench $^*Cr(bpy)_3^{3+}$ with a very high electron transfer rate constant. On the other hand, ferrocene and derivatives are well known as efficient quenchers of triplet states of many organic compounds. Chapple and co-workers[28] found that ferrocene can quench the triplet state of several organic compounds with a rate close to the limit of diffusion control if the triplet energy of the donor is larger than 16000 cm^{-1}. The energy quenching of electronically excited $Ru(bpy)_3^{2+}$ by d^6 metallocenes of Fe, Ru, and Os were studied by Wrighton and co-workers.[29] The quenching rate constants are in a range from 3.4 to 7.4 x 10^9 $M^{-1}s^{-1}$ for ferrocene and its derivatives but less than 10^7 for ruthenocene and acetylosmocene. Recently Ollino and Cherry[30] also studied the quenching of $^*Ru(bpy)_3^{2+}$ by ferrocene. Their results show good agreement. All of these observations are consistent with the high k_{en} found for ferrocene derivatives in this work. However, it is a little surprising to find that ruthenocene and osmocene both are efficient quenchers for $(^2E)Cr(bpy)_3^{3+}$.

The stability of ferrocenium ion may be the reason that only certain ferrocenes undergo electron transfer quenching

mechanism as the major pathway. Ferrocenium carboxylic acid was made by the oxidation of ferrocene carboxylic acid with p-quinone[31]. However, this particular compound decomposes in 70% CH_3CN. Ferrocenium carboxaldehyde couldn't be made by any method normally used for the preparation of ferrocenium salt. These experiments indicate that some ferrocenium ions are not stable which may be the reason they won't quench $(^2E)Cr(bpy)_3^{3+}$ by an electron transfer mechanism, especially since there is a competitive energy transfer pathway available.

Quenching of $^*Cr(bpy)_3^{3+}$ by ferrocenium ions

All the rate constants listed in Table I-6 indicate ferrocenium ions are good quenchers for $^*Cr(bpy)_3^{3+}$.

The second-order rate constants are 1.37 and 1.54 x 10^7 $M^{-1}s^{-1}$ for $^*Cr(4,4'\text{-}Me_2bpy)_3^{3+}$ and $^*Cr(5\text{-}Clphen)_3^{3+}$, respectively. Comparing these two values with the rate constant of $^*Cr(bpy)_3^{3+}$ with $Fe(C_5Me_5)_2^+$ (2.3 x 10^7 $M^{-1}s^{-1}$), obviously, there is no dependence on the potential[22] of $Cr^{*/2+}$ (1.25 V for 4,4'-Me_2bpy; 1.44 V for bpy and 1.53 V for 5-Clphen). These observations strongly suggest all the quenching reactions of $(^2E)Cr(bpy)_3^{3+}$ undergo energy-transfer mechanism as shown in equations (5) and (8).

$$Cr(bpy)_3^{3+} + h\nu \longrightarrow {}^*Cr(bpy)_3^{3+} \qquad (5)$$

$$^{*}Cr(bpy)_3^{3+} + Fe(Cp)_2^{+} \longrightarrow Cr(bpy)_3^{3+} + {}^{*}Fe(Cp)_2^{+} \qquad (8)$$

There are two possible pathways for energy-transfer between donors and acceptors: coulombic interactions and exchange interactions.[32]

The coulombic interaction occurs via the electromagnetic field and does not require physical contact of the interacting partners. A equation proposed by Forster[33] for coulombic interaction is shown in equation 15.

$$k_q(\text{coulombic}) = K\kappa^2 k_D^{\circ}/r_{DA}^6 \; J(\varepsilon_A) \qquad (15)$$

Where K is a constant determined by experimental conditions such as the solvent index of refraction, κ^2 is the interaction between two oscillating dipoles which depends on the orientation of the dipoles in space, r_{DA} is the donor-acceptor separation distance, and $J(\varepsilon_A)$ is the spectral overlap integral.

The exchange interaction occurs via overlap of electron clouds and requires physical contact between the interaction partners. A theory for energy transfer by electron exchange was worked out by Dexter[34] who proposed that for the rate constant of energy transfer:

$$k_q(\text{exchange}) = K\, J\exp(-2r_{DA}/L) \qquad (16)$$

where K is related to the specific orbital interactions, r_{DA} is the donor-acceptor separation, J is a spectral overlap integral normalized for the extinction coefficient of the acceptor, and L is an effective average Bohr radius for the excited and ground states of the donor and acceptor.

In this system, the individual electronic transitions are Laporte and spin forbidden, and the coulombic coupling mechanism leads to very small probabilities for energy-transfer. Furthermore, for a typical $^*Cr(bpy)_3^{3+}$-Fe^{3+} system, the critical Forster quenching radius is R_o~ 6 Å, and the rate constant for energy transfer is less than 2×10^3 s^{-1}.[35] Based on these factors, an electron exchange mechanism should be the dominant means of donor-acceptor coupling in $^*Cr(bpy)_3^{3+}$-Fe^{3+} energy transfer system. The spectral overlap integral is effectively a constant in the $^*Cr(bpy)_3^{3+}$-Fe^{3+} systems (see Table I-6).

The data in Table I-6 are in good accordance with expectation based on equation 16 as shown in Figure 3. It is convenient to use a normalized form in which one compound, $Fe(C_5H_5)_2^+$, is taken as a reference compound for the series. In that case we consider the relation given by Endicott, $(k_q/k_q')_{corr} = (k_q/k_q^{ref})\cdot(K_o^{ref}/K_o)$. The ion-pairing constants K_o were calculated according to equation 17-19 from Brown and Sutin.[36] This estimate employs a mean value of r_{DA}

$$K_o = (4\pi Nr^3/3000)\ \exp[-w_r/RT] \qquad (17)$$

$$w_r = z_1 z_2 e^2 / D_s r(1 + kr) \quad (18)$$

$$k = (8\pi N^2 e^2 \mu / 1000 D_s RT)^{1/2} \quad (19)$$

based on the geometric mean of the covalent radii along three Cartesian axes as shown in equation (20).[36]

$$r = 1/2(d_1 d_2 d_3)^{1/3} \quad (20)$$

The linear correlation in Fig. 3 results in a value of L = 0.5 Å. The simplest physical explanation of this parameter is that it equals the mean of the Cr-donor and Fe-acceptor 3d-orbital radii.

By studying the reaction of $^*Cr(bpy)_3^{3+}$ with cobalt complexes, Endicott and co-workers[37] also found that the reactivity appears to be determined by variations in the inefficient overlap of donor and acceptor orbitals. Therefore the value of k_q decreases with increasing quencher size. Recently, Endicott and co-workers[38] reported that the quenching rate of $^*Cr(bpy)_3^{3+}$ donors with a few dozen cobalt(III) complexes is dependent on the size of the quenchers. The distance dependence is compatible with expectation for energy-transfer mediated by an exchange mechanism with $(k_q/k_q')_{corr}$ proportional to $\exp(-2r_{DA}/L)$ and L = 1.8 Å.

Table I-6. Summary of electronic and kinetic data for the reaction of $^*Cr(bpy)_3^{3+}$ with ferrocenium ions ($Fe(C_5H_4R)(C_5H_4R')$)

Ferrocenium ion	$\varepsilon_{727}/M^{-1}cm^{-1}$	$10^{-8}k_q/M^{-1}s^{-1}$ [a]	r_{DA}/nm [b]	K_o/M^{-1} [c]
$Fe(Cp)_2^+$	10.3	4.4 ± 0.1	0.88	0.392
$Fe(Cp)(C_5H_4\text{-}nBu)^+$	<20	3.2 ± 0.1	0.94	0.55
$Fe(Cp)(C_5H_4CH_2NMe_2)^+$	<20	1.89 ± 0.03	0.93	0.517
$Fe(Cp)(C_5H_4CH_2OH)^+$	<20	1.62 ± 0.05	0.91	0.46
$Fe(C_5H_4CH_3)_2^+$	<20	1.40 ± 0.03	0.91	0.464
$Fe(C_5H_4\text{-}nBu)_2^+$	<20	0.30 ± 0.01	0.95	0.572
$Fe(C_5Me_5)_2^+$	242	0.23 ± 0.01	0.96	0.61

[a] At T= 25 °C and μ = 0.05 M ($HClO_4$). In 70% CH_3CN/30% H_2O.

[b] r_{Cr} = 0.68 nm.

[c] Calculated according to eq. 17-19 as in Ref 36.

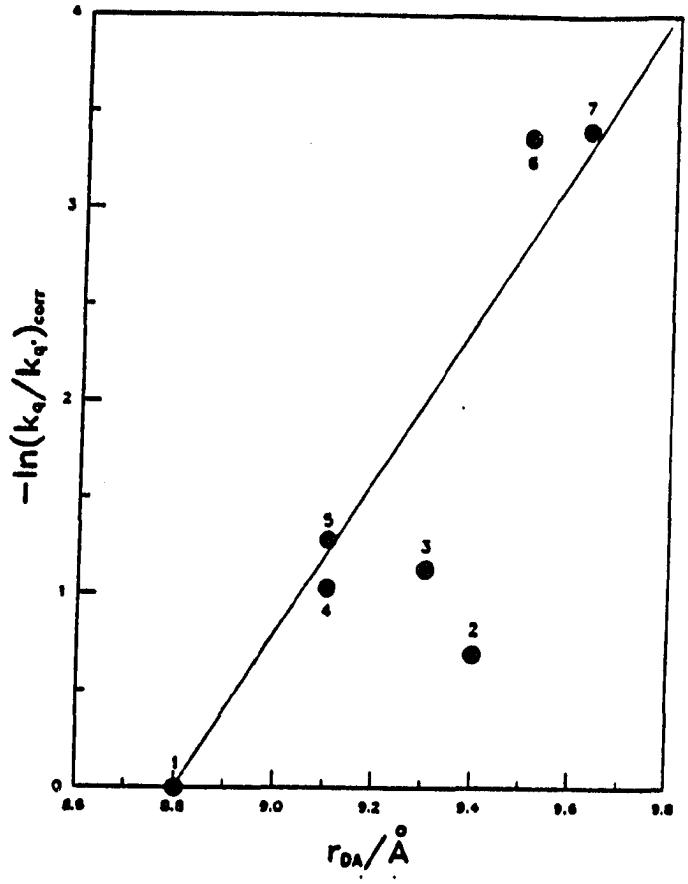

Figure I-3. Plot of $-\ln(k_q/k_q')_{corr}$ versus the donor-acceptor distance. The ferrocenium ions are numbered in order of their appearance in Table I-6

Kinetics of the reaction of $Cr(bpy)_3^{2+}$ with ferrocenium ions ($Fe(C_5H_4R)(C_5H_4R')^+$)

The kinetics of the reaction of $Cr(bpy)_3^{2+}$ with ferrocenium ion ($Fe(C_5H_4R)(C_5H_4R')^+$) suggest the rate law is first-order in both $[Cr(bpy)_3^{2+}]$ and $[Fe(C_5H_4R)(C_5H_4R')^+]$. Thus the rate law of this reaction is given as in equation (20).

$$-d[Cr(bpy)_3^{2+}]/dt = k\,[Cr(bpy)_3^{2+}]\,[Fe(C_5H_4R)(C_5H_4R')^+] \quad (20)$$

The Marcus equation has been applied in order to have a further understanding about the electron transfer mechanism of these reactions. The equations used are[39]:

$$\Delta G_{12}^* = 1/2(\Delta G_{11}^* + \Delta G_{22}^* + \Delta G_{12}^\ominus - \omega_{11} - \omega_{22} + \omega_{12} + \omega_{21}) + (\Delta G_{12}^\ominus + \omega_{21} - \omega_{12})^2/8(\Delta G_{11}^* - \omega_{11} + \Delta G_{22}^* - \omega_{22}) \quad (21)$$

$$k = Z \exp(-\Delta G^*/RT) \quad (22)$$

$$\omega_{ij} = 4.225 \times 10^{-8} z_i z_j / a(1 + 3.285 \times 10^7 a \mu^{1/2}) \quad (23)$$

Where ΔG is the change of free energy, ω the reorganization work, k the rate constant for the cross-reaction, Z a collision number, z_i the charge number of species i, and a the distance of closest approach.

Table I-7. Summary of electrochemical and kinetic data for the reaction of $Cr(bpy)_3^{2+}$ with ferrocenium ions ($Fe(C_5H_4R)(C_5H_4R')$)

ferricenium ion	E°(V, NHE)	$10^{-6}k_{ex}/M^{-1}s^{-1}$ [a] Fe^{II}/Fe^{III}	$10^9k/M^{-1}s^{-1}$ exptl.[b]	corr.	calcd.
$Fe(C_5H_4CH_3)_2^+$	0.43	8.3 ± 0.8	4.5	6.3	99
$Fe(Cp)(C_5H_4\text{-}nBu)^+$	0.50	6.5 ± 0.7	5.3	8.1	91
$Fe(Cp)(C_5H_4CH_2OH)^+$	0.52	4.2 ± 0.4	6.0	9.8	93
$Fe(Cp)_2^+$	0.51	5.7 ± 0.1	3.5	4.5	92
$Fe(Cnp)(C_5H_4CH_2NMe_2)^+$	0.55	——	3.6	4.7	——
$Fe(Cp)(C_5H_4CHO)^+$	0.55	——	8.8	20.3	——
$Fe(Cp)(C_5H_4COOH)^+$	0.77	——	6.2	10.3	——
$Fe(C_5H_4COOH)_2^+$	0.98	——	8.9	20.9	——

[a]Reference 19.

[b]At 25 °C and μ = 0.05 M ($HClO_4$)

For the following four ferrocenium ions, $Fe(C_5H_4CH_3)_2^+$, $Fe(Cp)(C_5H_4\text{-}nBu)^+$, $Fe(Cp)(C_5H_4CH_2OH)^+$, and $Fe(Cp)_2^+$, their self-exchange rate constants of +/0 couple are known as well as their reduction potentials. Application of the Marcus cross relation to the $Cr(bpy)_3^{2+}$ reaction yields a calculated rate constant as listed in Table I-7. However, these values are too high to be reliable. These results clearly suggest that these reactions are not good candidates for application of Marcus theory because of a large driving force and high value of self-exchange rate constant of the redox couples.

Summary

The kinetics of quenching of $^*Cr(bpy)_3^{3+}$ by d^6 metallocenes and by ferrocenium ions were studied by laser flash photolysis. The quenching by ferrocenium ions proceeds by energy transfer and is dependent on the donor-acceptor distance, as expected for an electron-exchange mechanism. The rate constants for quenching with d^6 metallocenes are at or near the diffusion-controlled limit. The reactions partition themselves between electron transfer and energy transfer. The $Cr(bpy)_2^{2+}$ and the ferroceniums, formed by electron transfer quenching, undergo rapid back electron transfer, $k = (3\text{-}9) \times 10^9\ M^{-1}s^{-1}$.

BIBLIOGRAPHY

1. Balzani, V.; Moggi, L.; Manfrin, M. F.; Bolletta, F.; Laurence, G. S.; Coord. Chem. Rev. 1975, 15, 321.
2. Balzani, V.; Bolletta, F,; Gandolfi, M. T.; Maestri, M. Top. Curr. Chem. 1978, 75, 1.
3. Sutin, N.; Creutz, C. Pure Appl. Chem. 1980, 52, 2717.
4. Maestri, M.; Bolletta, F.; Moggi, L.; Balzani, V.; Henry, M. S.; Hoffman, M. Z. J. Am. Chem. Soc. 1978, 100, 2694.
5. Jamieson, M. A.; Serpone, N.; Hoffman, M. Z. Coord. Chem. Rev. 1981, 39, 121.
6. Serpone, N.; Jamieson, M. A.; Henry, M. S.; Hoffman, M. Z.; Bolletta, F.; Maestri, M. J. Am. Chem. Soc. 1979, 101, 2907.
7. Juris, A.; Manfrin, M. F.; Maestri, M.; Serpone, N. Inorg. Chem. 1978, 17, 2258.
8. Gandolfi, M. T.; Maestri, M.; Sandrini, D.; Balzani, V. Inorg. Chem. 1983, 22, 3435.
9. Bolletta, F.; Maestri, M.; Balzani, V. J. Phys. Chem. 1976, 80, 2499.
10. Brunschwig, B.; Sutin, N. J. Am. Chem. Soc. 1978, 100, 7568.
11. Kealy, T. J.; Pauson, P. L.; Nature (London), 1951, 168, 1039.
12. Miller, S. A.; Tebboth, J. A.; Tremaine, J. F.

J. Chem. Soc. 1952, 632.

13. Wilkinson, G.; Rosenblum, M.; Whiting, M. C.; Woodward, R. B. J. Am. Chem. Soc. 1952, 74, 2125.
14. a. Sohn, Y. S.; Hendrickson, D. N.; Gray, H. B. J. Am. Chem. Soc. 1970, 92, 3233. b. Sohn, Y. S.; Hendrickson, D. N.; Gray, H. B. J. Am. Chem. Soc. 1971, 93, 3603.
15. Scott, D. R.; Becker, R. S. J. Chem. Phys. 1961, 35, 516.
16. Fry, A. J.; Liu, R. S. H.; Hammond, G. S.; J. Am. Chem. Soc. 1966, 88, 4781.
17. Bhaumik, M. L.; El-Sayed, M. A.; J. Phys. Chem. 1965, 69, 275.
18. Herkstroeter, W. G. J. Am. Chem. Soc. 1975, 97, 4161.
19. Carney, M. J.; Lesniak, J. S.; Likar, M. D.; Pladziewicz, J. R. J. Am. Chem. Soc. 1984, 106, 2565.
20. Pladziewicz, J. R.; Espenson, J. H. J. Am. Chem. Soc. 1973, 95, 56; J. Phys. Chem. 1971, 75, 3381.
21. Yang, E. S.; Chan, M. S.; Wahl, A. C.; J. Phys. Chem. 1975, 79, 2049; J. Phys. Chem. 1980, 84, 3094.
22. Konig, E.; Herzog, S. J. Inorg. Nucl. Chem. 1970, 32, 585.
23. Rosenblum, M. "Chemistry of the iron group metallocenes" Part one, John Wiley & Sons: New York, 1965, p40.
24. Pladziewicz, J. R.; Brenner, M. S.; Rodeberg, D. A.; Likar, M. D. Inorg. Chem. 1985, 24, 1450.
25. Connolly, P. Ph.D. Dissertation, Iowa State University, Ames, Iowa, 1985.
26. Hoselton, M. A.; Lin, C.-T.; Schwartz, H. A.; Sutin, N.

J. Am. Chem. Soc. 1978, 100,2383.

27. Ohno, T.; Kato, S. Bull. Chem. Soc. Jpn. 1984, 57, 1528.
28. Chapple, A. P.; Vikesland, J. P.; Wilkinson, F. Chemical Physics Letters 1977, 50, 81.
29. Wrighton, M. S.; Pdungsap, L.; Morse, D. L. J. Phys. Chem. 1975, 79, 66.
30. Ollino, M.; Cherry, W.R. Inorg. Chem. 1985, 24, 1417.
31. Hendrickson, D. N.; Sohn, Y. S.; Gray, H. B. Inorg. Chem. 1971, 10, 1559.
32. Turro, N. J. "Modern Molecular Photochemistry", Benjamin/Cummings: Menlo Park, CA, 1978; pp 296-311.
33. a. Forster, T. Disc. Faraday Soc. 1959, 27, 7. b. Forster, T. Ann. Physik. 1948, 2, 55.
34. Dexter, D. L. J. Chem. Phys. 1953, 21, 836.
35. Yardley, J. T. Introduction to Molecular Energy Transfer; Academic Press: New York, 1970.
36. Brown, G. M.; Sutin, N. J. Am. Chem. Soc. 1979, 101, 883.
37. Endicott, J. F.; Heeg, M. J.; Gaswick, D. C.; Pyke, S. C. J. Phys. Chem. 1981, 85, 1777.
38. Endicott, J. F.; Tamilarasan, R.; Brubaker, G. R. J. Am. Chem. Soc. 1986, 108, 5193.
39. Stanbury, D. M.; Gaswick, D.; Brown, G. M.; Taube, H. Inorg. Chem. 1983, 22, 1975.

APPENDIX

Table A-1. Kinetic data of the reaction of $Fe(Cp)_2$ with $^*Cr(bpy)_3^{3+}$

Conditions: $[Cr(bpy)_3^{3+}] = 1.0 \times 10^{-5}$ M

$\lambda = 727$ nm, $\mu = 0.05$ M

T = 25 °C, in 70% CH_3CN/H_2O

$10^6[Fe(Cp)_2]/M$	$10^{-4}k_{obs}/s^{-1}$
5.19	9.07
5.19	8.81
7.79	10.0
7.79	10.7
10.4	13.8
10.4	13.4
13.0	15.9
13.0	16.9
12.4	17.7
18.6	21.0
24.8	28.4

Table A-2. Kinetic data for the reaction of $Fe(Cp)(C_5H_4\text{-}nBu)$ with $^*Cr(bpy)_3^{3+}$

Conditions: $[Cr(bpy)_3^{3+}] = 1.13 \times 10^{-5}$ M

$\lambda = 727$ nm, $\mu = 0.05$ M

T = 25 °C, in 70% CH_3CN/H_2O

$10^5[Fe(Cp)(C_5H_4\text{-}nBu)]/M$	$10^{-4}k_{obs}/s^{-1}$
0.42	7.79
0.42	7.91
0.63	9.51
0.63	9.35
0.84	11.8
0.84	11.2
1.05	14.0
1.05	14.1
1.26	15.1
1.26	15.4

Table A-3. Kinetic data for the reaction of $Fe(C_5H_4CH_3)_2$ with $^*Cr(bpy)_3^{3+}$

Conditions: $[Cr(bpy)_3^{3+}] = 1.1 \times 10^{-5}$ M

$\lambda = 727$ nm, $\mu = 0.05$ M

T = 25 °C, in 70% CH_3CN/H_2O

$10^6[Fe(C_5H_4CH_3)_2]/M$	$10^{-4}k_{obs}/s^{-1}$
2.84[a]	5.84
2.84[a]	5.84
4.26[a]	7.32
4.26[a]	6.86
5.68	8.13
5.68	8.03
7.10	10.1
7.10	9.83
8.52	11.1
8.52	10.7
11.4	14.1
11.4	12.8

[a] $[Cr(bpy)_3^{3+}] = 5.6 \times 10^{-6}$ M.

Table A-4. Kinetic data for the reaction of $Fe(Cp)(C_5H_4CHO)$ with $^*Cr(bpy)_3^{3+}$

Conditions: $[Cr(bpy)_3^{3+}] = 1.1 \times 10^{-5}$ M

$\lambda = 727$ nm, $\mu = 0.05$ M

T = 25 °C, in 70% CH_3CN/H_2O

$10^5[Fe(Cp)(C_5H_4CHO)]/M$	$10^{-4}k_{obs}/s^{-1}$
0.00	3.00
0.49	7.49
0.49	7.82
0.82	8.43
0.82	7.90
1.14	13.0
1.14	12.8
1.47	14.2
1.47	14.4
1.79	17.9
1.79	18.8
2.12	21.4
2.12	20.4
4.70	32.0[a]

[a] $[Cr(bpy)_3^{3+}] = 5.0 \times 10^{-5}$ M.

Table A-5. Kinetic data of the reaction of $Fe(Cp)(C_5H_4CH_2OH)$ with $^*Cr(bpy)_3^{3+}$

Conditions: $[Cr(bpy)_3^{3+}] = 5 \times 10^{-5}$ M

$\lambda = 727$ nm, $\mu = 0.05$ M

T = 25 °C, in 70% CH_3CN/H_2O

$10^6[Fe(Cp)(C_5H_4CH_2OH)]/M$	$10^{-4}k_{obs}/s^{-1}$
5.17	7.63
5.17	7.70
7.75	9.22
7.75	9.36
10.3	11.0
10.3	11.6
12.9	14.4
12.9	13.3
15.5	15.3
15.5	15.5

Table A-6. Kinetic data for the reaction of $Fe(Cp)(C_5H_4COOH)$ with $^*Cr(bpy)_3^{3+}$

Condition: $[Cr(bpy)_3^{3+}] = 1 \times 10^{-5}$ M

$\lambda = 727$ nm, $\mu = 0.05$ M

T = 25 °C, in 70% CH_3CN/H_2O

$10^5[Fe(Cp)(C_5H_4COOH)]/M$	$10^{-4}k_{obs}/s^{-1}$
0.62	7.1
0.62	6.7
1.04	9.8
1.04	9.2
1.45	12.1
1.45	12.4
1.87	14.3
2.28	19.8
2.28	18.5
2.50	19.6
4.72	33.2
4.72	33.1

Table A-7. Kinetic data for the reaction of $Fe(C_5H_4COOH)_2$ with $^*Cr(bpy)_3^{3+}$

Conditions: $[Cr(bpy)_3^{3+}] = 5.7 \times 10^{-6}$ M

$\lambda = 727$ nm, $\mu = 0.05$ M

T = 25 °C, in 70% CH_3CN/H_2O

$10^6[Fe(C_5H_4COOH)_2]/M$	$10^{-4}k_{obs}/s^{-1}$
3.02	4.85
3.02	4.80
4.50	6.84
4.50	6.88
6.04	8.55
6.04	7.87
7.55	9.28
7.55	8.94
9.06	9.67
9.06	9.60
10.3	9.60
10.3	10.1
12.1	11.9
12.1	11.7
13.6	12.9
13.6	13.1
15.1	13.7
15.1	13.0

Table A-8. Kinetic data for the reaction of $Fe(Cp)(C_5H_4CH_2NMe_2)$ with $^*Cr(bpy)_3^{3+}$

Conditions: $[Cr(bpy)_3^{3+}] = 1.1 \times 10^{-5}$ M

$\lambda = 727$ nm, $\mu = 0.05$ M

T = 25 °C, in 70% CH_3CN/H_2O

$10^5[Fe(Cp)(C_5H_4CH_2NMe_2)]$	$10^{-4}k_{obs}/s^{-1}$
0.00	3.09
1.16	7.18
1.16	7.28
1.62	9.92
1.62	9.80
2.08	12.4
2.08	11.4
2.54	14.4
2.54	13.7
3.00	18.3
3.00	18.8
3.47	19.1
3.47	17.2
3.93	20.3
3.93	22.1
4.39	22.7
4.39	22.9

Table A-9. Kinetic data for the reaction of $Ru(Cp)_2$ with $^*Cr(bpy)_3^{3+}$

Conditions: $[Cr(bpy)_3^{3+}] = 1.1 \times 10^{-5}$ M

$\lambda = 727$ nm, $\mu = 0.05$ M

T = 25 °C, in 70% CH_3CN/H_2O

$10^6[Ru(Cp)_2]/M$	$10^{-4}k_{obs}/s^{-1}$
3.85[a]	4.87
3.85[a]	4.85
6.16[a]	6.41
6.16[a]	6.35
7.70	7.18
7.70	7.58
9.24	8.19
9.24	8.14
11.5	9.46
11.5	9.54
13.1	11.3
13.1	10.7
15.4	11.4
15.4	11.5
19.2	13.2
19.2	14.0

[a] $[Cr(bpy)_3^{3+}] = 5.6 \times 10^{-6}$ M.

Table A-10. Kinetic data for the reaction of $Os(Cp)_2$ with $^*Cr(bpy)_3^{3+}$

Conditions: λ = 727 nm, μ = 0.05 M

T = 25 °C, in 70% CH_3CN/H_2O

$10^6[Cr(bpy)_3^{3+}]/M$	$10^6[Os(Cp)_2]/M$	$10^{-4}k_{obs}/s^{-1}$
4.72	3.02	5.65
4.72	3.02	6.00
4.72	4.83	7.45
4.72	4.83	7.20
4.72	6.04	8.61
4.72	6.04	8.97
11.3	10.3	9.85
11.3	10.3	10.1
11.3	12.1	13.1
11.3	12.1	13.6
11.3	13.3	14.1
11.3	13.3	13.8
11.3	15.1	14.9
11.3	15.1	14.9

Table A-11. Kinetic data for the reaction of $Fe(Cp)_2PF_6$ with $^*Cr(bpy)_3^{3+}$

Conditions: $[Cr(bpy)_3^{3+}] = 3.77 \times 10^{-4}$ M

$\lambda = 727$ nm, $\mu = 0.05$ M ($HClO_4$)

T = 25 °C, in 70% CH_3CN/H_2O

$10^4[Fe(Cp)_2^+]/M$	$10^{-4}k_{obs}/s^{-1}$
0.39	4.34
0.39	4.49
0.77	5.86
0.77	6.10
1.15	7.75
1.15	8.19
1.54	9.50
1.54	9.45
1.92	11.6
1.92	11.7
2.31	12.5
2.31	13.2
0.77	6.09[a]
0.77	6.24[a]
1.54	9.18[a]
1.54	9.06[a]
2.31	11.2[a]
2.31	11.4[a]

[a]Ionic strength was adjusted by HCl.

Table A-12. Kinetic data for the reaction of $Fe(Cp)(C_5H_4\text{-}nBu)PF_6$ with $^*Cr(bpy)_3^{3+}$

Conditions: $[Cr(bpy)_3^{3+}] = 5 \times 10^{-5}$ M

$\lambda = 727$ nm, $\mu = 0.05$ M

T = 25 °C, in 70% CH_3CN/H_2O

$10^4[Fe(Cp)(C_5H_4\text{-}nBu)^+]/M$	$10^{-4}k_{0bs}/s^{-1}$
1.13	7.60
1.13	7.60
2.36	9.81
2.36	9.95
2.81	12.6
2.81	12.3
3.55	14.1
3.55	14.4
7.80	27.8
7.80	27.2

Table A-13. Kinetic data for the reaction of $Fe(Cp)(C_5H_4CH_2NMe_2)PF_6$ with $*Cr(bpy)_3^{3+}$

Conditions: $[Cr(bpy)_3^{3+}] = 5.0 \times 10^{-5}$ M

$\lambda = 727$ nm, $\mu = 0.05$ M

T = 25 °C, in 70% CH_3CN/H_2O

$10^4[Fe(Cp)(C_5H_4CH_2NMe_2)(PF_6)]/M$	$10^{-4}k_{obs}/s^{-1}$
0.73	4.47
0.73	4.40
1.46	5.94
1.46	5.96
2.19	7.17
2.19	7.11
2.92	8.02
2.92	7.66
3.65	9.56
3.65	9.42
4.38	10.6
4.38	10.3
5.11	13.1
5.11	12.4
5.84	13.4
5.84	13.3
7.30	17.6
7.30	17.2
8.76	21.9
8.76	21.5

Table A-14. Kinetic data for the reaction of $Fe(Cp)(C_5H_4CH_2OH)PF_6$ with $^*Cr(bpy)_3^{3+}$

Conditions: $[Cr(bpy)_3^{3+}] = 5 \times 10^{-5}$ M

$\lambda = 727$ nm, $\mu = 0.05$ M

T = 25 °C, in 70% CH_3CN/H_2O

$10^4[Fe(Cp)(C_5H_4CH_2OH)^+]/M$	$10^{-4}k_{obs}/s^{-1}$
1.30	4.58
1.30	4.73
2.02	6.62
2.02	6.70
3.30	8.73
3.30	8.99
4.06	10.9
4.06	10.8
5.45	11.6
5.45	11.5
5.76	11.5
5.76	11.5

Table A-15. Kinetic data for the reaction of $Fe(C_5H_4CH_3)_2PF_6$ with $^*Cr(bpy)_3^{3+}$

Conditions: $[Cr(bpy)_3^{3+}] = 5 \times 10^{-5}$ M

$\lambda = 727$ nm, $\mu = 0.05$ M

T = 25 °C, in 70% CH_3CN/H_2O

$10^4[Fe(C_5H_4CH_3)_2^+]/M$	$10^{-4}k_{obs}/s^{-1}$
1.11	4.71
1.11	4.79
2.23	6.19
2.23	6.46
3.34	7.66
3.34	8.03
4.45	9.54
4.45	9.19
5.57	10.9
5.57	11.2

Table A-16. Kinetic data for the reaction of $Fe(C_5H_4\text{-}nBu)_2PF_6$ with $^*Cr(bpy)_3^{3+}$

Conditions: $[Cr(bpy)_3^{3+}] = 3.7 \times 10^{-4}$ M

$\lambda = 727$ nm, $\mu = 0.05$ M

T = 25 °C, in 70% CH_3CN/H_2O

$10^4[Fe(C_5H_4\text{-}Bu)_2^+]/M$	$10^{-4}k_{obs}/s^{-1}$
0.00	2.90
2.34	3.52
4.29	4.21
5.97	4.66
7.63	5.35
9.68	5.64

Table A-17. Kinetic data for the reaction of $Fe(Cp^*)_2PF_6$ with $^*Cr(bpy)_3^{3+}$

Conditions: $[Cr(bpy)_3^{3+}] = 5 \times 10^{-5}$ M

$\lambda = 727$ nm, $\mu = 0.05$ M

T = 25 °C, in 70% CH_3CN/H_2O

$10^3[Fe(Cp^*)_2^+]/M$	$10^{-4}k_{obs}/s^{-1}$
0.95	4.51
0.95	4.53
1.60	5.68
1.60	5.68
1.94	6.60
1.94	6.94
2.61	8.47
2.61	8.13
3.04	9.86
3.04	9.76
3.70	11.7
3.70	11.5
4.01	12.6
4.01	12.6

Table A-18. Kinetic data for the reaction of $Fe(C_5H_4COOH)_2^+$ with $Cr(bpy)_3^{2+}$

Conditions: λ = 560 nm, μ = 0.05 M

T = 25 °C, in 70% CH_3CN/H_2O

$10^4[Cr(bpy)_3^{3+}]/M$	$10^4[Fe(C_5H_4COOH)_2]/M$	$10^9 k/M^{-1}s^{-1}$ [a]
3.77	1.81	8.75
3.77	1.81	8.98
3.77	3.60	9.98
3.77	3.60	9.20
5.66	1.21	8.94
5.66	2.42	9.00
5.66	2.42	8.03
7.55	1.81	9.08
7.55	1.81	9.22
7.55	3.60	8.49
7.55	3.60	8.58

[a]The average is (8.9 ± 0.3) x 10^9 $M^{-1}s^{-1}$.

Table A-19. Kinetic data for the reaction of $Fe(Cp)(C_5H_4CHO)^+$ with $Cr(bpy)_3^{2+}$
Conditions: λ = 560 nm, μ = 0.05 M
T = 25 °C, in 70% CH_3CN/H_2O

$10^4[Cr(bpy)_3^{3+}]/M$	$10^4[Fe(Cp)(C_5H_4CHO)]/M$	$10^9 k/M^{-1}s^{-1}$ [a]
3.77	1.99	9.17
3.77	1.99	8.83
3.77	3.98	8.85
3.77	7.90	8.85
3.77	7.90	8.62
5.66	1.99	8.32
5.66	1.99	8.76
5.66	3.98	8.61
5.66	3.98	8.57
5.66	7.90	9.47
5.66	7.90	9.33
7.55	1.99	8.53
7.55	1.99	7.85
7.55	3.98	9.05
7.55	3.98	8.25

[a]The average is (8.8 ± 0.3) x 10^9 $M^{-1}s^{-1}$.

Table A-20. Kinetic data for the reaction of $Fe(Cp)(C_5H_4COOH)^+$ with $Cr(bpy)_3^{2+}$
Conditions: λ = 560 nm, μ = 0.05 M
T = 25 °C, in 70% CH_3CN/H_2O

$10^4[Cr(bpy)_3^{3+}]/M$	$10^4[Fe(Cp)(C_5H_4COOH)^+]/M$	$10^9 k/M^{-1}s^{-1}$ [a]
1.88	2.86	6.36
1.88	2.86	5.63
1.88	4.30	6.32
1.88	4.30	6.85
1.88	5.74	7.05
1.88	5.74	6.37
3.77	2.86	6.02
3.77	2.86	6.02
3.77	4.30	5.64
3.77	4.30	5.67
3.77	5.74	6.53
3.77	5.74	6.16
5.66	2.86	5.70
5.66	2.86	5.64
5.66	5.74	6.26
5.66	5.74	6.29

[a]The average is (6.2 ± 0.3) x 10^9 $M^{-1}s^{-1}$.

Table A-21. Kinetic data for the reaction of $Fe(Cp)(C_5H_4CH_2OH)^+$ with $^*Cr(bpy)_3^{2+}$
Conditions: λ = 560 nm, μ = 0.05 M
T = 25 °C, in 70% CH_3CN/H_2O

$10^4[Cr(bpy)_3^{3+}]/M$	$10^4[Fe(Cp)(Cp\text{-}CH_2OH)]/M$	$10^{-9}k/M^{-1}s^{-1}$ [a]
3.77	3.4	5.89
3.77	5.2	5.88
3.77	5.2	5.79
3.77	6.9	8.03[b]
3.77	6.9	7.82[b]
1.89	5.2	6.48
1.89	5.2	6.84
1.89	3.4	5.50
1.89	3.4	5.53

[a]The average is (6.0 ± 0.4) x 10^9 $M^{-1}s^{-1}$.

[b]Excluded from the average.

Table A-22. Kinetic data for the reaction of $Fe(Cp)(C_5H_4\text{-}nBu)^+$ with $Cr(bpy)_3^{2+}$
Conditions: λ = 560 nm, μ = 0.05 M
T = 25 °C, in 70% CH_3CN/H_2O

$10^4[Cr(bpy)_3^{3+}]/M$	$10^4[Fe(Cp)(C_5H_4\text{-}nBu)]/M$	$10^{-9}k/M^{-1}s^{-1}$ [a]
1.88	5.01	5.34
1.88	5.01	5.41
1.88	6.26	5.30
1.88	6.26	5.47
3.77	3.76	5.16
3.77	3.76	5.27
3.77	5.01	5.50
3.77	5.01	5.35
3.77	6.26	5.33
3.77	6.26	5.27
5.66	3.76	5.34
5.66	3.76	5.22
5.66	6.26	5.23
5.66	6.26	5.24

[a]The average is (5.3 ± 0.1) x 10^9 $M^{-1}s^{-1}$.

Table A-23. Kinetic data for the reaction of $Fe(C_5H_4CH_3)_2^+$ with $Cr(bpy)_3^{2+}$

Conditions: λ = 560 nm, μ = 0.05 M

T = 25 °C, in 70% CH_3CN/H_2O

$10^4[Cr(bpy)_3^{3+}]/M$	$10^4[Fe(C_5H_4\text{-}Me)_2]/M$	$10^{-9}k/M^{-1}s^{-1}$ [a]
1.88	2.56	4.52
1.88	2.56	4.44
1.88	3.41	4.75
1.88	3.41	4.59
1.88	4.26	4.30
1.88	4.26	4.41
3.77	2.56	4.47
3.77	2.56	4.59
3.77	5.12	4.59
3.77	5.12	4.74
5.66	2.56	4.38
5.66	2.56	4.49
5.66	5.12	4.55
5.66	5.12	4.54

[a]The average is (4.5 ± 0.1) x 10^9 $M^{-1}s^{-1}$.

Table A-24. Kinetic data for the reaction of $Fe(Cp)(C_5H_4CH_2NMe_2)^+$ with $Cr(bpy)_3^{2+}$
Conditions: λ = 727 nm, μ = 0.05 M
T = 25 °C, in 70% CH_3CN/H_2O

$10^4[Fe(Cp)(C_5H_4CH_2NMe_2)]/M$	$10^4[Cr(bpy)_3^{3+}]/M$	$10^9 k/M^{-1}s^{-1}$ [a]
1.89	1.89	3.89
1.89	3.77	3.45
1.89	3.77	3.62
3.77	3.77	3.56
3.77	5.66	3.48
3.77	5.66	3.58
5.66	5.66	3.65
5.66	5.66	3.57
5.66	7.54	3.83
5.66	7.54	3.74

[a]The average is (3.6 ± 0.1) x 10^9 $M^{-1}s^{-1}$.

Table A-25. Kinetic data for the reaction of $Fe(Cp)_2^+$ with $Cr(bpy)_3^{2+}$

Conditions: $[Cr(bpy)_3^{3+}] = 3.77 \times 10^{-4}$ M

$\lambda = 560$ nm, $\mu = 0.01$ M

T = 25 °C, in 70% CH_3CN/H_2O

$10^4[Fe(Cp)_2]/M$	$10^5[Fe(Cp)_2^+]/M$	$10^{-9}k/M^{-1}s^{-1}$ [a]
3.77	1.24	3.33
2.83	1.47	3.30
2.83	1.50	3.93
1.89	1.35	3.33
1.89	1.42	3.57
0.94	1.10	3.66
0.94	1.01	3.49
4.72	1.14	3.73

[a]The average is $(3.5 \pm 0.2) \times 10^9$ $M^{-1}s^{-1}$.

Table A-26. Kinetic data for the reaction of $Fe(Cp^*)_2PF_6$ with $^*Cr(4,4'\text{-}Me_2bpy)_3^{3+}$

Conditions: $[Cr(4,4'\text{-}Me_2bpy)_3^{3+}] = 2.0 \times 10^{-5}$ M

$\lambda = 727$ nm, $\mu = 0.05$ M (HCl)

T = 25 °C, in 70% CH_3CN/H_2O

$10^3[Fe(Cp^*)_2^+]/M$	$10^{-4}k_{ob}s/s^{-1}$
0.00	1.11
0.00	1.25
0.99	2.47
0.99	2.44
1.87	3.66
1.87	3.58
2.85	4.92
2.85	5.08
3.72	6.11
3.72	6.11
4.69	7.54
4.69	7.73

Table A-27. Kinetic data for the reaction of $Fe(Cp^*)_2PF_6$ with $^*Cr(5\text{-Clphen})_3^{3+}$

Conditions: $[Cr(5\text{-Clphen})_3^{3+}] = 2.0 \times 10^{-5}$ M

$\lambda = 727$ nm, $\mu = 0.05$ M (HCl)

T = 25 °C, in 70% CH_3CN/H_2O

$10^3[Fe(Cp^*)_2^+]$/M	$10^{-4}k_{obs}/s^{-1}$[a,b]
0.00	3.01
0.00	3.44
1.14	5.02
1.14	5.26
2.07	6.87
2.07	6.74
3.11	6.79
3.11	6.97
4.03	9.54
4.03	9.14
5.14	10.9
5.14	10.8

CHAPTER II. PREPARATION AND HOMOLYSIS OF A SERIES MACROCYCLIC ORGANOCOBALT COMPLEXES

INTRODUCTION

Since the discovery that coenzyme B_{12} contains a cobalt(III)-carbon bond,[1] there has been much interest in the preparation and properties of similar inorganic analogues.[2] However, complexes with saturated macrocycles are still quite rare. The saturated macrocyclic ligands were thought to impose too much instability on the Co-C bond for these complexes to exist. Roche and Endicott[3,4] did succeed in the preparation of several interesting organocobalt mac-N_4 complexes by following a photochemical approach as shown in Scheme I. Obviously the predicted effect of the macrocycle

Scheme I.

$$Co(NH_3)_5O_2CR^{2+} + h\nu \longrightarrow Co^{2+} + 5NH_4^+ + CO_2 + R\cdot \qquad (1)$$

$$R\cdot + CoN_4^{2+} \longrightarrow RCoN_4^{2+} \qquad (2)$$

R = CH_3 or C_2H_3

N_4 = Me_6[14]4,11-dieneN$_4$, meso-Me_6[14]aneN$_4$, [14]aneN$_4$, and Me_4[14]tetraeneN$_4$

saturation is less severe than originally thought. However their attempts to prepare the higher alkyl analogues were unsuccessful.

Recently, Bakac and Espenson[5] reported a new approach to the preparation of a series of organo Co([14]aneN$_4$)$^{2+}$ complexes. The photochemical steps are as shown in Scheme II.

Scheme II.

$(py)(dmgH)_2CoR + h\nu \longrightarrow (H_2O)(py)Co(dmgH)_2 + R\cdot$ (3)

$(H_2O)(py)Co(dmgH)_2 + 3H^+ \longrightarrow Co(H_2O)_6^{2+} + 2dmgH_2 + pyH^+$ (4)

$R\cdot + (H_2O)_2LCo^{2+} \longrightarrow (H_2O)LCoR^{2+} + H_2O$ (5)

R = primary alkyl, substituted primary alkyl, and benzyl

and the capture of the radical is quite efficient, yielding nearly quantitative amounts of $(H_2O)LCoR^{2+}$ in solution. The high absorption coefficients of organocobaloximes relative to those of the product organocobalt complex prevent the product itself from ready photolysis. This also may be the reason for low yields of the methyl complex and the inability to prepare complexes with other alkyl groups in the preparation with $(NH_3)_5CoO_2CR^{2+}$.[3,4]

Since complexes of organocobalt with saturated macrocycles are still rare, it is desirable to prepare additional macrocyclic organocobalt complexes. Two macrocycle ligands, C-meso-Me_6[14]aneN_4 and Me_6[14]4,11-dieneN_4, are chosen as candidates (as shown in Figure I) in this study. The six methyl groups on the macrocycle add a lot of steric hindrance to attack at the metal center. Therefore the potential of $Co^{III/II}$ for Co(meso-Me_6[14]aneN_4)$^{2+}$ and Co(Me_6[14]4,11-dieneN_4)$^{2+}$ are ~ 0.2 V higher than that of Co([14]aneN_4)$^{2+}$.[6] This steric effect may make the preparation become difficult.

Homolytic metal-carbon bond cleavage occurs by both

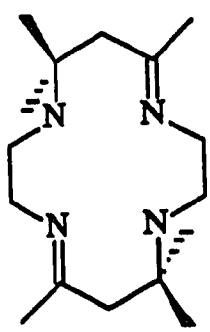

$Me_6[14]4,11\text{-dieneN}_4$

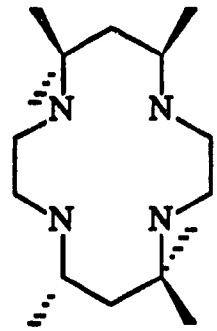

C-meso-$Me_6[14]$aneN$_4$

Figure II-1. Structures of $Me_6[14]4,11\text{-dieneN}_4$ and C-meso-$Me_6[14]$aneN$_4$

unimolecular[7-14] and bimolecular[15-20] homolytic reactions. Both mechanisms, especially the former, are important in determing metal-carbon bond dissociation enthalpies. The approach is based on the assumption that the BDE can be approximated as ΔH for the unimolecular homolysis since the recombination reaction has a negligibly small activation enthalpy. The rate constants for homolysis of the cobalt-carbon bond of these organocobalt complexes will be investigated. Because the cobalt-carbon bond is much weaker in $Co(Me_6[14]4,11\text{-dieneN}_4)(H_2O)CH_3^{2+}$ than in $Co([14]aneN_4)(H_2O)CH_3^{2+}$,[21] a rapid homolysis process may be observed for $Co(Me_6[14]4,11\text{-dieneN}_4)(H_2O)CH_3^{2+}$ and its

analogues. Based on the kinetic experiments of homolysis at different temperatures, thermodynamic parameters will be obtained for these reactions. Therefore, these results may be able to tell if there is any stabilization for the cobalt-carbon bond from the unsaturation of the macrocycle ligand.

EXPERIMENTAL

Reagents

Organocobaloximes ($RCo(dmgH)_2$)py, R= Me, Et, nPr, CH_2Cl, CH_2Br, i-Pr, $PhCH_2$) Organocobaloximes were prepared by following the literature method.[22] 16.3 g $dmgH_2$ and 16.7 g $CoCl_2 \cdot 6H_2O$ were stirred in 200 mL MeOH under argon until the cobalt salt dissolved. 6 g of NaOH were added as a 50% aqueous solution then followed by the addition of 5.6 g of pyridine. The red suspension was cooled to -10°C in a rock-salt/ice bath and stirred for ~15 minutes under argon. A further 3 g of NaOH, also as a 50 wt.% solution, was added then followed by 1.3 g $NaBH_4$. To the dark blue solution an equivalent amount of appropriate alkyl halide was added. The reaction solution was allowed to slowly warm to room temperature over 90 minutes. The volume of the solution was reduced to 1/3 of the original by rotatory evaporation. The solution was then added to 200 mL H_2O containing 2 mL pyridine. The product was filtered and washed with cold water.

5,7,7,12,14,14-Hexamethyl-1,4,8,11-tetra-azacyclotetradeca-4,11-diene To 1,2-diaminoethane dihydrobromide (11.1 g, 0.05 mole) were added acetone (100 mL) and 1,2-diaminoethane (3.0 g, 0.05 mol).[23] The mixture was stirred and heated at 45 °C for 45 minutes; during which time a copious white precipitate of the macrocycle dihydrobromide

formed. The solution was cooled and the product filtered, washed with ice-cold acetone, then ether, and dried in air.

C-meso-5,7,7,12,14,14-Hexamethyl-1,4,8,11-tetraazacyclotetradecane trans-[14]-Diene dihydrobromide dihydrate (16 g) was dissolved in methanol (200 mL), and sodium borohydride (3 g) was added in small portions to the warmed solution.[23] When the addition was completed and bubbling ceased, 2 M KOH was added till the solution was basic to litmus. When the volume of the solution was reduced to ~1/3 of the original by rotatory evaporation, a white precipitate formed. This was filtered and dissolved in water. Addition of 2 M KOH caused the white product to precipitate. This was filtered and washed with water, ether and dried in air; m.p. 147-148 °C. The product can be recrystalized from aqueous methanol.

$CoL(ClO_4)_2$ (L = Me_6[14]4,11-dieneN$_4$, C-meso-Me_6[14]aneN$_4$) An anhydrous solution of $CoCl_2$ was prepared by stirring $CoCl_2 \cdot 6H_2O$ (1.5 g, 6.3 mmol) in 10 mL 2,2-dimethoxypropane for one hour under a steady flow of argon. Following the method of Rillema and Endicott,[24] the appropriate ligand (3.1 mmol) dissolved in 20 mL DMF was added and the mixture was heated to 70 °C for one hour. Cooling yielded a blue-green precipitate of cobalt tetrachloro salt which was filtered, washed with 1:2.5 methanol-ether and with ether, and air-dried.

The tetrachlorocobaltate salt was then stirred in 30 mL H_2O and NH_4ClO_4 was added. The slurry was filtered, washed

with 1:5 methanol-ether and ether, and air-dried to yield the desired product, $CoL(ClO_4)_2$ (L = Me_6[14]4,11-dieneN$_4$, C-meso-Me_6[14]aneN$_4$).

Other reagents The chromium(III) perchlorate was prepared by the reduction of CrO_3 in an aqueous perchloric acid medium using H_2O_2. The chromium(II) perchlorate was prepared by reducing acidic Cr(III) perchlorate solutions on zinc amalgam. The 4-hydroxy-2,2,6,6-tetramethylpiperidinyloxy free radical was used as purchased. The $ABTS^-$ (2,2'-azino-bis(3-ethylbenzthiazoline-6-sulfonic acid) ammonium salt) was prepared by oxidizing its 2- salt with cerium(IV) perchlorate.[25] The concentration of the $ABTS^-$ was determined by UV-vis spectroscopic method(λ_{max} = 650 nm, ε = 10050 M^{-1} cm^{-1}).

2-Methyl-2-butyl hydroperoxide, 2,3-dimethyl-2-butyl hydroperoxide, and 2-methyl-1-phenylpropyl-2hydroperoxide were prepared from the corresponding alcohols by following the method in the literature.[26] These hydroperoxides were characterized by their ^1H NMR spectra. The concentrations of the hydroperoxides were determined spectrophotometrically by measuring the extent of the formation of their corresponding organochromium(III).

The 1,2-diaminoethane dihydrobromide was prepared as follows. A solution of 1,2-diaminoethane(10 mL, 0.15 mol) in methanol (100 mL) was cooled in an ice-bath, and concentrated (49%) hydrobromic acid (34 mL, 0.32 mol) was added dropwise.

The white solid was filtered off. A second crop could be isolated by addition of ether to the filtrate. The product was then washed with n-butanol and ether, and dried in air.

Methanol (Aldrich), hydrogen peroxide (Aldrich), t-butyl hydroperoxide (Aldrich), potassium hydroxide (Fisher), sodium borohydride (Fisher), hydrobromic acid, ethylenediamine and perchloric acid were used as purchased.

Synthesis of organocobalt complexes

Photolytic method The organocobalt complexes were prepared by photolyzing acidic aqueous solutions of appropriate organocobaloximes in the presence of $Co(Me_6[14]4,11\text{-}dieneN_4)^{2+}$.[5] A typical procedure is given below for the ethyl complex. A 8-mL aliquot of 0.394 g (1 mmol) $EtCo(dmgH)_2py$ in 1 M $HClO_4$ was added to 100 mL of a deaerated aqueous solution of 0.56 g (1 mmol) $Co(Me_6[14]4,11\text{-}diene)^{2+}$ in a 200-mL Erlenmeyer flask. The stirred suspension was cooled and irradiated by use of a 300-W sun lamp till all the organocobaloxime was consumed. The solid $dmgH_2$ produced was removed by filtration and the yellow filtrate was kept in a freezer for a few hours. Warming up to room temperature, the precipitate was obtained after filtration. The product was washed with ether and air-dried. Other complexes were prepared by the same procedure from appropriate organocobaloximes. All of these crude products have been characterized by their ^1H NMR spectrum.

Fenton's reaction The hydroxymethyl, methoxymethyl, and methyl cobalt(diene) complexes were prepared by following Fenton's reaction. A 0.5 g sample of $Co(Me_6[14]4,11\text{-}dieneN_4)^{2+}$ was dissolved in 70mL H_2O in the presence of MeOH (or Me_2O, or DMSO; respectively) and 2 mL 1.0 M $HClO_4$, and 0.97 M H_2O_2 was added. The solution was kept stirring in the dark for 30 minutes. After filtration, sodium perchlorate was added to the filtrate directly to form a precipitate. The product was filtered and washed with ether then air-dried.

Reaction with hydroperoxide The methyl cobalt complexes were prepared by the reaction with hydroperoxides. A typical procedure was as follows. A 0.5 g sample of $Co(Me_6[14]4,11\text{-}dieneN_4)^{2+}$ was dissolved in 100 mL H_2O ($[H^+]$= 0.02 M). An aqueous solution of tert-butyl hydroperoxide was added slowly. The solution was kept stirring for 30 minutes. After filtration, sodium perchlorate was added to the filtrate to form the precipitate. The product was filtered, washed with ether, and air-dried.

Methods

Ultraviolet-visible spectroscopy Uv-vis spectra and single wavelength absorbance vs. time data were acquired using a Cary model 219 recording spectrophotometer, or a Cary model 14 recording spectrophotometer interfaced with an OLIS 3820 data system. Temperature control of $\pm$ 0.1°C was maintained by circulating water from a constant-temperature bath through the jacket of a water-filled cell holder within the

spectrophotometer. The fitting of the data to linear and nonlinear equations was accomplished using an Apple IIe computer with the appropriate software for the analysis of kinetic data or standard first-order routines on the OLIS computer system.

^{1}H NMR spectrum Routine ^{1}H NMR spectra were collected using a Nicolet NT-300. The NMR experiments were all done in D_2O with HOD as the reference at δ4.63 ppm.

Gas chromatograph Gas chromatography was carried out on a Hewlett Packard 5790A series gas chromatograph with 3390a series integrator. A VZ-10 column was used for the determinations.

Laser flash photolysis The laser system used has been described by Connolly[27] and is based on another system in the literature.[28] The signal from the photomultiplier tube was collected and stored on a Nicolet model 2090-3a digitizing oscilloscope. The Nicolet oscilloscope was interfaced with an Apple II plus microcomputer which converted the voltage vs time data from the oscilloscope to absorbance vs time data (voltage being proportional to transmittance).

X-ray crystallography of rac-$CH_2ClCo(Me_6[14]4,11\text{-}dieneN_4)(CLO_4)_2$

An orange-yellow crystal of the title compound was mounted on a glass fiber in a random orientation and moved into the cold stream of the low-temperature device on the

diffractometer. The cell constants were determined from a list of reflections found by an automated search routine.

A total of 3861 reflections were collected in the $+h,+k,\pm l$ quadrant, of which 3291 were unique and not systematically absent. The agreement factor for the averaging of 802 observed reflections was 2.2% based on intensity and 1.6% based on F_{obs}. The intensities of three standards, checked hourly over the course of the data collection, indicated only random variations within the errors of the measurement. Lorentz and polarization corrections were applied.

The space group $P2_1/c$ was uniquely defined by the observed systematic absences. The position of all 34 non-hydrogen atoms were taken from a direct methods E-map[x]. Following isotropic least-squares refinement of all atoms, hydrogen atoms were added in calculated positions for all carbon atoms and used for the calculation of structure factors only. Since no initial absorption correction was made, a numerical correction was made at this time on the unaveraged data set, and the data re-averaged. In the final stage of refinement, the cobalt, chlorine, oxygen, and nitrogen atoms were given anisotropic temperature factors. Following convergence, the discrepancy indices were $R = 0.0421$ and $R_w = 0.0538$. A difference Fourier map was calculated, and the positions of the four highest peaks were found to correspond to the expected positions of hydrogen atoms on the water

molecule coordinated to Co and on atoms N(1) and N(3). The position of the four hydrogen atoms were then included in the refinement (isotropic thermal parameters were fixed for the hydrogen atoms).

The final cycle of refinement included 234 variable parameters and converged with unweighted and weighted agreement factors of:

$$R_1 = \Sigma|F_o - F_c|/\Sigma F_o = 0.0394$$

$$R_2 = \mathrm{SQRT}[\Sigma w(F_o - F_c)^2/\Sigma w(F_o^2)] = 0.0497$$

The stanard deviation of an observation of unit weight was 1.29. The largest positive peak in the final difference Fourier had a height of 0.368 e/Å^3.

X-ray data collection and structure solution were carried out at the Iowa State Molecular Structure Laboratory. All calculations were performed on a Digital Equipment Corp. MicroVAX II computer using the CaD4/SDP package.

RESULTS

^{1}H NMR and UV-Visible spectra

The visible spectra of the alkyl complexes, Table II-1, exhibit two weakly allowed transitions at λ = 460-510 nm and λ = 360-390 nm. The spectrum of the methyl complex agrees well with that reported previously.[3,4] The ^{1}H NMR spectra of the alkyl cobalt complexes, Table II-2, also show agreement with the previous report.

A detailed spectral analysis for $(H_2O)LCoCH_3^{2+}$ in terms of three-center bonding model has been published.[29] The similarity of the spectral data in Table II-1 indicates comparable orbital energy levels for all the alkyl complexes.

X-ray crystal structure of $[(H_2O)(Me_6[14]4,11\text{-dieneN}_4CoCH_2Cl](ClO_4)_2$

The crystal structure of $CH_2ClCo(Me_6[14]4,11\text{-dieneN}_4)^{2+}$ consists of six coordinate cobalt cations, in which the cobalt center is surrounded by four nitrogen atoms from the equatorial macrocyclic ligand, $Me_6[14]4,11\text{-dieneN}_4$, and an aquo ad chloromethyl group in the axial positions, and uncoordinated perchlorate ions.

The structure of the complex is represented by the ORTEP drawing shown in Figure II-2. The stereoview of the cation is shown in Figure II-3. The crystallographic data are collected in Table II-3. The calculated bond distances and bond angles are reported in Tables II-4 and II-5, respectively.

Table II-1. UV-Visible spectra data for the $RCoL^{2+}$

	λ, nm (ε, $M^{-1}cm^{-1}$)[a]	
	λ_1 (ε_1)	λ_2 (ε_2)
$MeCo(Me_6[14]4,11\text{-}dieneN_4)^{2+}$	470(214)	376(391)
	470(228)[b]	376(404)[b]
$EtCo(Me_6[14]4,11\text{-}dieneN_4)^{2+}$	480(185)	380(401)
$n\text{-}PrCo(Me_6[14]4,11\text{-}dieneN_4)^{2+}$	480(156)	381(345)
$ClCH_2Co(Me_6[14]4,11\text{-}dieneN_4)^{2+}$	466(152)	356(280)
$CH_2OHCo(Me_6[14]4,11\text{-}dieneN_4)^{2+}$	464(148)	373(358)
$CH_3OCH_2Co(Me_6[14]4,11\text{-}dieneN_4)^{2+}$	466(155)	364(336)
$MeCo(Me_6[14]aneN_4)^{2+}$	498(74)[b]	384(133)[b]
$EtCo(Me_6[14]aneN_4)^{2+}$	504(57)	392(115)
$n\text{-}PrCo(Me_6[14]aneN_4)^{2+}$	508(58)	390(134)

[a]In 0.01M $HClO_4$.

[b]Reference 4.

Table II-2. ^1H NMR spectra data[a] for $RCoL^{2+}$

	R (δ,ppm)	CH_3 (ligand) (δ, ppm)
$MeCo(Me_6[14]4,11\text{-}dieneN_4)^{2+}$	1.61(3H)	2.18(6H),1.25(6H),1.12(3H),0.99(3H)
$EtCo(Me_6[14]4,11\text{-}dieneN_4)^{2+}$	0.10(3H,t)	2.19(6H),1.28(6H),1.12(3H),1.08(3H)
$n\text{-}PrCo(Me_6[14]4,11\text{-}dieneN_4)^{2+}$	–	2.1096H),1.26(6H),1.13(3H),1.08(3H)
$ClCH_2Co(Me_6[14]4,11\text{-}dieneN_4)^{2+}$	–	2.19(6H),1.30(6H),1.03(6H)
$CH_2OHCo(Me_6[14]4,11\text{-}dieneN_4)^{2+}$	–	2.04(6H),1.21(6H),1.03(3H),0.82(3H)
$CH_3OCH_2Co(Me_6[14]4,11\text{-}dieneN_4)^{2+}$	3.15(3H,s)	2.15(6H),1.21(6H),1.10(3H),0.88(3H)
$MeCo(Me_6[14]aneN_4)^{2+}$	2.01(3H,s)	1.04-1.13(15H),0.95(3H)
$EtCo(Me_6[14]aneN_4)^{2+}$	0.28(3H,t)	1.03-1.11(15H),0.91(3H)
$n\text{-}PrCo(Me_6[14]aneN_4)^{2+}$	–	1.0-1.12(15H),0.92(3H)
$ClCH_2Co(Me_6[14]aneN_4)^{2+}$	–	1.03-1.16(15H),0.87(3H)

[a]In D_2O with HOD as the reference at δ4.63 ppm.

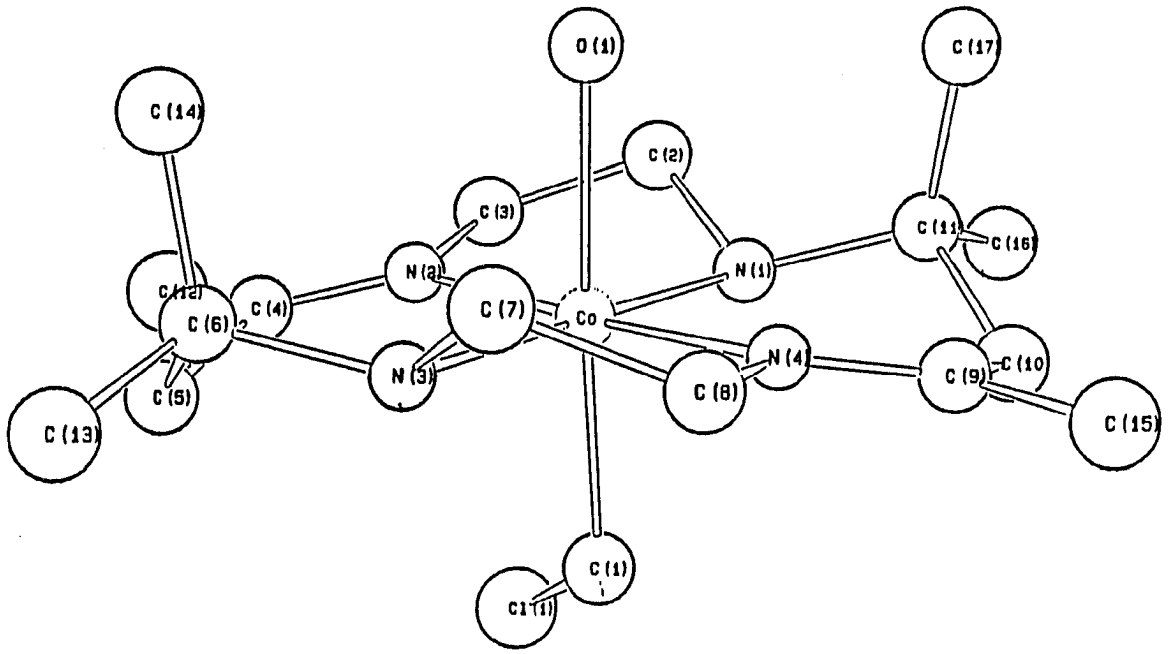

Figure II-2. The ORTEP of $CH_2ClCo(Me_6[14]4,11\text{-dieneN}_4)(H_2O)^{2+}$

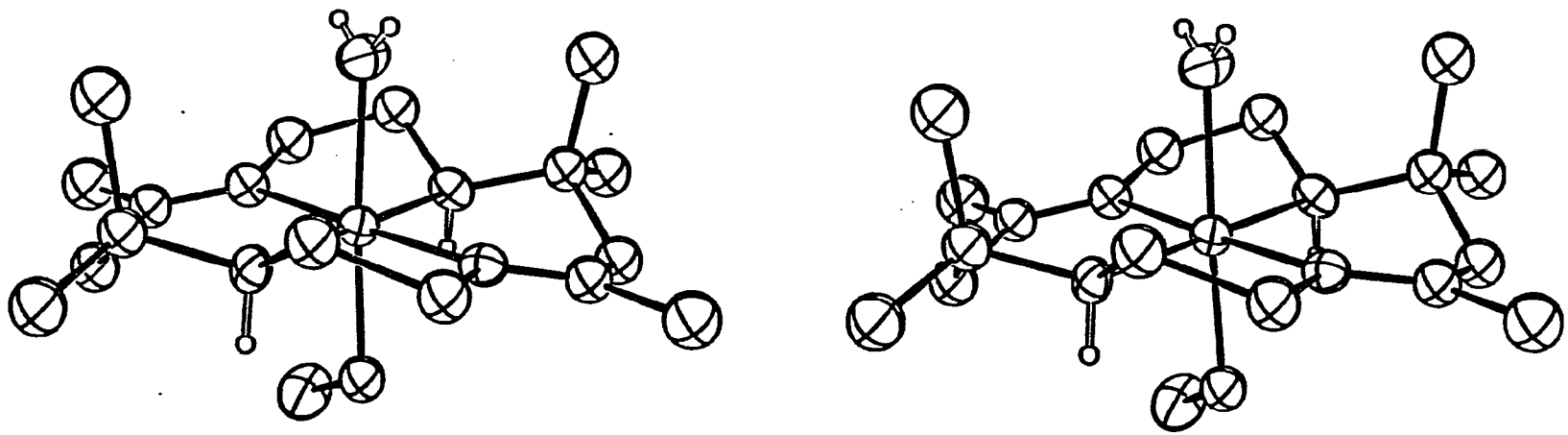

Figure II-3. The stereoview of $CH_2ClCo(Me_6[14]4,11\text{-dieneN}_4)(H_2O)^{2+}$

Table II-3. Crystallographic data for $CoC_{17}H_{36}Cl_3N_4O_9$

empirical formula	$CoC_{17}H_{36}Cl_3N_4O_9$
formula weight	605.79
space group	$P2_1/c$ (no. 14)
a, Å	15.315(2)
b, Å	9.012(3)
c, Å	18.998(5)
β, deg	105.47(2)
V, $Å^3$	2527(2)
Z, molecules/unit cell	4
d_{calc}, g/cm^3	1.592
crystal size, mm	0.24x0.42x0.13
μ(MoKα), cm^{-1}	10.48
data collection instrument	Enraf-Nonius CAD4
radiation (monochromated in incident beam)	MoKα(λ = 0.71073 Å)
orientation reflections, number, range(2θ)	21, 21.0-31.1
temperature, °C	-30
scan method	ω-scans
data col. range, 2θ, deg	4-45
no. unique data, total	3291
with $F_o^2 > 3\sigma(F_o^2)$	2229
number of parameters refined	234
correction factors, max., min.	1.12, 0.852
R[a]	0.0394
R_w[b]	0.0497
quality-of-fit indicator[c]	1.29
largest shift/esd, final cycle	0.01
largest peak, e/ $Å^3$	0.368

[a] $R = \Sigma||F_o| - |F_c|/ \Sigma|F_o|$.

[b] $R_w = [\ \Sigma w(|F_o| - |F_c|)^2/ \Sigma w|F_o|^2]^{1/2}$; $w = 1/\sigma^2(|F_o|)$.

[c] quality-of-fit$=[\Sigma w(|F_o|-|F_c|)^2/(N_{obs} - N_{parameters})]^{1/2}$.

Table II-4. Calculated bond distances for $CH_2ClCo(Me_6[14]4,11\text{-dieneN}_4)(H_2O)(ClO_4)_2$

atom pair	distance (Å)	atom pair	distance (Å)
Co-O1	2.062(4)	C2-C3	1.499(7)
Co-N1	1.985(4)	C4-C5	1.489(7)
Co-N2	1.923(4)	C4-C12	1.500(7)
Co-N3	1.981(4)	C5-C6	1.535(7)
Co-N4	1.929(4)	C6-C13	1.531(7)
Co-C1	1.965(5)	C6-C14	1.523(7)
C11-C1	1.796(5)	C7-C8	1.512(7)
O1-H1(O1)	0.76(7)	C9-C10	1.512(7)
O1-H2(O1)	0.62(8)	C9-C15	1.480(7)
N1-C2	1.499(6)	C10-C11	1.524(7)
N1-C11	1.510(6)	C11-C16	1.530(7)
N1-H(N1)	0.90(7)	C11-C17	1.520(7)
N2-C3	1.480(6)	C12-O2	1.434(3)
N2-C4	1.275(6)	C12-O3	1.399(5)
N3-C6	1.504(6)	C12-O4	1.397(4)
N3-C7	1.481(6)	C13-O6	1.418(4)
N3-H(N3)	0.83(7)	C13-O7	1.432(4)
N4-C8	1.481(6)	C13-O8	1.397(4)
N4-C9	1.287(6)	C13-O9	1.410(4)

Table II-5. Bond angles in $CH_2ClCo(Me_6[14]4,11\text{-}dieneN_4)(H_2O)(ClO_4)_2$

atoms	angle	atoms	angle
O1-Co-N1	90.0(2)	Co-N2-N4	128.1(3)
O1-Co-N2	88.7(1)	C3-N2-C4	119.0(4)
O1-Co-N3	90.4(2)	Co-N3-C6	120.8(3)
O1-Co-N4	88.7(1)	Co-N3-C7	105.7(3)
O1-Co-C1	176.6(2)	Co-N3-H(N3)	105.(5)
N1-Co-N2	85.6(1)	C6-N3-C7	115.8(4)
N1-Co-N3	179.7(2)	C6-N3-H(N3)	101.(5)
N1-Co-N4	94.6(1)	C7-N3-H(N3)	108.(5)
N1-Co-C1	89.6(1)	Co-N4-C8	111.9(3)
N2-Co-N3	94.3(2)	Co-N4-C9	128.7(3)
N2-Co-N4	177.4(1)	C8-N4-C9	119.2(4)
N2-Co-C1	94.6(2)	Co-C1-C11	115.4(2)
N3-Co-N4	85.5(2)	N1-C2-C3	108.0(4)
N3-Co-C1	90.1(2)	N2-C3-C2	110.7(4)
N4-Co-C1	88.0(1)	N2-C4-C5	121.0(5)
Co-O1-H1(O1)	129.(6)	N2-C4-C12	122.2(5)
Co-O1-H2(O1)	124.(8)	C5-C4-C12	116.6(4)
H1(O1)-O1-H2(O1)	107.(9)	C4-C5-C6	116.4(4)
Co-N1-C2	106.0(3)	N3-C6-C5	106.1(3)
Co-N1-C11	121.1(3)	N3-C6-C13	109.3(4)
Co-N1-H(N1)	102.(4)	N3-C6-C14	113.0(4)

Table II-5 (Continued)

atoms	angle	atoms	angle
C2-N1-C11	114.2(4)	C5-C6-C13	108.3(4)
C2-N1-H(N1)	106.(4)	C5-C6-C14	111.1(4)
C11-N1-H(N1)	106.(4)	C13-C6-C14	108.9(3)
CO-N2-C3	112.4(2)	N3-C7-C8	107.1(4)
N4-C8-C7	109.3(4)	C16-C11-C17	109.3(4)
N4-C9-C10	121.2(4)	O2-C12-O3	107.7(3)
N4-C9-C15	123.1(4)	O2-C12-O4	110.5(2)
C10-C9-C15	115.7(4)	O3-C12-O4	110.4(4)
C9-C10-C11	117.9(4)	O6-C13-O7	108.2(2)
N1-C11-C10	107.6(4)	O6-C13-O8	109.4(4)
N1-C11-C16	108.3(4)	O6-C13-O9	108.3(3)
N1-C11-C17	113.1(3)	O7-C13-O8	110.0(2)
C10-C11-C16	108.3(3)	O7-C13-O9	110.5(3)
C10-C11-C17	110.0(4)	O8-C13-O9	110.5(3)

Table II-6. Atomic coordinates for $CH_2ClCo(Me_6[14]4,11\text{-}dieneN_4)(H_2O)(ClO_4)_2$

atom	x	y	z	B(Å^2)
Co	0.26266(4)	0.13705(8)	0.91055(4)	1.81(1)
Cl1	0.41976(9)	0.0450(2)	1.05029(4)	3.84(4)
O1	0.1392(2)	0.1021(4)	0.8360(2)	2.64(8)
N1	0.3099(3)	-0.0479(5)	0.8774(2)	2.21(9)
N2	0.2236(3)	0.0116(4)	0.9782(2)	1.96(9)
N3	0.2161(2)	0.3216(4)	0.9441(2)	1.92(9)
N4	0.2964(2)	0.2620(5)	0.8397(2)	1.96(9)
C1	0.3830(3)	0.1754(6)	0.9769(3)	2.4(1)[a]
C2	0.2499(3)	-0.1705(6)	0.8903(3)	2.8(1)[a]
C3	0.2347(4)	-0.1480(7)	0.9643(3)	2.9(1)[a]
C4	0.1999(3)	0.0498(6)	1.0351(3)	2.2(1)[a]
C5	0.1957(3)	0.2090(6)	1.0548(3)	2.6(1)[a]
C6	0.1524(3)	0.3154(6)	0.9921(3)	2.4(1)[a]
C7	0.1873(3)	0.4172(6)	0.8787(3)	2.5(1)[a]
C8	0.2630(3)	0.4158(6)	0.8414(3)	2.4(1)[a]
C9	0.3478(3)	0.2311(6)	0.7980(3)	2.2(1)[a]

[a]Atoms were defined isotropically. Anistropically refined atoms are given in the form of the isotropic equivalent displacement parameter defined as : $(4/3)x[a^2xB(1,1)+b^2xB(2,2)+C^2xB(3,3)+ab(cos\gamma)xB(1,2)+ac(cos\beta)xB(1,3)+bc(cos\alpha)xB(2,3)]$.

Table II-6 (Continued)

atom	x	y	z	B(Å^2)
C10	0.3894(3)	0.0787(6)	0.7985(3)	2.6(1)[a]
C11	0.3312(3)	-0.0556(6)	0.8043(3)	2.4(1)[a]
C12	0.1837(4)	-0.0616(7)	1.0889(3)	3.7(1)[a]
C13	0.1462(4)	0.4692(7)	1.0246(3)	3.0(1)[a]
C14	0.0575(4)	0.2643(7)	0.9515(3)	3.1(1)[a]
C15	0.3721(4)	0.3407(7)	0.7484(3)	3.1(1)[a]
C16	0.3870(4)	-0.1957(7)	0.8027(3)	3.2(1)[a]
C17	0.2469(4)	-0.0581(7)	0.7402(3)	3.0(1)[a]
Cl2	0.01143(8)	0.2800(2)	0.67401(7)	3.07(3)
Cl3	0.58482(9)	0.0638(2)	0.41554(7)	2.85(3)
O2	0.1073(2)	0.2700(5)	0.7059(2)	4.2(1)
O3	-0.0142(4)	0.1602(7)	0.6262(3)	8.7(2)
O4	-0.0348(3)	0.2759(8)	0.7282(2)	7.7(2)
O5	0.0080(3)	-0.0876(6)	0.8677(3)	7.3(1)
O6	0.6070(3)	-0.0651(5)	0.3811(2)	5.5(1)
O7	0.6356(3)	0.0611(5)	0.4907(2)	3.8(1)
O8	0.4921(3)	0.0638(8)	0.4104(3)	7.7(2)
O9	0.6082(4)	0.1892(5)	0.3801(2)	7.1(2)
H(N1)	0.363(4)	-0.059(8)	0.911(3)	4.0[a]
H(N3)	0.261(4)	0.360(8)	0.972(4)	4.0[a]
H1(O1)	0.116(4)	0.147(8)	0.802(4)	4.0[a]
H2(O1)	0.112(4)	0.054(8)	0.840(4)	4.0[a]

Table II-7. Torsion angles in $CH_2ClCo(Me_6[14]4,11\text{-}dieneN_4)(H_2O)^{2+}$

atom1	atom2	atom3	atom4	angle
O1	Co	N1	C2	-58.85(0.32)
O1	Co	N1	C11	72.20(0.38)
N2	Co	N1	C2	29.70(0.33)
N2	Co	N1	C11	160.75(0.40)
N3	Co	N1	C2	120.66(10.03)
N3	Co	N1	C11	-108.30(10.03)
N4	Co	N1	C2	-147.69(0.33)
N4	Co	N1	C11	-16.65(0.40)
C1	Co	N1	C2	124.49(0.35)
C1	Co	N1	C11	-104.47(0.40)
O1	Co	N2	C3	81.69(0.35)
O1	Co	N2	C4	-106.25(0.47)
N1	Co	N2	C3	-8.70(0.36)
N1	Co	N2	C4	163.35(0.49)
N3	Co	N2	C3	172.31(0.35)
N3	Co	N2	C4	-15.64(0.49)
N4	Co	N2	C3	83.95(4.14)
N4	Co	N2	C4	-104.00(4.07)
C1	Co	N2	C3	-97.62(0.38)
C1	Co	N2	C4	74.43(0.49)
O1	Co	N3	C6	74.48(0.36)
O1	Co	N3	C7	-58.01(0.32)
N1	Co	N3	C6	-105.02(10.06)
N1	Co	N3	C7	122.48(10.02)
N2	Co	N3	C6	-14.15(0.38)
N2	Co	N3	C7	-146.64(0.32)
N4	Co	N3	C6	163.25(0.37)
N4	Co	N3	C7	30.75(0.32)
C1	Co	N3	C6	-108.85(0.38)

Table II-7 (Continued)

atom1	atom2	atom3	atom4	angle
C1	Co	N3	C7	118.65(0.34)
O1	Co	N4	C8	84.15(0.34)
O1	Co	N4	C9	-101.78(0.47)
N1	Co	N4	C8	174.34(0.34)
N1	Co	N4	C9	-11.59(0.48)
N2	Co	N4	C8	81.89(4.14)
N2	Co	N4	C9	-104.03(4.07)
N3	Co	N4	C8	-6.67(0.34)
N3	Co	N4	C9	167.40(0.48)
C1	Co	N4	C8	-96.55(0.36)
C1	Co	N4	C9	77.53(0.48)
O1	Co	C1	Cl1	-148.87(3.22)
N1	Co	C1	Cl1	-66.18(0.31)
N2	Co	C1	Cl1	19.33(0.32)
N3	Co	C1	Cl1	113.75(0.30)
N4	Co	C1	Cl1	-160.74(0.31)
Co	N1	C2	C3	-44.35(0.48)
C11	N1	C2	C3	-179.18(0.45)
Co	N1	C11	C10	50.21(0.53)
Co	N1	C11	C16	166.77(0.36)
Co	N1	C11	C17	-71.88(0.55)
C2	N1	C11	C10	177.63(0.44)
C2	N1	C11	C16	-65.81(0.56)
C2	N1	C11	C17	55.53(0.62)
Co	N2	C3	C2	-14.82(0.55)
C4	N2	C3	C2	172.32(0.49)
Co	N2	C4	C5	3.07(0.76)
Co	N2	C4	C12	-170.04(0.41)
C3	N2	C4	C5	174.69(0.48)
C3	N2	C4	C12	0.88(0.78)

Table II-7 (Continued)

atom1	atom2	atom3	atom4	angle
Co	N3	C6	C5	50.46(0.51)
Co	N3	C6	C13	166.73(0.34)
Co	N3	C6	C14	-71.63(0.54)
C7	N3	C6	C5	178.68(0.43)
C7	N3	C6	C13	-65.04(0.55)
C7	N3	C6	C14	56.60(0.62)
Co	N3	C7	C8	-47.82(0.46)
C6	N3	C7	C8	176.78(0.43)
Co	N4	C8	C7	-18.87(0.51)
C9	N4	C8	C7	166.42(0.46)
Co	N4	C9	C10	1.78(0.75)
Co	N4	C9	C15	-176.84(0.39)
C8	N4	C9	C10	175.48(0.47)
C8	N4	C9	C15	-3.14(0.76)
N1	C2	C3	N2	39.18(0.60)
N2	C4	C5	C6	43.58(0.74)
C12	C4	C5	C6	-142.28(0.52)
C4	C5	C6	N3	-68.62(0.58)
C4	C5	C6	C13	174.55(0.47)
C4	C5	C6	C14	54.90(0.64)
N3	C7	C8	N4	44.02(0.55)
N4	C9	C10	C11	39.72(0.73)
C15	C9	C10	C11	-141.56(0.51)
C9	C10	C11	N1	-64.32(0.59)
C9	C10	C11	C16	179.06(0.46)
C9	C10	C11	C17	59.97(0.63)

The atomic coordinates, Table II-6, and the torsion angles, Table II-7, have also been included in the crystallographic data.

Isomerization of $RCo(Me_6[14]4,11\text{-}dieneN_4)^{2+}$

The isomerization for $RCo(Me_6[14]4,11\text{-}dieneN_4)^{2+}$(R = Me, Et, and n-Pr) has been observed from their ^1H NMR spectrum study. A typical example of $CH_3Co(Me_6[14]4,11\text{-}dieneN_4)^{2+}$ is shown in Figure II-4. The $Co\text{-}CH_3$ singlet is located at δ1.65 and 1.38 ppm for N-meso and N-racemic isomers of $CH_3Co(Me_6[14]4,11\text{-}dieneN_4)^{2+}$, respectively. The chemical shifts for the $Co\text{-}CH_3$ resonance in these two isomers are consistent with those conducted by Roche and Endicott.[3] Figure II-4a shows the ^1H NMR spectrum of the N-meso isomer with little amount of N-racemic isomer as a result of isomerization. In the course of study, the peak at δ1.65 shift to δ1.38 ppm as shown in Figure II-4b and II-4c. Eventually, all the N-meso isomer converts to N-racemic isomer as shown in Figure II-4d. It is interesting to notice that the two smaller singlets, δ1.12(3H) and δ0.99(3H) ppm, collapsed into a larger singlet, δ1.05 ppm(6H). This clearly suggests that the configuration of the macrocycle ligand has been changed in the course of study.

Homolysis of $EtCo(Me_6[14]4,11\text{-}dieneN_4)^{2+}$

Dilute acidic aqueous[4] solutions of $EtCo(Me_6[14]4,11\text{-}dieneN_4)^{2+}$, hereafter $EtCoL^{2+}$, decompose at room temperature to yield equivalent amount of C_2H_4 and C_2H_6. Since very

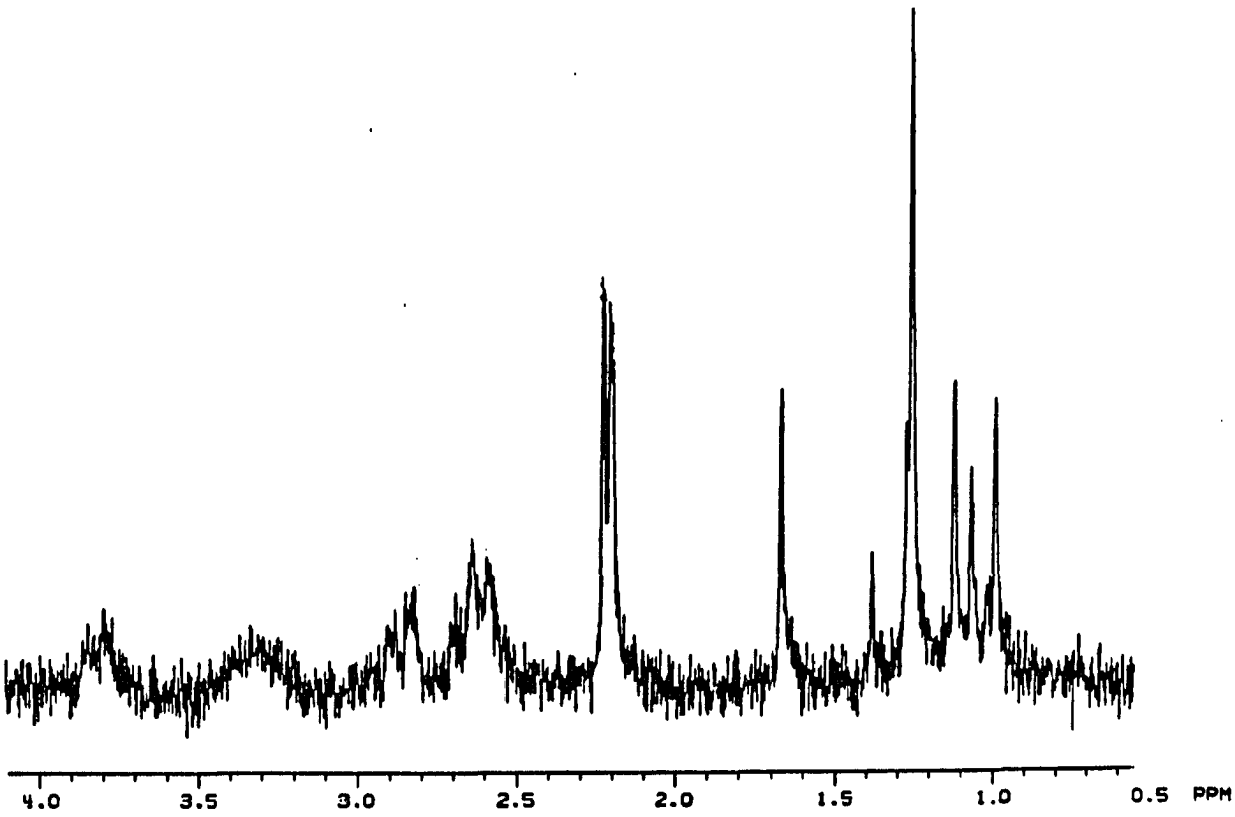

Figure II-4a. ^{1}H NMR spectrum of $MeCo(Me_6[14]4,11\text{-}dieneN_4)^{2+}$ in D_2O, t = 20 min

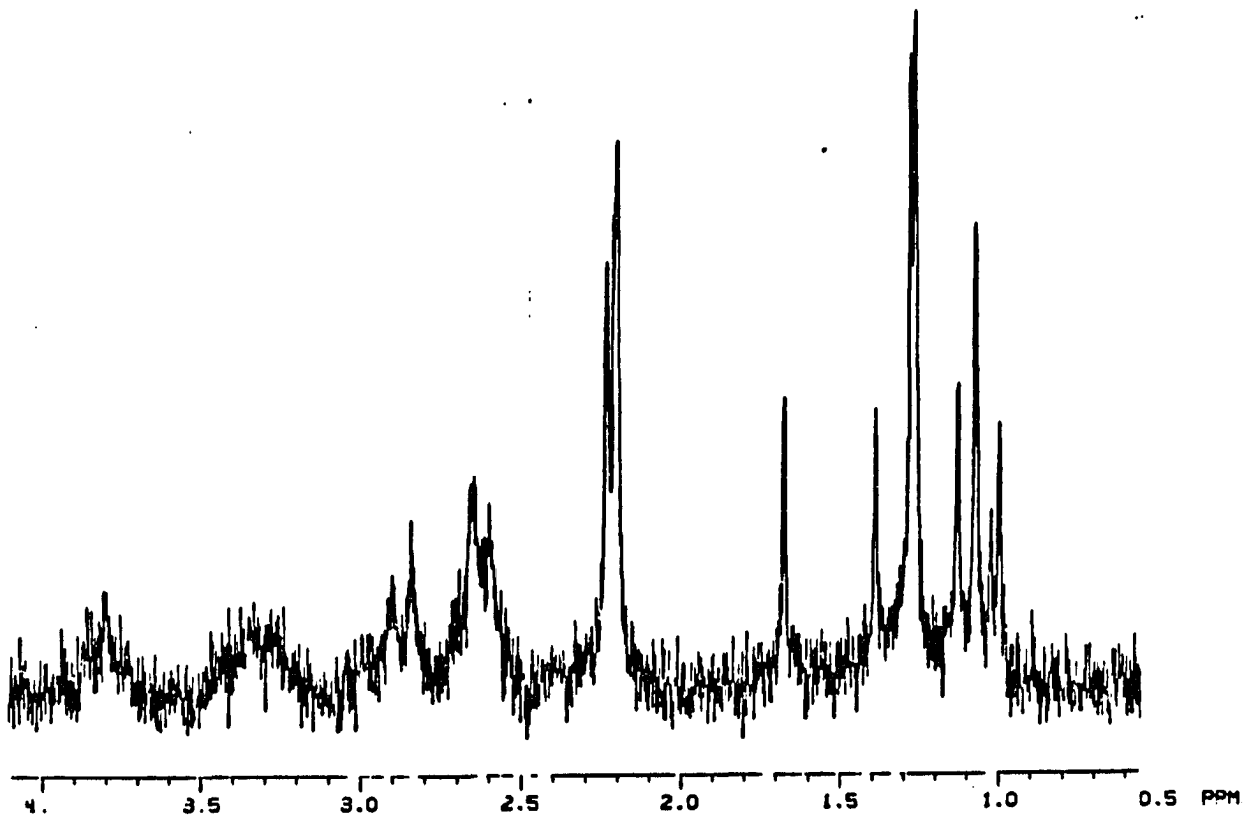

Figure II-4b. ^1H NMR spectrum of $MeCo(Me_6[14]4,11\text{-dieneN}_4)^{2+}$ in D_2O, t = 45 min

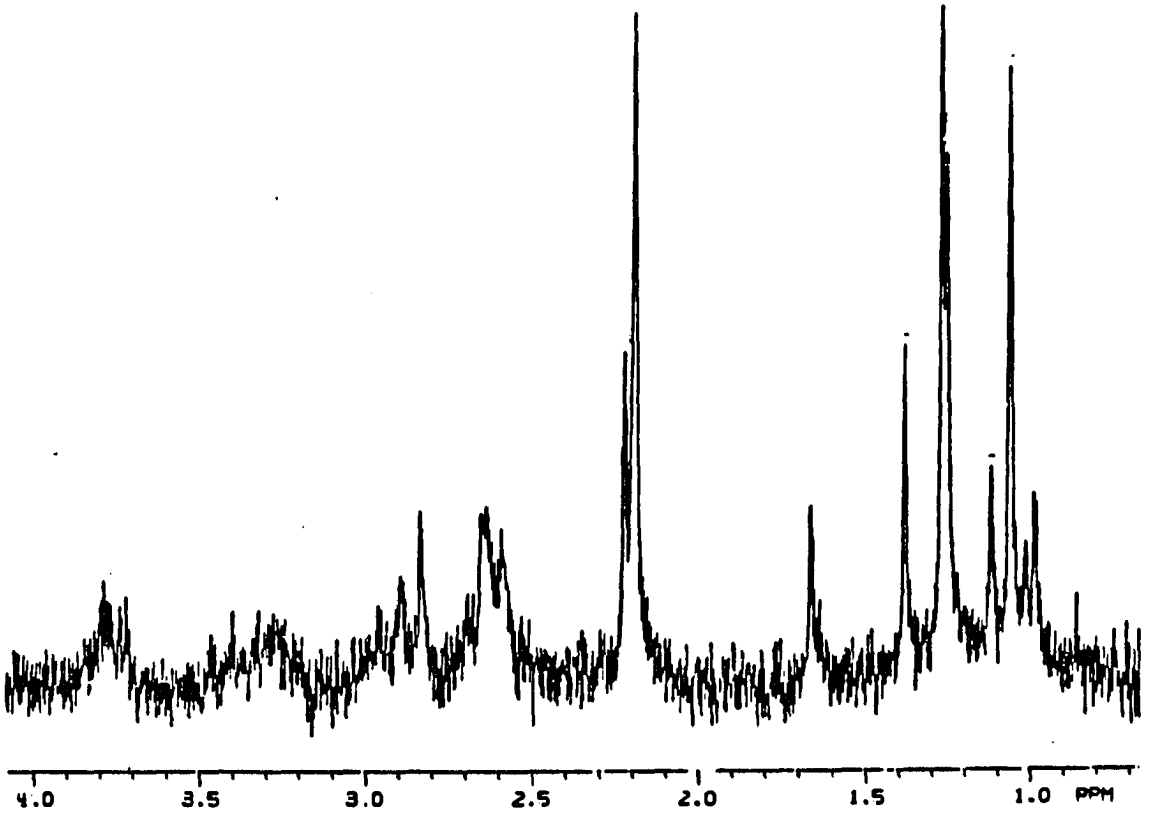

Figure II-4c. ^{1}H NMR spectrum of $MeCo(Me_6[14]4,11\text{-dieneN}_4)^{2+}$ in D_2O, t = 86 min

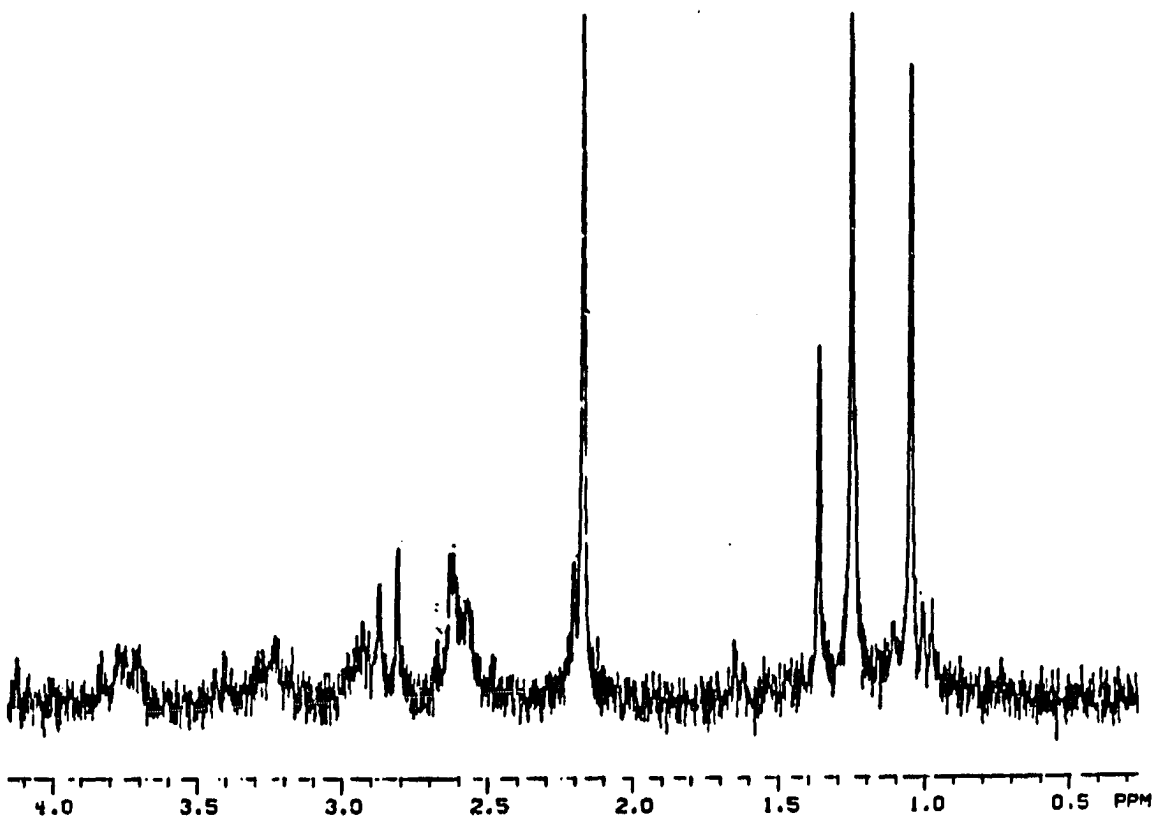

Figure II-4d. ^1H NMR spectrum of $MeCo(Me_6[14]4,11\text{-dieneN}_4)^{2+}$ in D_2O, t = 775 min

little of $n\text{-}C_4H_{10}$ was observed (~3%), this strongly suggests that ethyl radical was attacked by $EtCoL^{2+}$ especially the concentration of ethyl radical at steady state was low in this case. The visible spectrum shows two peaks (λ440, 325 nm) which are diagnostic of CoL^{2+}.[5] All the reactions involved are listed in Scheme III.

Scheme III.

$$EtCoL^{2+} \longrightarrow Et\cdot + CoL^{2+} \qquad (6)$$

$$Et\cdot + EtCoL^{2+} \longrightarrow C_2H_4 + C_2H_6 + CoL^{2+} \qquad (7)$$

The loss of organocobalt is accelerated by addition of Cr^{2+}, Fe^{3+}, $Co(NH_3)_5Br^{2+}$, O_2 and HTMPO; i.e., reagents that react rapidly with CoL^{2+} or ethyl radical.[6] The kinetics of these reactions were studied under pseudo-first-order conditions with the scavenger in excess. The pseudo-first-order rate constants are listed in Table A-1 and A-2. The kinetic result shows no dependence on the concentration of scavenger except the reaction with Cr^{2+}. The k_h, unimolecular homolysis rate constant, was obtained as an intercept from the plot of k_{obs} vs. $[Cr^{2+}]$ in the reaction with Cr^{2+}. All the k_h values and products observed from the G.C. spectrum are listed in Table II-8.

Activation parameters ($\Delta H^{\neq}$, $\Delta S^{\neq}$)

The kinetics of homolysis were studied at different temperatures for these organocobalt complexes ($RCoL^{2+}$; R =

Table II-8. Kinetic result and product analysis from the decomposition of $EtCo(Me_6[14]4,11\text{-dieneN}_4)^{2+}$ with the presence of scavengers[a]

scavenger	k_h/s^{-1}	product
Cr^{2+}	3.4×10^{-4}[b]	C_2H_6(~95%), C_2H_4(~5%)
$Co(NH_3)_5Br^{2+}$	4.2×10^{-4}[c]	C_2H_5Br, C_2H_4, C_2H_6
O_2	3.9×10^{-4}[d]	C_2H_4
HTMPO	4.7×10^{-4}[d]	C_2H_4

[a] $T = 25 \pm 0.1$ °C.

[b] $\mu = 0.14$ M. Extrapolated to $[Cr^{2+}] = 0$ M.

[c] $\mu = 0.5$ M.

[d] $\mu = 0.1$ M.

Et, n-Pr; L = $Me_6[14]aneN_4$, $Me_6[14]4,11\text{-}dieneN_4$). All these rate constants are listed in Table A-3 to A-6 for $EtCo(Me_6[14]4,11\text{-}dieneN_4)^{2+}$, $n\text{-}PrCo(Me_6[14]4,11\text{-}dieneN_4)^{2+}$, $EtCo(Me_6[14]aneN_4)^{2+}$, $n\text{-}PrCo(Me_6[14]aneN_4)^{2+}$ respectively. The plots of ln(k/T) against 1/T are linear for all the cases as shown in Figure A-1 to A-4. The values of ΔH and ΔS are calculated from Eyring equation and listed in Table II-9.

Rate constant of the reaction of Me· with $MeCo(Me_6[14]4,11\text{-}dieneN_4)^{2+}$

A check of the distribution of the products for the reaction of Fe^{2+} with t-amyl hydroperoxide in the presence of $MeCo(Me_6[14]4,11\text{-}dieneN_4)^{2+}$ was made. The products are methane, ethane, ethylene, propane and butane with a ratio as 3:27:21:30:19. The reaction was slower than that in the absence of methylcobalt complex (the amounts of the products formed in the same time scale). It suggests there are many steps as the following:

$$Fe^{2+} + EtC(CH_3)_2OOH \longrightarrow Fe(OH)^{2+} + Et(CH_3)_2CO\cdot \quad (8)$$

$$Et(CH_3)_2CO\cdot \longrightarrow Et\cdot + (CH_3)_2CO \quad (9)$$

$$Et(CH_3)_2CO\cdot \longrightarrow \cdot CH_3 + (Et)(CH_3)CO \quad (10)$$

$$2\cdot CH_3 \longrightarrow C_2H_6 \quad (11)$$

$$2Et\cdot \begin{cases} \longrightarrow C_2H_4 + C_2H_6 \\ \longrightarrow C_4H_{10} \end{cases} \quad (12)$$

$$Et\cdot + MeCoL^{2+} \longrightarrow C_3H_8 + CoL^{2+} \quad (13)$$

Table II-9. Activation parameters of unimolecular homolysis and D_{Co-C} of alkylcobalt complexes, $RCoL^{n+}$

$RCoL^{n+}$	$\Delta H^{\neq}$/kcal mol^{-1}	$\Delta S^{\neq}$/cal$mol^{-1}K^{-1}$	D_{Co-C}/kcal mol^{-1}
$EtCo(Me_6[14]4,11\text{-}dieneN_4)^{2+}$	25.1 ± 0.9	10 ± 3	23
$n\text{-}PrCo(Me_6[14]4,11\text{-}dieneN_4)^{2+}$	26.6 ± 0.9	14 ± 3	25
$EtCo(Me_6[14]aneN_4)^{2+}$	25.6 ± 0.6	12 ± 2	24
$n\text{-}PrCo(Me_6[14]aneN_4)^{2+}$	26.5 ± 0.8	15 ± 3	25

$$Et\cdot + MeCoL^{2+} \rightleftharpoons Me\cdot + EtCoL^{2+} \quad (14)$$

$$Et\cdot + EtCoL^{2+} \longrightarrow C_2H_4 + C_2H_6 + CoL^{2+} \quad (7)$$

The decreased ratio of butane to ethane and ethylene could be explained by equation (14) and (7). Owing to the high concentration of $MeCoL^{2+}$, the equilibrium of the reaction (14) could be driven to the right although ethyl radical is more stable than methyl radical. However, the formation of propane strongly suggests there is a reaction between ethyl radical and methylcobalt complex.

The kinetics of the reaction of Me· with $MeCo(Me_6[14]4,11\text{-dieneN}_4)^{2+}$ was then studied by using laser flash photolysis. The $ABTS^-$ was used as a chromophore in these reactions. The reaction steps are presented as the following. The methyl radical is formed by photohomolysis

$$MeCoL^{2+} \longrightarrow Me\cdot + CoL^{2+} \ (L = Me_6[14]4,11\text{-dieneN}_4) \quad (15)$$

$$Me\cdot + MeCoL^{2+} \xrightarrow{k_2} C_2H_6 + CoL^{2+} \quad (16)$$

$$Me\cdot + Me\cdot \xrightarrow{k_c} C_2H_6 \quad (11)$$

$$Me\cdot + ABTS^- \xrightarrow{k_{ABTS}} \text{products} \quad (17)$$

of $MeCo(Me_6[14]4,11\text{-dieneN}_4)^{2+}$. Then the radical reacts with methylcobalt complex and $ABTS^-$ as well as itself to give different products. The rate law of this reaction is presented in equation 18. The disappearance of methyl radical

$$-d[Me\cdot]/dt = (k_2\,[MeCoL^{2+}] + k_{ABTS}\,[ABTS^-] + 2k_c\,[Me\cdot])\,[Me\cdot] \quad (18)$$

$$k_{obs} = k_2[MeCoL^{2+}] + k_{ABTS}[ABTS^-] + 2k_c[Me\cdot] \quad (19)$$

can be measured by monitoring the disappearance of $ABTS^-$ at λ650 nm ($\varepsilon = 10050\ M^{-1}cm^{-1}$). Table A-7 gives k_{obs} as well as k_{corr} ($k_{corr} = k_{obs} - k_{ABTS}[ABTS^-] - 2k_c[Me\cdot]$). The plot of k_{corr} vs. $[MeCoL^{2+}]$, Figure II-5, is linear, showing the first-order dependence of the rate on the methylcobalt complex concentration. The k_2 is therefore calculated from the slope of the line as $4.7 \times 10^7\ M^{-1}s^{-1}$.

Reaction of $RCoL^{2+}$ with Cr^{2+}

The reactions occur according to equation 20. Then

$$RCoL^{2+} + Cr^{2+} \longrightarrow CrR^{2+} + CoL^{2+} \quad (20)$$

the organochromium complex will follow an acid hydrolysis as

$$(H_2O)_5CrR^{2+} + H^+ \longrightarrow RH + Cr(H_2O)_6{}^{3+} \quad (21)$$

shown in equation 21. All the reactions of $RCoL^{2+}$ with Cr^{2+} were studied kinetically under pseudo-first-order conditions with Cr^{2+} in excess. For L = Me_6[14]4,11-dieneN$_4$, the rate constants for the reactions were obtained from an analysis of the decrease in absorbance at λ480 nm vs. time data. For L =

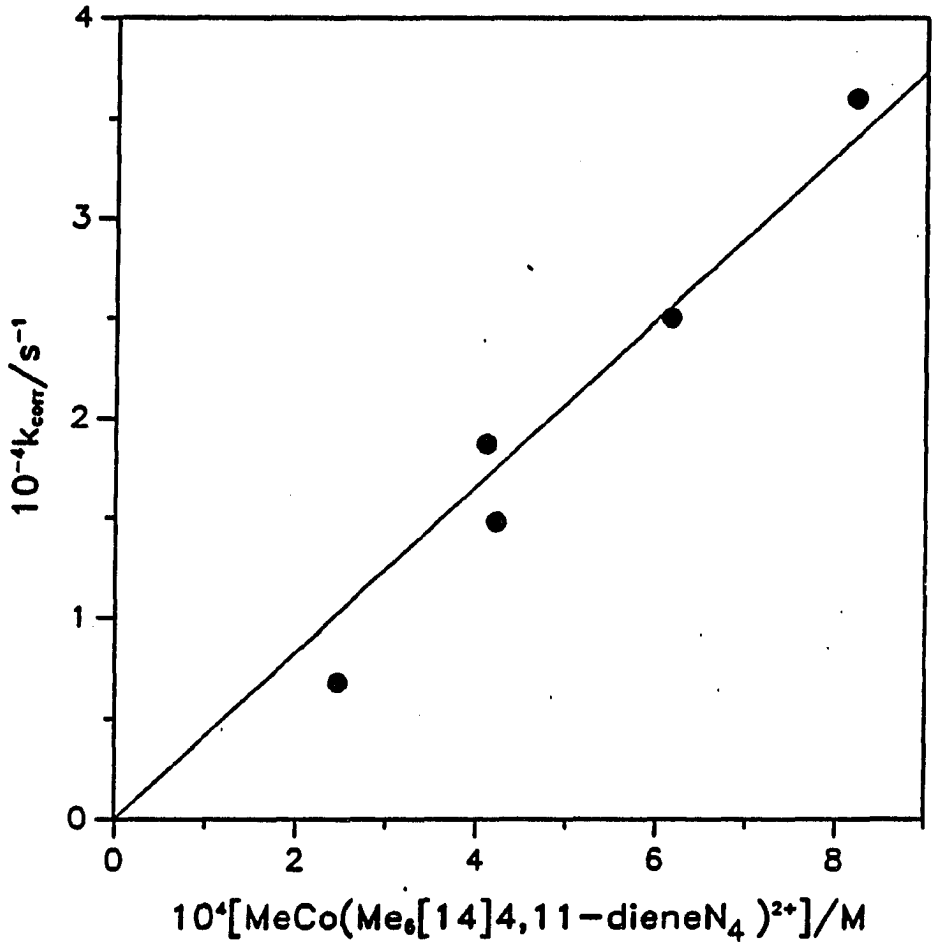

Figure II-5. The dependence of k_{corr} on $[CH_3Co(Me_6-[14]4,11\text{-}dieneN_4)^{2+}]$ for the reaction of $\cdot CH_3$ with $MeCo(Me_6[14]4,11\text{-}dieneN_4)^{2+}$

$Me_6[14]aneN_4$, the reactions were followed by monitoring at λ390 nm. which is the maximum of CrR^{2+}. Therefore an increase in absorbance were observed owing to reaction 20, then a decrease in absorbance was observed owing to reaction 21. In the case of $Etco(Me_6[14]aneN_4)^{2+}$, a consecutive treatment was made. Tables A-8 to A-12 give the pseudo-first-order rate constants, k_{obs}. Plots of k_{obs} vs. $[Cr^{2+}]$ were linear in all cases, showing the first-order dependence of the rate on Cr^{2+} concentration. A typical example for the reaction of $MeCoL^{2+}$ with Cr^{2+} is shown in Figure II-6. The intercept shows the value for unimolecular homolysis rate constant in the cases of R = Et, n-Pr. These results also show good agreement with those obtained by using different scavengers. Table II-10 gives all the second order rate constant and the final product analysis of these reactions. Thus the reaction between $RCoL2^{+}$ and Cr^{2+} follows the second-order rate law shown in equation 22.

$$-d[RCoL^{2+}]/dt = (k_h + k\,[Cr^{2+}])\,[RCoL^{2+}] \qquad (22)$$

$$k_{obs} = k_h + k\,[Cr^{2+}] \qquad (23)$$

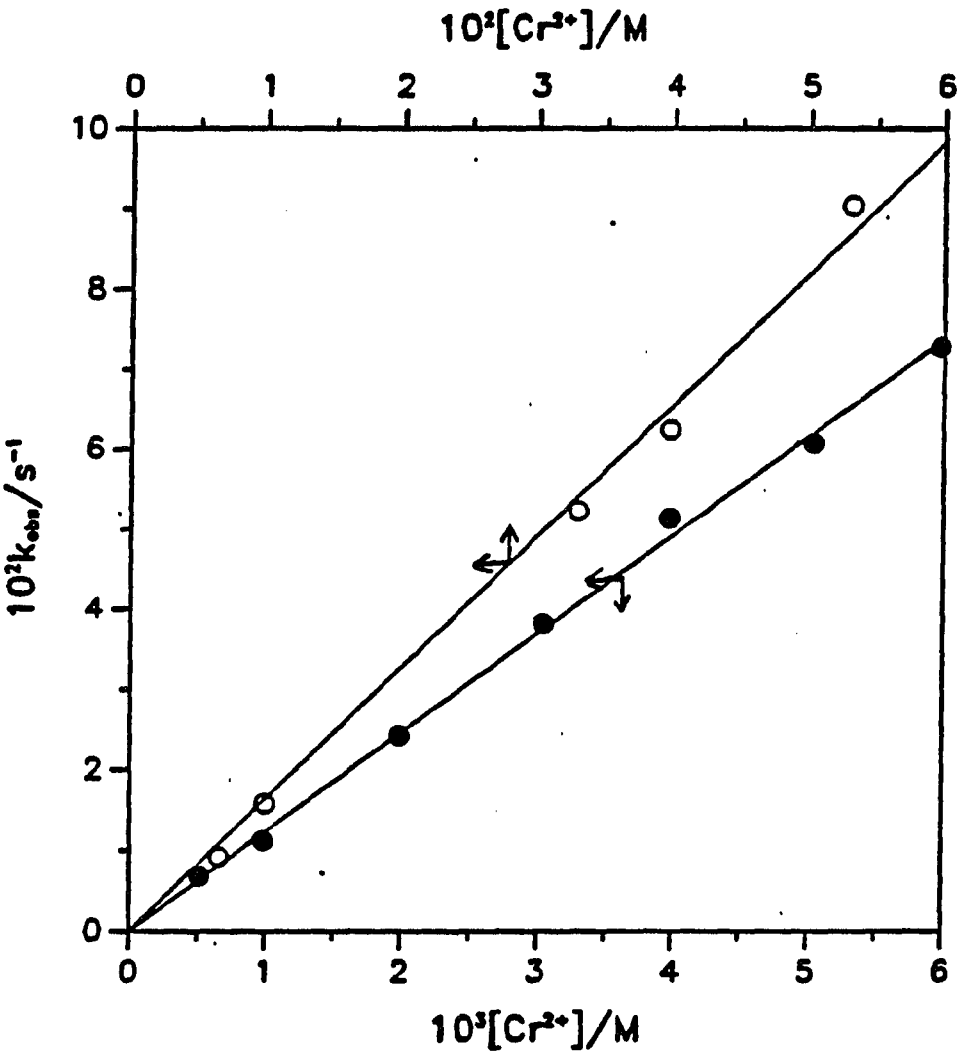

Figure II-6. The dependence of k_{obs} on $[Cr^{2+}]$ for the reaction of $MeCoL^{2+}$ with Cr^{2+}. The upper line is for $MeCo(Me_6[14]aneN_4)^{2+}$. The lower line is for $MeCo(Me_6[14]4,11\text{-}dieneN_4)^{2+}$

Table II-10. Summary of kinetic results for the reaction of $RCoL^{2+}$ with Cr^{2+}

$RCoL^{2+}$	$k/M^{-1}s^{-1}$ [a]
$MeCo(Me_6[14]4,11\text{-}dieneN_4)^{2+}$	12.3 ± 0.2
$EtCo(Me_6[14]4,11\text{-}dieneN_4)^{2+}$	(3.6 ± 0.2) x 10^{-2}
$n\text{-}PrCo(Me_6[14]4,11\text{-}dieneN_4)^{2+}$	(5 ± 1) x 10^{-4}
$MeCo(Me_6[14]aneN_4)^{2+}$	1.64 ± 0.03
$EtCo(Me_6[14]aneN_4)^{2+}$	(5.4 ± 0.4) x 10^{-3}

[a] At T = 25.0 ± 0.1 °C and μ = 1.0 M.

DISCUSSION

Preparation of the organocobalt complexes

The preparation of the organocobalt complexes is based on the photochemistry of the organocobaloximes. Photolysis yields an alkyl radical and $Co(dmgH)_2$. In the acidic solution

$$RCo(dmgH)_2py \longrightarrow R\cdot + Co(dmgH)_2py \qquad (3)$$

$Co(dmgH)_2py$ will decompose to Co^{2+}, pyH^+ and $dmgH_2$ rapidly.[30]

$$Co(dmgH)_2py + 3H^+ \longrightarrow Co^{2+} + 2dmgH_2 + pyH^+ \qquad (4)$$

This rapid decomposition minimizes the recapture of R· by

$$R\cdot + CoL^{2+} \longrightarrow RCoL^{2+} \qquad (5)$$

$Co(dmgH)_2$ to form organocobaloximes. The relatively strong absorption of these organocobaloximes provides a good protection during the course of the preparation of these product organocobalt complexes which are photosensitive. In the original preparation of the methyl complex,[3,4] the radical was generated by photohomolysis of $(NH_3)_5CoO_2CCH_3^{2+}$. The low yield of the methyl complex and the inability to prepare complexes with other alkyl groups may be related to the low absorption coefficients of $(NH_3)_5CoO_2CCH_3^{2+}$ relative to those

of product organocobalt complex and the ready photohomolysis of the latter. The photochemical steps and the capture of the radical are quite efficient, resulting in a good yield of $(H_2O)LCoR^{2+}$ in solution.

$MeCoL^{2+}$ (L = $Me_6[14]aneN_4$, $Me_6[14]4,11\text{-}dieneN_4$) can be prepared from the reaction of CoL^{2+} with t-butyl hydroperoxide. The ^1H NMR and visible spectra of these products are identical to those of the products obtained from different preparative methods. This method is also available for preparing $EtCo(Me_6[14]4,11\text{-}dieneN_4)^{2+}$. The possible reaction mechanism is described as follows. Since the organocobalt complex is easily separated from the Co^{3+} complex and the reaction is fast, this method provides a simple way to prepare methylcobalt complexes.

$$RCMe_2OOH + CoL^{2+} \longrightarrow RCMe_2O\cdot + CoLOH^{2+} \quad (24)$$

$$RCMe_2O\cdot \longrightarrow R\cdot + Me_2CO \quad (25)$$

$$R\cdot + CoL^{2+} \longrightarrow RCoL^{2} \quad (5)$$

The $CH_2OHCo(Me_6[14]4,11\text{-}dieneN_4)^{2+}$ and $CH_3OCH_2Co(Me_6[14]4,11\text{-}dieneN_4)^{2+}$ were prepared by the reaction of $(H_2O)LCo^{2+}$ with H_2O_2 in the presence of methanol or dimethyl ether (Fenton's reaction). The reaction mechanism is described as follows.

$$CoL^{2+} + H_2O_2 \longrightarrow CoLOH^{2+} + OH\cdot \quad (26)$$

$$MeOH\ (MeOCH_3) + OH\cdot \longrightarrow \cdot CH_2OH\ (\cdot CH_2OCH_3) + H_2O \quad (27)$$

$$\cdot CH_2OH(\cdot CH_2OCH_3) + CoL^{2+} \longrightarrow CH_2OHCoL^{2+}(CH_3OCH_2CoL^{2+}) \quad (28)$$

The decomposition product of $CH_2OHCo(Me_6[14]4,11\text{-dieneN}_4)^{2+}$ is formaldehyde, as expected. An attempt to prepare a crystalline sample of this complex was not successful. The Fenton's reaction method was employed to prepare $MeCo(Me_6[14]4,11\text{-dieneN}_4)^{2+}$, in the presence of DMSO, too. The ^1H NMR and visible spectra of this product are the same as those of the product obtained from different preparative methods. This strongly suggests Fenton's reaction is a successful preparation method in diene system. However, only the Co(III) complex was observed when this method was employed to prepare $CH_2OHCo(Me_6[14]aneN_4)^{2+}$.

Two peaks, λ_{max} = 366(s), 502 nm, were observed when t-butyl alcohol was present in the reaction of $Co(Me_6[14]4,11\text{-dieneN}_4)^{2+}$ with H_2O_2. It indicates the product could be $(CH_3)_2COHCH_2Co(Me_6[14]4,11\text{-diene})^{2+}$. However, this product is not stable and will decompose in about 30 min to give isobutene. The possible decomposition reaction is shown in equation (27). Attempts to isolate this product were not

$$(CH_3)_2COHCH_2CoL^{2+} + H^+ \longrightarrow (CH_3)_2C{=}CH_2 + CoL^{3+} + H_2O \quad (29)$$

successful.

Unfortunately this method is not working for the other free radicals such as $CH_3C{\cdot}HOH$ or $\cdot CH_2CHO$. Only the formation of CoL^{3+} was observed after the injection of H_2O_2.

Elroi and Meyerstein[31] found out there is a reaction between CoL^{2+} and $\cdot CH_2OH$ by means of radiolysis. The rate constant for this reaction is $(7 \pm 1) \times 10^7$ $M^{-1}s^{-1}$ and is independent of the pH of the solution. The spectrum of this intermediate is very similar to the one observed in this study. However this intermediate decomposes in a first-order process with $k = 0.10 \pm 0.02$ s^{-1}. This is very different from the product in this study which is stable for hours.

Attempts to prepare i-propyl,i-butyl, neo-pentyl and benzyl cobalt complex have been made for L = Me_6[14]4,11-dieneN$_4$. Unfortunately, neither the photolysis method nor the reaction with hydroperoxide works. There is no evidence to tell whether there is no reaction between these radicals and CoL^{2+} or these organocobalt complexes are so unstable. Previous results[5,32] show great differences in stability among benzyl,isopropyl, and ethyl cobaltcyclam complexes. $PhCH_2Co([14]aneN_4)^{2+}$ will undergo homolysis with a rate constant $k = 0.0941$ s^{-1} (25 °C)[32]; the attempt to prepare i-$PrCo([14]aneN_4)^{2+}$ was not successful and $EtCo([14]aneN_4)^{2+}$(or any other primary alkyl cobaltcyclam complexes) is stable at room temperature for several hours. Tsou et al.[33] also found that the homolysis rate constant of n-$PrCo(saloph)^{2+}$ and i-$PrCo(saloph)^{2+}$ are 4.7×10^{-4} and 5.7×10^{-2} s^{-1} (70 °C),

respectively. All these observations suggest the secondary organocobalt complexes must be very unstable, especially since primary organocobalt complexes will decompose completely within several hours in the absence of scavengers. Therefore the failure to prepare these sterically crowded organocobalt complexes is not surprising.

Crystal structure of $CH_2ClCo(Me_6[14]4,11\text{-dieneN}_4)^{2+}$

The rac(N) isomer of $CH_2ClCo(Me_6[14]4,11\text{-dieneN}_4)^{2+}$ is characterized by having hydrogen atoms of both amino groups (N1, N3) pointing to the same side of the coordinated methyl group. It is expected that these amine hydrogen atoms would occupy the axial positions, allowing the larger methylene group (C_2, C_7), to occupy the more stable equatorial position.

Among cobalt complexes with equatorialy coordinated 14-membered tetraaza macrocycles there is a remarkable similarity of equatorial Co-N bond lengths, independent of the formal oxidation state of the metal, the axial ligands, or the nature of the macrocycle.[34] However, the Co-N bond length does depend on the hybridization of the donor atom: 1.92 Å for -Co-imine (N2, N4); 1.98 Å for Co-amine (N1, N3).[33,35]

The Co-C bond distance 1.965 Å is normal for an alkyl cobalt(III) complex (Table II-11), indicating that the effect of the macrocycle saturation on the Co-C bond dissociation energy is perhaps quiet moderate. An increase in the Co-C bond distance would be expected for a complex with a BDE

Table II-11. Comparison of axial bond lengths in macrocyclic cobalt(III) complexes

L	R	Co-C	Co-OH_2
rac(N)Me_6[14]4,11-dieneN_4	Me	1.971(6)[a]	2.115(4)
rac(N)Me_6[14]4,11-dieneN_4	CH_2Cl	1.965(5)[b]	2.062(4)
$dmgH^-$	Me	1.990(5)[c]	2.058(3)
Me_4[14]tetraneN_4	Me	2.01[a]	2.11
[14]aneN_4	Me	1.99[a]	2.16
[14]aneN_4	Et	1.99(2)[d]	2.20(1)
rac(N)Me_6[14]4,11-dieneN_4	H_2O	—	1.91[e]

[a]Reference 36.

[b]This study.

[c]Reference 37.

[d]Reference 5.

[e]Reference 38.

Table II-12. Least-Squares plane[a]

atom	dev Å
N(1)[b]	-0.025 ± 0.005
N(2)[b]	0.025 ± 0.004
N(3)[b]	-0.025 ± 0.004
N(4)[b]	0.025 ± 0.004
Co	-0.0193 ± 0.0007
O(1)	2.047 ± 0.003
C(1)	-1.981 ± 0.005

[a]Orthonormal equation of plane
-0.7395X + -0.1499Y + -0.6603Z - -10.7395 = 0
crystallographic equation of plane
-11.2697X + -1.3512Y + -8.3614Z - -10.7395 = 0.

[b]Atoms defining the plane.

significantly smaller than that of the other alkyl cobalt complexes.

The Co-O bond length is 2.06 Å which is shorter than that of rac(N)-MeCo(Me_6[14]4,11-dieneN$_4$)(H_2O)$^{2+}$ but longer than that of related Co(Me_6[14]4,11-dieneN$_4$)(H_2O)$_2^{3+}$. This is consistent with a strong trans effect of the alkyl group.

Table II-12 contains the least-squares plane calculation and shows that the cobalt atom is in the plane defined by the

four nitrogen atoms. This is also true for the rac(N)MeCo(Me_6[14]4,11-dieneN_4)$^{2+}$ complex.[36] In the case of EtCo([14]aneN_4)$^{2+}$, however the cobalt atom is displaced towards the ethyl group by 0.05 Å.[5] This difference is thought to arise from the steric effect of the terminal methyl groups on the ring in the former case. The former has two axial methyl groups on the ring toward the side of the water molecule which requires the cobalt atom to be in the plane of the four nitrogen atoms to get more space.

The ORTEP of this molecule shows that the terminal methyl groups occupy axial positions in the ring (C_{14}, C_{17}), in this case directed toward the coordinated water molecule. Therefore it should have three unequivalent methyl groups (each has two equivalent methyl groups). This is consistent with its ^{1}H NMR spectrum (3 singlets with same intensity in the range of δ 0.9-2.2 ppm). However this structure is different from that found by Szalda, et al.[39] recently. They prepared the methylcobalt complex(MeCo(Me_6[14]4,11-dieneN_4)$^{2+}$) by following the reaction of $\cdot CH_3$ with rac-Co(Me_6[14]4,11-dieneN_4)$^{2+}$ directly. The crystal structure of the product shows the two methyl groups on the ring toward to the side with the methyl group on the cobalt atom. This is probably because the original rac(N)-Co(Me_6[14]4,11-dieneN_4)$^{2+}$ complex has a five coordinated cobalt center and the two axial methyl groups on the ring are directed towards the side of the vacancy (opposite the side of the water molecule).[39] This

vacancy provides a good opportunity for $\cdot CH_3$ to attack on cobalt. Therefore the methyl group on cobalt will be on the same side with the two axial methyl groups on the ring.

Isomerization of $RCo(Me_6[14]4,11\text{-diene})^{2+}$

Based on the observations of the ^1H NMR spectrum of $RCo(Me_6[14]4,11\text{-dieneN}_4)^{2+}$, it is clearly indicated that there is a isomerization reaction for these organocobalt complexes. The $Co(Me_6[14]4,11\text{-dieneN}_4)^{2+}$ complexes being employed in this study are most likely to be predominantly of the N-meso isomer of the ligand.[2] The preparative reactions were carried out in acidic solution; therefore a predominantly N-meso isomer of the product $RCo(Me_6[14]4,11\text{-dieneN}_4)^{2+}$ would be expected. The ^1H NMR spectrum of N-meso organocobalt complexes shows that the two (and only these two) axial methyl groups in the ring are not equivalent. They experience different local fields owing to the asymmetry along the axis perpendicular to the CoN_4 plane. Although there is no crystal structure of any of these N-meso isomers yet, their structures are pretty well confirmed by their ^1H NMR spectra. However, in basic or neutral solution, the N-meso isomer would convert to N-racemic isomer which is confirmed by previous result as well as the crystal structure of $CH_2ClCo(Me_6[14]4,11\text{-dieneN}_4)^{2+}$ in this study. These assignments are confirmed by the ^1H NMR spectra for most alkylcobalt complexes (R= CH_3, C_2H_5, and n-C_3H_7). In acidic solution, the isomerization reaction is prevented. Therefore the isomerization probably proceeds via

deprotonation and inversion of a secondary nitrogen (N-1 or N-8).

Recently Szalda et al.[39] found there is a equilibration between N-meso and N-racemic $Co(me_6[14]4,11\text{-dieneN}_4)^{2+}$. Equilibration of the two isomers is slow at room temperature ($< 2 \times 10^{-7}$ s^{-1}) in organic solvents and in acidic aqueous solutions; it is rapid in alkaline media and the N-rac isomer is favored at equilibrium. These results are exactly consistent with those observed in this study.

Although an attempt to measure the isomerization rate has not been made, the relative reaction rate can be stated as n-Pr > Et > Me which shows that the rate is dependent on the size of the alkyl group on cobalt atom. This is due to the steric effect from the axial methyl group in the ring towards the side of the alkyl group on the cobalt atom. This also makes the N-meso isomer become a relatively unstable isomer in the equilibrium.

Homolysis

The unimolecular homolysis of $EtCo(Me_6[14]4,11\text{-dieneN}_4)^{2+}$ has been studied carefully with a series of different scavengers. The general possible mechanism for these reactions are the following:

$$EtCoL^{2+} \xrightarrow{k_h} Et\cdot + CoL^{2+} \quad (L = Me_6[14]4,11\text{-dieneN}_4) \qquad (6)$$

$$Et\cdot + EtCoL^{2+} \xrightarrow[k_{-1}]{k_2} C_2H_4 + C_2H_6 + CoL^{2+} \qquad (7)$$

$$Et\cdot + S \xrightarrow{k_3} \text{products} \qquad (30)$$

The rate law is represented in equation (29).

$$-\frac{d[EtCoL^{2+}]}{dt} = \frac{2k_2k_h[EtCoL^{2+}]^2 + k_hk_3[EtCoL^{2+}][S]}{k_{-1}[CoL^{2+}] + k_2[EtCoL^{2+}] + k_3[S]} \quad (31)$$

Under these conditions $[S]>[EtCoL^{2+}]>>[CoL^{2+}]$ and k_3 at least is comparable with k_{-1} and k_2. This equation (31) can be simplified as equation (32).

$$-\frac{d[EtCoL^{2+}]}{dt} = k_h\,[EtCoL^{2+}] \quad (32)$$

The k_{obs} should be independent of the concentration of scavenger as well as the identity of scavenger being used in these kinetic studies. The results listed in Table II-8 show that the kinetic reactions are independent on the scavenger used. This result strongly suggests that the kinetic rate constants reported do, indeed, refer to the homolysis step as shown in equation 6.

In this study all the scavengers being used are the quenchers for the radical which is formed from the homolysis step. The possible mechanisms are described as follows:

i. O_2

$$Et\cdot + O_2 \longrightarrow EtOO\cdot \quad (33)$$

$$EtOO\cdot + CoL^{2+} \longrightarrow EtOOCoL^{2+} \quad (34)$$

($L = Me_6[14]4,11\text{-dieneN}_4$)

ii.HTMPO

$$Et\cdot + HTMPO \longrightarrow C_2H_4 + HTMPOH \qquad (35)$$

iii. $Co(NH_3)_5Br^+$

$$Et\cdot + Co(NH_3)_5Br^{2+} \longrightarrow EtBr + Co^{2+} + 5NH_4^+ \qquad (36)$$

$$Et\cdot + Co(NH_3)_5Br^{2+} \longrightarrow C_2H_4 + Co^{2+} + 5NH_4^+ + HBr$$

iv.Cr^{2+}

$$Et\cdot + Cr^{2+} \longrightarrow EtCr^{2+} \qquad (37)$$

$$EtCr^{2+} + H^+ \longrightarrow C_2H_6 + Cr^{3+} \qquad (38)$$

$$EtCoL^{2+} + Cr^{2+} \longrightarrow EtCr^{2+} + CoL^{2+} \qquad (39)$$

Since there is a bimolecular homolysis reaction between Cr^{2+} and $EtCo(Me_6[14]4,11\text{-dieneN}_4)^{2+}$, equation 39, the k_h was obtained as a intercept in the plot of k_{obs} vs. the concentration of Cr^{2+}. This probably is the reason that the rate constant is a little different from the others. When oxygen was used as scavenger, ethylene but not ethane was observed in the G.C. spectrum. This simply indicates there is a reaction between $EtOO\cdot$ and $EtCo(Me_6[14]4,11\text{-dieneN}_4)^{2+}$ as in equation 40. The kinetic result shows this reaction must be

$$EtOO\cdot + EtCoL^{2+} \longrightarrow EtOOH + C_2H_4 + CoL^{2+} \qquad (40)$$

a minor pathway, otherwise the k_{obs} should be equal to $2k_h$. However, a comparison between the yield of the ethylene and that of the radical formed in the homolysis reaction was made.

The result shows there is only ~10% of ethylene formed in the presence of oxygen relative to the amount of radical formed in homolysis. This clearly confirms that reaction 38 is not important.

The activation parameters, $\Delta H^{\neq}$ and $\Delta S^{\neq}$, are basically the same for these four cobalt complexes as listed in Table II-9. This is also a supportive of a homolytic process.

Recombination of cobalt(II) complexes with alkyl radicals has previously been demonstrated[40,41,42] to be close to diffusion controlled. Assuming ΔH_{-1} ~ 2 kcal/mol for such a diffusion-controlled process permits the the Co-R bond dissociaton energy, D_{Co-R}, to be deduced reliably from the measured values of $\Delta H^{\neq}$. Values of D_{Co-R} obtained in this way are listed in Table II-9.

The values of the activation parameters and rate constants for homolysis of macrocyclic alkylcobalt complexes in aqueous solutions, along with four examples in nonaqueous solvents, are summarized in Table II-13.[33,43,44] The rate constants span 4 orders of magnitude. The highest one is that for i-PrCo(cobalamin) which is a secondary organocobalt complex. From the last two examples in Table II-13, it is clear to see that secondary organocobalt complexes are much less stable

Table II-13. Kinetic data[a] and activation parameters of unimolecular homolysis for alkylcobalt complexes, $RCoL^{n+}$

$RCoL^{n+}$	k_h/s^{-1}	$\Delta H^{\ddagger}$/kcal mol^{-1}	$\Delta S^{\ddagger}$/cal $mol^{-1}K^{-1}$
$EtCo(Me_6[14]4,11\text{-}dieneN_4)^{2+}$[b]	3.9×10^{-4}	25.1 ± 0.9	10 ± 3
$n\text{-}PrCo(Me_6[14]4,11\text{-}dieneN_4)^{2+}$[b]	3.3×10^{-4}	26.6 ± 0.9	14 ± 3
$EtCo(Me_6[14]aneN_4)^{2+}$[b]	6.7×10^{-4}	25.6 ± 0.6	12 ± 2
$n\text{-}PrCo(Me_6[14]aneN_4)^{2+}$[b]	4.4×10^{-4}	26.5 ± 0.8	15 ± 3
neopentylCo(cobalamin)[c]	1.5×10^{-4}	23.4 ± 0.2	2.6 ± 0.1
neopentylCo(cobinamide)[c]	1.1×10^{-7}	32.1 ± 0.1	17.3 ± 0.4
i-PrCo(cobalamin)[c]	3.8×10^{-3}	20.7 ± 0.5	-0.3 ± 1.8
i-PrCo(cobinamide)[c,f]	2.5×10^{-6}	28.3 ± 0.2	10.8 ± 0.7
neopentylCo[C_2(DO)(DOH)pn][d,f]	1.3×10^{-7}	32.2 ± 2.0	18 ± 6
neopentylCo(saloph)py[e,f]	3.9×10^{-4}	20.3 ± 0.6	-6.2
n-PrCo(saloph)py[e,f]	2.1×10^{-7}	27.1 ± 1.1	2.6
i-PrCo(saloph)py[e,f]	1.5×10^{-4}	21.8 ± 1.0	-2.9

[a] At T = 25 °C.

[b] This study.

[c] Reference 43.

[d] In o-dichlorobenzene, reference 44. $C_2(DO)(DOH)_{pm}$ = 11-hydroxy-2,10-diethyl-3,9-dimethyl-1,4,8,11-tetraazaundeca-1,3,8,10-tetraen-1-olato.

[e] In pyridine, reference 33. saloph = N,N'-(bis(salicylidene)-o-phenylene)diamino.

[f] Calculated from $\Delta H^{\ddagger}$ and $\Delta S^{\ddagger}$.

than primary ones. Their homolysis rate constants are different by almost three orders of magnitude at room temperature. However, the difference of homolysis rate constant between i-PrCo(cobalamin) and $EtCo(Me_6[14]aneN_4)^{2+}$ is only a factor of five. This simply suggests that the homolysis rate constants found in this study are quite unusual among the similar primary alkylcobalt macrocycle complexes. The range of activation enthalpy for unimolecular homolysis of a metal-carbon bond is from 20 to 32 kcal/mole. The values found in this study are in the middle of this range. It is clear to see that these complexes have larger ΔS values than the other alkyl cobalt complexes. These results strongly suggest that the steric effect of the methyl groups on the ring give a large contribution to the homolytic cleavage of the Co-C bond.

Reaction of radical(R·) with $RCoL^{2+}$ complexes

The equivalent distribution of RH and R(-H) observed in the decomposition of $EtCo(Me_6[14]4,11\text{-}dieneN_4)^{2+}$ is strongly indicative of a mechanism consisting of a unimolecular homolysis, followed by the fast reaction 42.

$$RCoL^{2+} \longrightarrow R\cdot + CoL^{2+} \qquad (41)$$

$$R\cdot + RCoL^{2+} \longrightarrow R(-H) + RH + CoL^{2+} \qquad (42)$$

This reaction (eq. 42) was confirmed by checking the distribution of the products for the reaction of Fe^{2+} with t-

amyl hydroperoxide in the presence of $EtCo(Me_6[14]4,11\text{-}dieneN_4)^{2+}$. The products are ethane, ethylene and butane with a ratio as 44:36:20. In the absence of ethyl cobalt complex, the products are still the same as the former but with a different ratio as 16:13:71. The dramatic decrease of the amount of butane and equivalent distribution of ethane and ethylene strongly support the reaction as shown in eq. 38. This reaction probably proceeds by the abstraction of a β-proton from the alkyl group on the cobalt atom.

An attempt to measure the rate constant of equation 42 was made. Because the instability of some of these organo cobalt complexes, $MeCo(Me_6[14]4,11\text{-}dieneN_4)^{2+}$ was chosen as the candidate. In this case the reaction being studied (equation 16) is different from reaction 40 but still comparable.

$$Me\cdot + MeCoL^{2+} \longrightarrow C_2H_6 + CoL^{2+} \qquad (16)$$

Though there are a great many examples of electrophilic and nucleophilic attack at saturated carbon, examples of homolytic attack have proved particularly elusive.[45] In the coupling reaction of a Grignard reagent with an alkyl halide catalyzed by silver, a homolytic displacement and substitution on alkyl silver reaction was proposed as a possible pathway.[46] However, there is no sole evidence to support this. Johnson and co-workers[47] found that allylbis(dimethylglyoximato)pyridinecobalt(III) reacts with

trichloromethyl radical in chloroform to give quantitative yields of 4,4,4-trichlorobut-1-ene. This was probably the first clear example of homolytic displacement of any transition metal from carbon. Then they also found, in the reaction of benzylcobaloximes with bromotrichloromethane, that a homolytic displacement of the cobaloxime by attack of the trichloromethyl radicals at the α-carbon of the benzyl group was involved as the key step in the reaction mechanisms.[48] Espenson and co-workers[49] found that 2-hydroxy-2-propyl radical would react with benzyl cobaltoxime to give 1-phenyl-2-methyl-2-propanol. The reaction rate is 1.2×10^7 $M^{-1}s^{-1}$ at 25.0 °C and 1.0 M H^+. Recently, Sauer et al.[50] reported there is a reaction between methyl radical and methylnickel cyclam with $k = 4.7 \times 10^7$ $M^{-1}s^{-1}$. All these results show agreement to the one found (4.3×10^7 $M^{-1}s^{-1}$) in this study.

Reaction of $RCoL^{2+}$ with Cr^{2+}

Kinetic studies clearly show that there is a bimolecular reaction between $RCoL^{2+}$ and Cr^{2+}. The bimolecular rate constants are dependent on the size of the coordinated alkyl group. The remarkable decrease of the rate from ethyl to n-propyl indicates that there is a severe steric hindrance for these organocobalt complexes. It is interesting to notice that the rate constants for diene ligand are higher than those for $Me_6[14]aneN_4$ ligand. This also indicates that the former is less sterically crowded owing to the double bonds which make the ring configuration become more planar. The reaction

mechanism appears to consist of an S_H2 displacement at the saturated carbon.[16]

Summary

The preparations of a series of organocobalt complexes, $RCo(Me_6[14]4,11\text{-}dieneN_4)^{2+}$ and $RCo(Me_6[14]aneN_4)^{2+}$(R = primary and substituted primary alkyl group), are presented. The complexes were characterized by ^1H NMR spectroscopy, UV-visible spectroscopy and a crystal structure determination for $ClCH_2Co(Me_6[14]4,11\text{-}dieneN_4)(H_2O)(ClO_4)_2$.

The unimolecular homolysis have been studied for some of these complexes. The Co-C bond energy is about 23 kcal/mol for these complexes. The rates of the alkyl group transfer from CoL^{2+} to Cr^{2+}(L = $Me_6[14]4,11\text{-}dieneN_4$ and $Me_6[14]aneN_4$) show a strong dependence of steric effect on the alkyl group, consistent with a S_H2 mechanism.

BIBLIOGRAPHY

1. Lenhart, P. G.; Hodgkin, D. C. Nature (London) 1961, 192, 937.
2. Busch, D. H.; Farmery, K.; Goedken, V.; Katavic, V.; Melnyk, A. C.; Sperati, C. R.; Tokel, N. Advan. Chem. Ser. 1970, 100, 44.
3. Roche, T. S.; Endicott, J. F. J. Am. Chem. Soc. 1972, 94, 8622.
4. Roche, T. S.; Endicott, J. F. Inorg. Chem. 1974, 13, 1575.
5. Bakac, A.; Espenson, J. H. Inorg. Chem. 1987, 26, 4353.
6. Heckman, R. A.; Espenson, J. H. Inorg. chem. 1979, 18, 38.
7. Nohr, R. S.; Espenson, J. H. J. Am. Chem. Soc. 1975, 97, 3392.
8. a. Kirker, G. W.; Bakac, A.; Espenson, J. H. J. Am. Chem. Soc. 1982, 104, 1249.

   b. Espenson, J. H.; Connolly, P.; Meyerstein, D.; Cohen, H. Inorg Chem. 1983, 22, 1009.

   c. Bakac, A.; Espenson, J. H. J. Am. Chem. Soc. 1984, 106, 5197.
9. a. Ng, F. T. T,; Rempel, G. L.; Halpern, J. J. Am. Chem. Soc. 1982, 104, 621.

   b. Halpern, J.; Ng, F. T. T.; Rempel. G. L. J. Am. Chem. Soc. 1979, 101, 7124.

   c. Halpern, J. Acc. Chem. Res. 1982, 15, 238.

10. Grate, G. W.; Schrauzer, G. N. Organometallics 1982, 1, 1155.

11. Tamblyn, W. H.; Klingler, R. J.; Hwang, W. S.; Kochi, J. K. J. Am. Chem. Soc. 1981, 103, 3161.

12. Pohl, M. C.; Espenson, J. H. Inorg. Chem. 1980, 19, 235.

13. Mulac, W. A.; Cohen, H.; Meyerstein, D. Inorg. Chem. 1982, 21, 4016.

14. Fergusson, S. B.; Baird, M. C.; Inorg. Chim. Acta 1982, 63, 41.

15. Van den Bergen, A.; West, B. O. J. Organomet. Chem. 1974, 64, 1125.

16. a. Espenson, J. H.; Shveima, J. S. J. Am. Chem. Soc. 1973, 95, 4468.

b. Espenson, J. H.; Sellers, T. D., Jr. J. Am. Chem. Soc. 1974, 96, 94.

c. Espenson, J. H.; Leslie, J. P. II J. Am. Chem Soc. 1974, 96, 1954.

17. Dizikes, L. J.; Ridley, W. P.; Wood, J. M. J. Am. Chem. Soc. 1978, 100, 1010.

18. Parris, M.; Ashbrook, A. W. Can. J. Chem. 1979, 57, 1233.

19. Chrzastowski, J. Z.; Cooksey, C. J.; Johnson, M. D.; Lockman, B. L.; Steggles, P. N. J. Am. Chem. Soc. 1975, 97, 932.

20. Dodd, D.; Johnson, M. D.; Lockman, B. L. J. Am. Chem. Soc. 1977, 99, 3664.

21. Endicott, J. F.; Balakrishnan, K. P.; Wong, C.-L. J. Am. Chem. Soc., 1980, 102, 5519.

22. Schrauzer,G. N. Inorg. Synth. 1965, 11, 65.

23. Hay, R. W.; Lawrance, G. A.; Curtis, N. F. J. Chem. Soc. Perkin, 1975, 591.

24. Rillema, D. P.; Endicott, J. F.; Papaconstantinou, E. Inorg. Chem. 1971, 10, 1739.

25. Maruthamuthu, P; Venkatasubramanian, L.; Dharmalingam, P. Bull. Chem. Soc. Jpn. 1987, 60, 1113.

26. a. Milas, N. A.; Sugenor, D. M. J. Am. Chem. Soc. 1946, 68, 205.

b. Leslie, II, J. P.; Espenson, J. H. J. Am. Chem. Soc. 1976, 98, 4839.

27. Connolly, P. Ph. D. Dissertation, Iowa State University, Ames, Iowa, 1985.

28. Hoselton, M. A.; Lin, C.-T.; Schwartz, H. A.; Sutin, N. J. Am. Chem. Soc. 1978, 100, 2383.

29. a. Mok, C. Y.; Endicott, J. F. J. Am. Chem. Soc. 1977, 99, 1276.

b. Mok, C. Y.; Endicott, J. F. J. Am. Chem. Soc. 1978, 100, 123.

c. Endicott, J. F. Inorg. Chem. 1977, 16, 494.

30. Gjerde, H. B.; Espenson, J. H. Organometallics 1982, 1, 435.

31. Elroi, H.; Meyerstein, D. J. Am. Chem. Soc. 1978, 100, 5540.

32. Bakac, A.; Espenson, J. H. Inorg. Chem. 1987, 26, 4307.

33. Tsou, T. T.; Loots, M.; Halpern, J. J. Am. Chem. Soc. 1982, 104, 623.

34. Endicott, J. F.; Durham, B.; Glick, M. D.; Anderson, T. J.; Kuszaj, J. M.; Schmonsees, W. G.; Balakrishnan, K. P. J. Am. Chem. Soc. 1981, 103, 1431.

35. Endicott, J. F.; Lilie, J.; Kuszaj, J. M.; Ramaswamy, B.S.; Schmonsees, W. G., Simic, M. G.; Glick, M. D.; Rilleman, D. P. J. Am. Chem. Soc. 1977, 99, 429.

36. Heeg, M. J.; Endicott, J. f.; Glick, M. D. Inorg. Chem. 1981, 20, 1196.

37. McFadden, D. L.; McPhail, A. T. J. Chem. Soc. Dalton Trans. 1974, 363.

38. Glick, M. D.; Kuszaj, J. M.; Endicott, J. F. J. A. Chem. Soc. 1973, 95, 5097.

39. Szalda, D. J.; Schwarz, C. L.; Endicott, J. F.; Fujita, E.; Creutz, C. Inorg. Chem. 1989, 28, 3214.

40. Halpern, J. Pure. Appl. Chem. 1979, 51, 217.

41. Endicott, J. F.; Ferraudi, G. J. J. Am. Chem. Soc. 1977, 99, 243.

42. Bakac, A.; Espenson, J. H. Inorg Chem 1989, 28, 0000.

43. Schrauzer, G. N.; Grate, J. H. J. Am. Chem. Soc. 1981, 103, 541.

44. Finke, R. G.; Smith, B, L.; Mayer, B. J.; Molinero, A. A. Inorg. Chem. 1983, 22, 3679.

45. Ingold, K. U.; Roberts, B. P. "Free Radical Substitution Reactions", Wiley-Interscience, New York, 1970.

46. Tamura, M.; Kochi, J. J. Am. Chem. Soc. 1971, 93, 1483.

47. Dass Gupta, B.; Funabiki, T.; Johnson, M. D. J. Am. Chem. Soc. 1976, 98, 6697.

48. Funabiki, T.; Dass Gupta, B.; Johnson, M. D. J. C. S. Chem. Comm. 1977, 653.

49. McHatton, R. C.; Espenson, J. H.; Bakac, A. J. Am. Chem. Soc. 1982, 104, 3531.

50. Sauer, A.; Cohen, H.; Meyerstein, D. Inorg. Chem. 1988, 27, 4578.

APPENDIX

Table A-1. Kinetic data for the reaction of Cr^{2+} with $EtCo(Me_6[14]4,11\text{-dieneN}_4)^{2+}$

Conditions: λ = 480 nm, μ = 0.14 M

T = 25.0 ± 0.1 °C

$10^{-3}[Cr^{2+}]/M$	$10^{-4}k_{obs}/s^{-1}$
9.0	4.65
18.0	7.22
22.5	6.97
45.0	12.12[a]

[a] μ = 0.23 M.

Table A-2. Kinetic data for the reaction of $Co(NH_3)_5Br^{2+}$ with $EtCo(Me_6[14]4,11\text{-dieneN}_4)^{2+}$

Conditions: λ = 480 nm, μ = 0.5 M

T = 25.0 ± 0.1 °C

$10^{-3}[Co(NH_3)_5Br^{2+}/M$	$10^{-4}k_{obs}/s^{-1}$
10.3	4.22
15.5	4.25
20.7	4.11

Table A-3. Homolysis rate constants of $EtCo(Me_6[14]4,11\text{-}dieneN_4)^{2+}$ at different temperatures

Temp./°C	k_h/s^{-1} [a,c]
11.0	4.90×10^{-5}
12.1	5.59×10^{-5}
15.7	1.09×10^{-4} [b]
16.3	9.30×10^{-5}
20.7	2.70×10^{-4} [b]
21.4	2.16×10^{-4}
25.0	3.90×10^{-4}
25.0	4.70×10^{-4} [b]
31.1	9.35×10^{-4}
35.9	1.60×10^{-3}
39.9	3.09×10^{-3}

[a]The scavenger is oxygen, except as noted.

[b]The scavenger is HTMPO.

[c]μ = 0.1 M.

Table A-4. Homolysis rate constants for nPrCo(Me_6[14]4,11-dieneN$_4$)$^{2+}$ at different temperatures

Temp./°C	k_h/s^{-1} [a,c]
11.9	3.05×10^{-5}
15.7	5.00×10^{-5} [b]
19.9	1.20×10^{-4}
20.8	1.89×10^{-4} [b]
25.0	3.30×10^{-4}
30.2	6.64×10^{-4}
35.2	1.16×10^{-3}
39.5	2.15×10^{-3}
46.6	5.70×10^{-3}

[a]The scavenger is oxygen except as noted.

[b]The scavenger is HTMPO.

[c]μ = 0.1 M.

Table A-5. Homolysis rate constants for $EtCo(Me_6[14]aneN_4)^{2+}$ at different temperatures

Temp./°C	k_h/s^{-1} [a,b]
14.9	1.22×10^{-4}
21.6	3.42×10^{-4}
25.3	6.66×10^{-4}
30.3	1.17×10^{-3}
35.3	2.51×10^{-3}
40.5	5.17×10^{-3}

[a]The scavenger is HTMPO.

[b]μ = 0.1 M.

Table A-6. Homolysis rate constants for $nPrCo(Me_6[14]aneN_4)^{2+}$ at different temperatures

Temp./°C	k_h/s^{-1} [a,b]
11.4	4.43×10^{-5}
15.3	8.68×10^{-5}
20.5	2.51×10^{-4}
25.0	4.45×10^{-4}
30.6	9.49×10^{-4}
35.6	1.79×10^{-3}
40.7	4.50×10^{-3}

[a]The scavenger is HTMPO.

[b]μ = 0.1 M.

Table A-7. Kinetic result of the reaction of Me· with $MeCo(Me_6[14]4,11\text{-}dieneN_4)^{2+}$

$10^4[MeCoL^{2+}]/M$	$10^5[ABTS^-]/M$	$10^4k_{obs}/s^{-1}$	$10^4k_{corr}/s^{-1}$
2.46	2.47	5.67	0.68
4.11	2.02	6.14	1.87
4.11	1.81	5.38	1.48
6.16	1.63	7.42	3.92
6.16	0.96	4.65	2.50
8.21	0.98	5.82	3.60

Table A-8. Kinetic data for the reaction of Cr^{2+} with $MeCo(Me_6[14]4,11\text{-dieneN}_4)^{2+}$

Conditions: λ = 470 nm, μ = 1.0M

T = 25.0 ± 0.1 °C

$10^3[Cr^{2+}]/M$	$10^2k_{obs}/s^{-1}$
0.99	1.13
1.99	2.42
3.05	3.82
3.98	5.14
5.04	6.08
5.20	6.79
5.97	7.28

Table A-9. Kinetic data for the reaction of Cr^{2+} with $EtCo(Me_6[14]4,11\text{-dieneN}_4)^{2+}$

Conditions: λ = 480 nm, μ = 1.0 M

T = 25 .0 ± 0.1 °C

$10^2[Cr^{2+}]/M$	$10^3k_{obs}/s^{-1}$
1.33	0.95
3.98	2.20
6.63	2.68
9.29	3.72
11.3	4.63
13.3	5.40
13.3	5.42

Table A-10. Kinetic data for the reaction of Cr^{2+} with n-PrCo(Me_6[14]4,11-dieneN$_4$)$^{2+}$

Conditions: λ = 480 nm, μ = 1.0 M

T = 25.0 ± 0.1 °C

$10[Cr^{2+}]/M$	$10^4 k_{obs}/s^{-1}$
0.50	2.95
1.0	3.19
1.5	3.05
2.0	3.39
2.5	4.00

Table A-11. Kinetic data for the reaction of Cr^{2+} with $MeCo(Me_6[14]aneN_4)^{2+}$

Conditions: λ = 480 nm, μ = 1.0 M

T = 25.0 ± 0.1 °C

$10^2[Cr^{2+}]/M$	$10^2k_{obs}/s^{-1}$
0.66	0.92
1.00	1.58
3.32	5.23
3.98	6.25
5.31	9.04

Table A-12. Kinetic data for the reaction of Cr^{2+} with $EtCo(Me_6[14]aneN_4)^{2+}$

Conditions: λ = 390 nm, μ = 1.0 M

T 25.0 ± 0.1 °C

$10^2[Cr^{2+}]/M$	$10^3k_{obs}/s^{-1}$
1.33	0.84
3.98	0.93
7.30	1.16
9.96	1.40
20.0	1.82

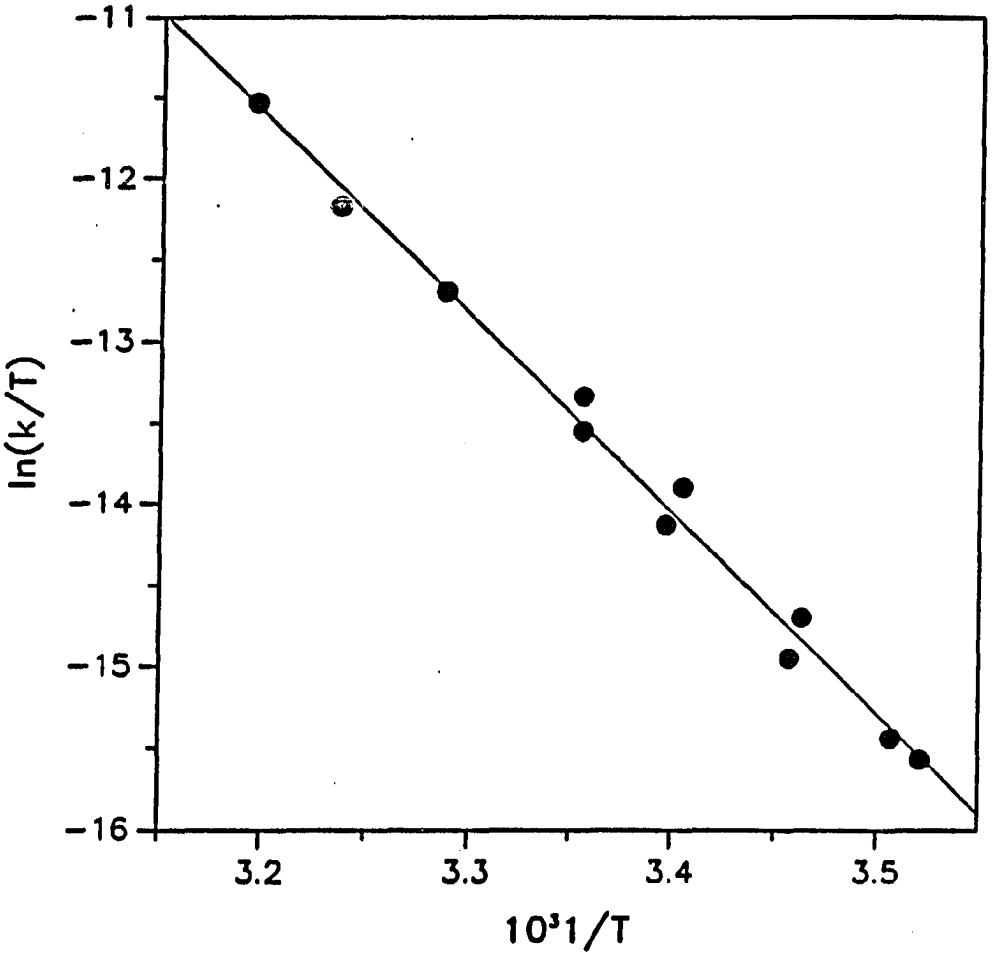

Figure A-1. The plot of Eyring equation for the homolysis of $EtCo(Me_6[14]4,11\text{-}dieneN_4)^{2+}$

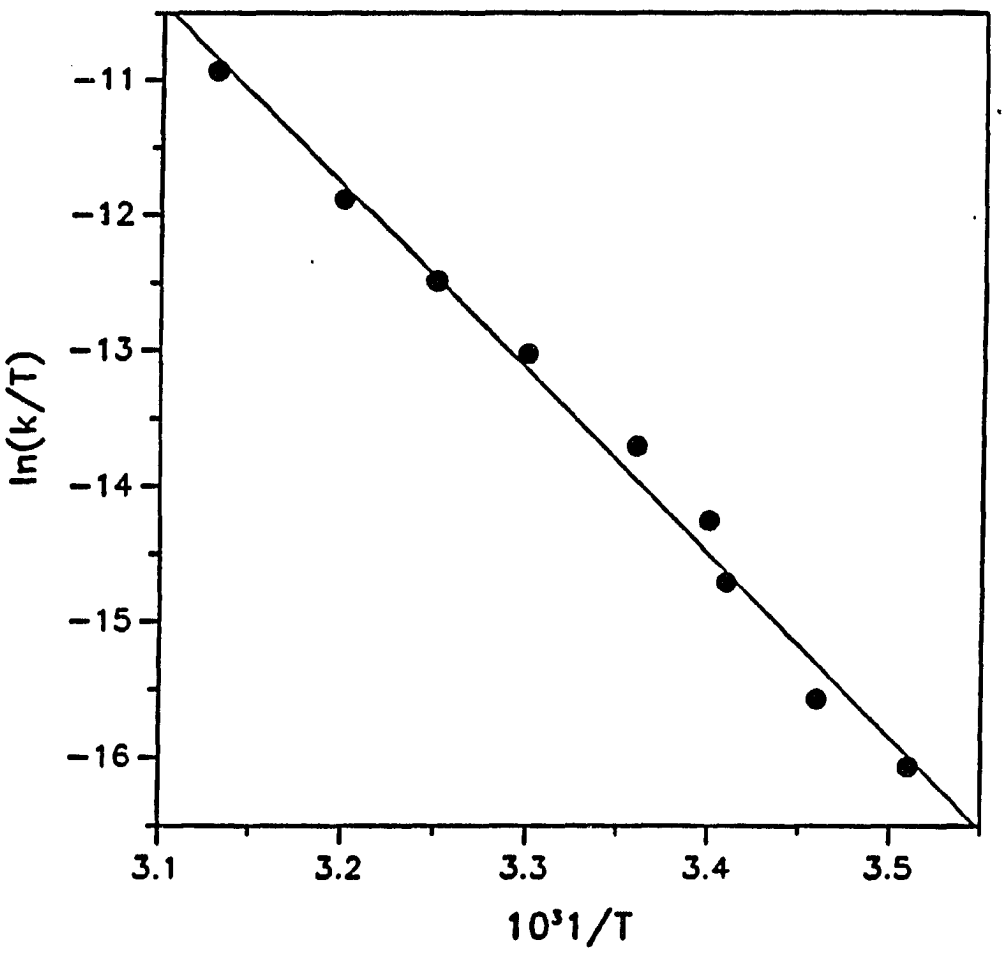

Figure A-2. The plot of Eyring equation for the homolysis of n-PrCo(Me_6[14]4,11-dieneN$_4$)$^{2+}$

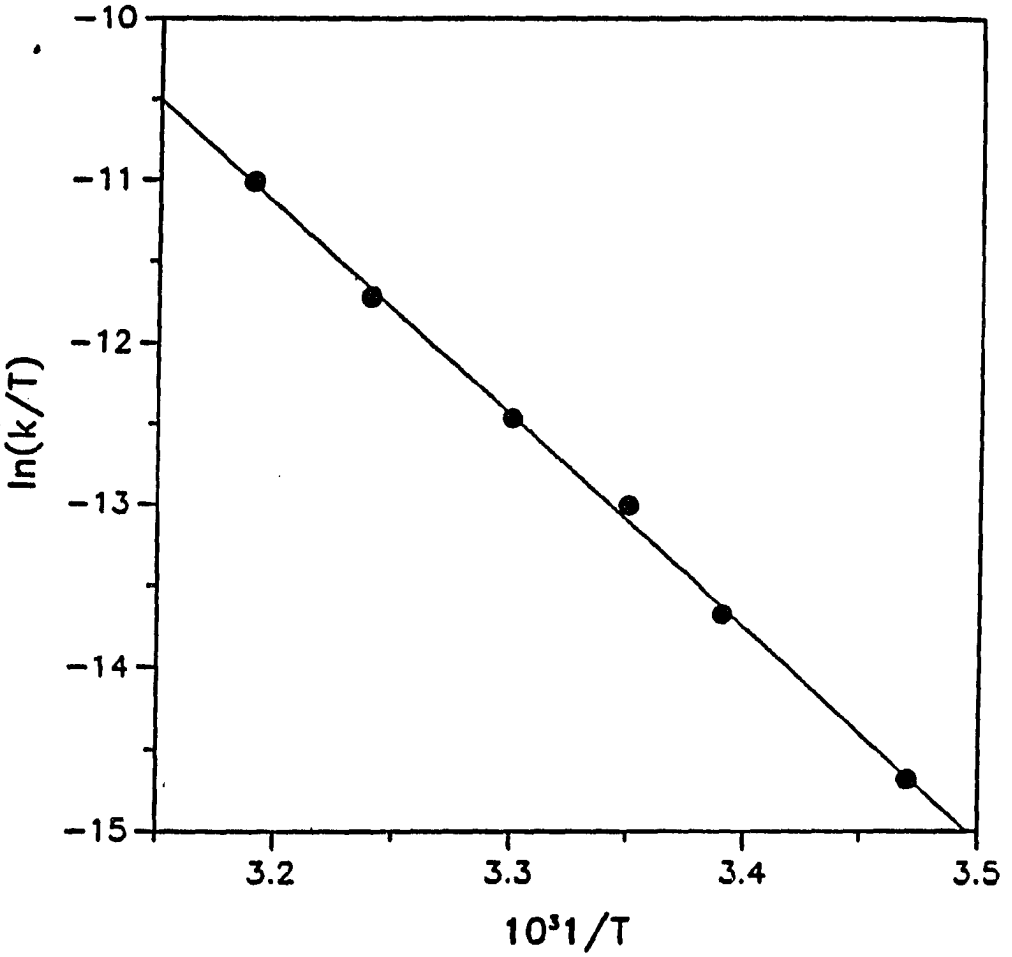

Figure A-3. The plot of Eyring equation for the homolysis of $EtCo(Me_6[14]aneN_4)^{2+}$

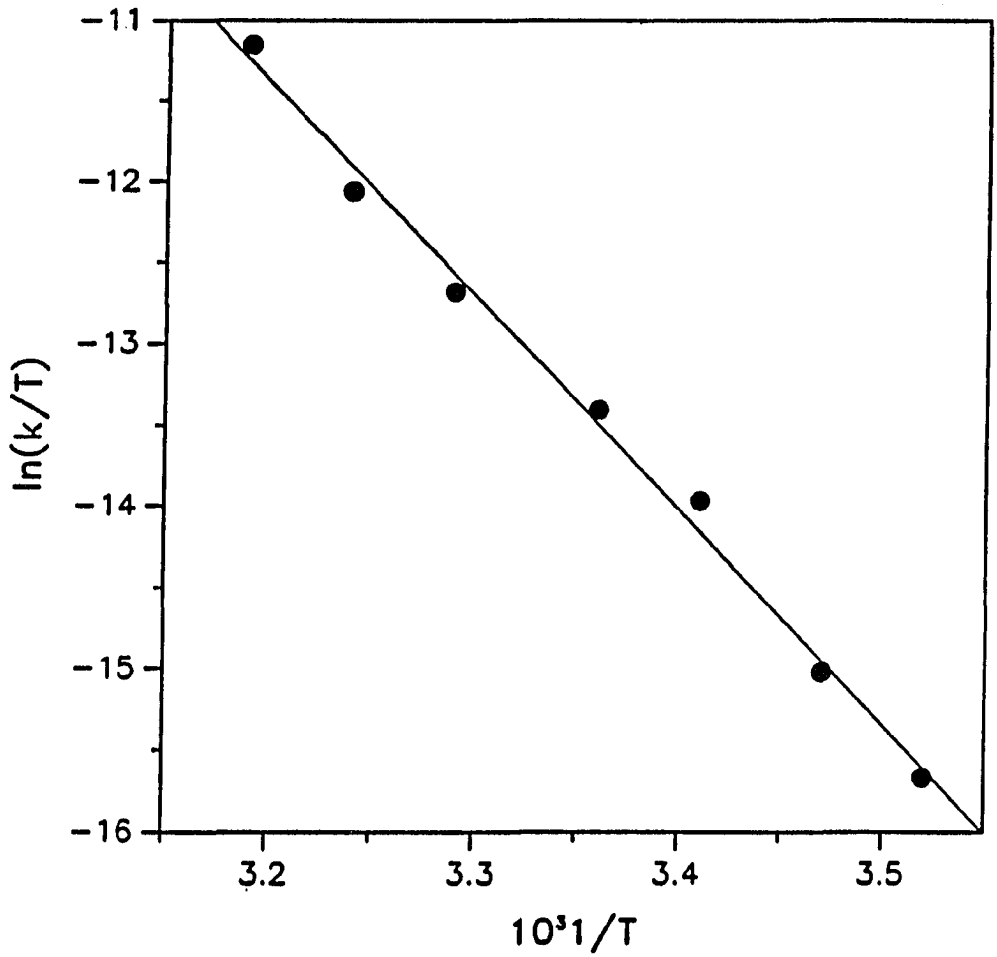

Figure A-4. The plot of Eyring equation for the homolysis of n-PrCo(Me_6[14]aneN_4)$^{2+}$

GENERAL SUMMARY

The quenching by ferrocenium ions proceeds by energy transfer and is dependent on the donor-acceptor distance, as expected for an electron-exchange mechanism. The rate constants for quenching with d^6 metallocenes are at or near the diffusion-controlled limit. The reactions partition themselves between electron transfer and energy transfer. The $Cr(bpy)_2^{2+}$ and the ferroceniums, formed by electron transfer quenching, undergo rapid back electron transfer, $k = (3-9) \times 10^9\ M^{-1}s^{-1}$.

The preparations of a series of organocobalt complexes, $RCo(Me_6[14]4,11\text{-}dieneN_4)^{2+}$ and $RCo(Me_6[14]aneN_4)^{2+}$(R = primary and substituted primary alkyl group), are presented. The complexes were characterized by ^1H NMR spectroscopy, UV-visible spectroscopy and a crystal structure determination for $ClCH_2Co(Me_6[14]4,11\text{-}dieneN_4)(H_2O)(ClO_4)_2$.

The unimolecular homolyses have been studied for some of these complexes. The Co-C bond energy was estimated as 23 Kcal/mol for these complexes. The rates of the alkyl group transfer from CoL^{2+} to Cr^{2+}(L = $Me_6[14]4,11\text{-}dieneN_4$ and $Me_6[14]aneN_4$) show a strong dependence of steric effect on the alkyl group, consistent with a S_H2 mechanism.

ACKNOWLEDGMENTS

I would like to thank Professor Espenson and Dr. Andrejia Bakac for their guidance during my graduate career. I am also grateful to the members of my research group for their helpful discussions. I am grateful to Dr. L. Daniels for his assistance with the X-ray crystal structure determination.

I would also like to thank my parents and my wife for the endless encouragement and their faith in me.